Electronic Supplementary Material (ESI) for Dalton Transactions.

Electronic Supporting Information (ESI) for:

Synthesis, characterization, and catalytic evaluation of ruthenium–diphosphine complexes bearing xanthate ligands

Mohammed Zain Aldin,[a] Anthony Maho,[b] Guillermo Zaragoza,[c] Albert Demonceau,[a] and Lionel Delaude*[a]

[a]*Laboratory of Organometallic Chemistry and Homogeneous Catalysis, Institut de chimie (B6a), Allée du six Août 13, Quartier Agora, Université de Liège, 4000 Liège, Belgium*

[b]*GreenMAT, Institut de Chimie (B6a), Allée du six Août 13, Quartier Agora, Université de Liège, 4000 Liège, Belgium*

[c]*Unidade de Difracción de Raios X, Edificio CACTUS, Universidade de Santiago de Compostela, Campus Vida, 15782 Santiago de Compostela, Spain*

Table of content

Part 1 – NMR spectra

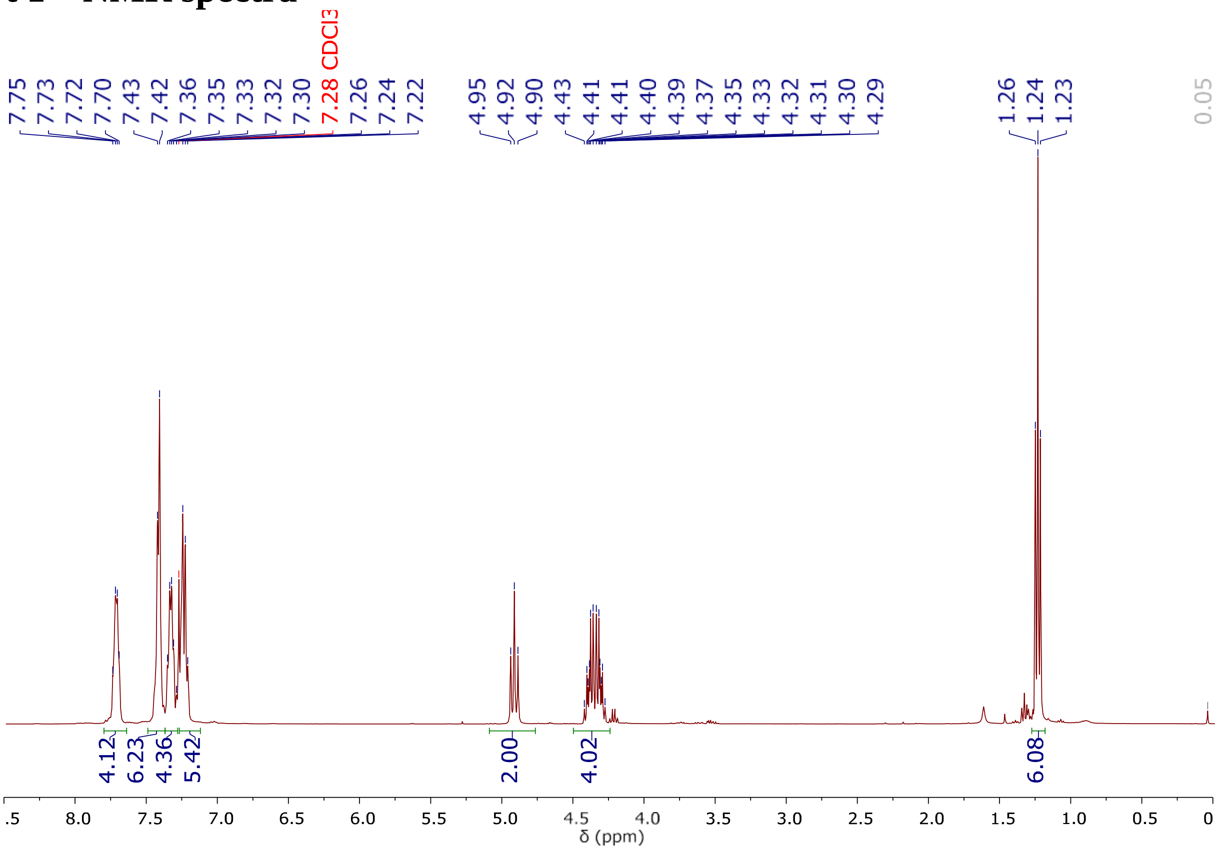

Fig. S1. ^{1}H NMR spectrum (400 MHz, $CDCl_3$, 298 K) of [Ru(S_2COEt)$_2$(dppm)] (**1**)

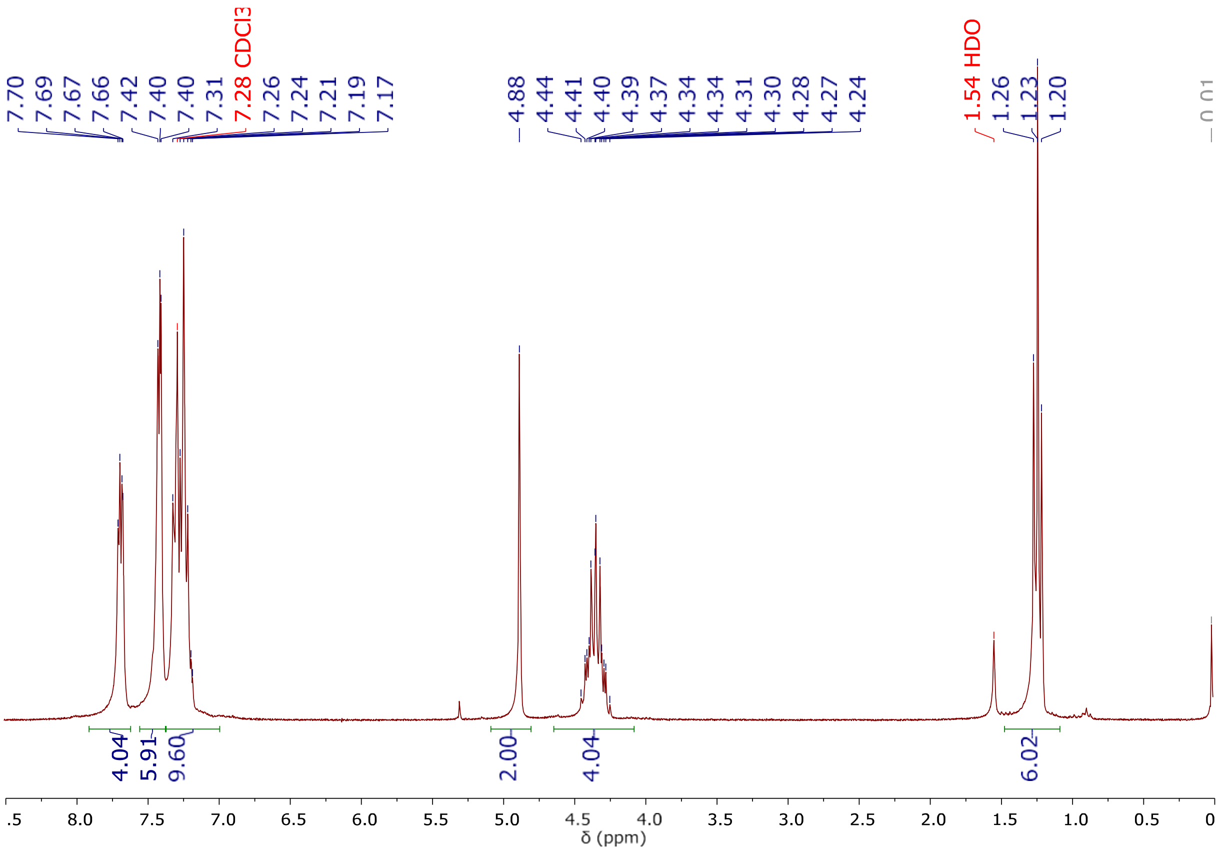

Fig. S2. ^{1}H{^{31}P} NMR spectrum (250 MHz, $CDCl_3$, 298 K) of [Ru(S_2COEt)$_2$(dppm)] (**1**)

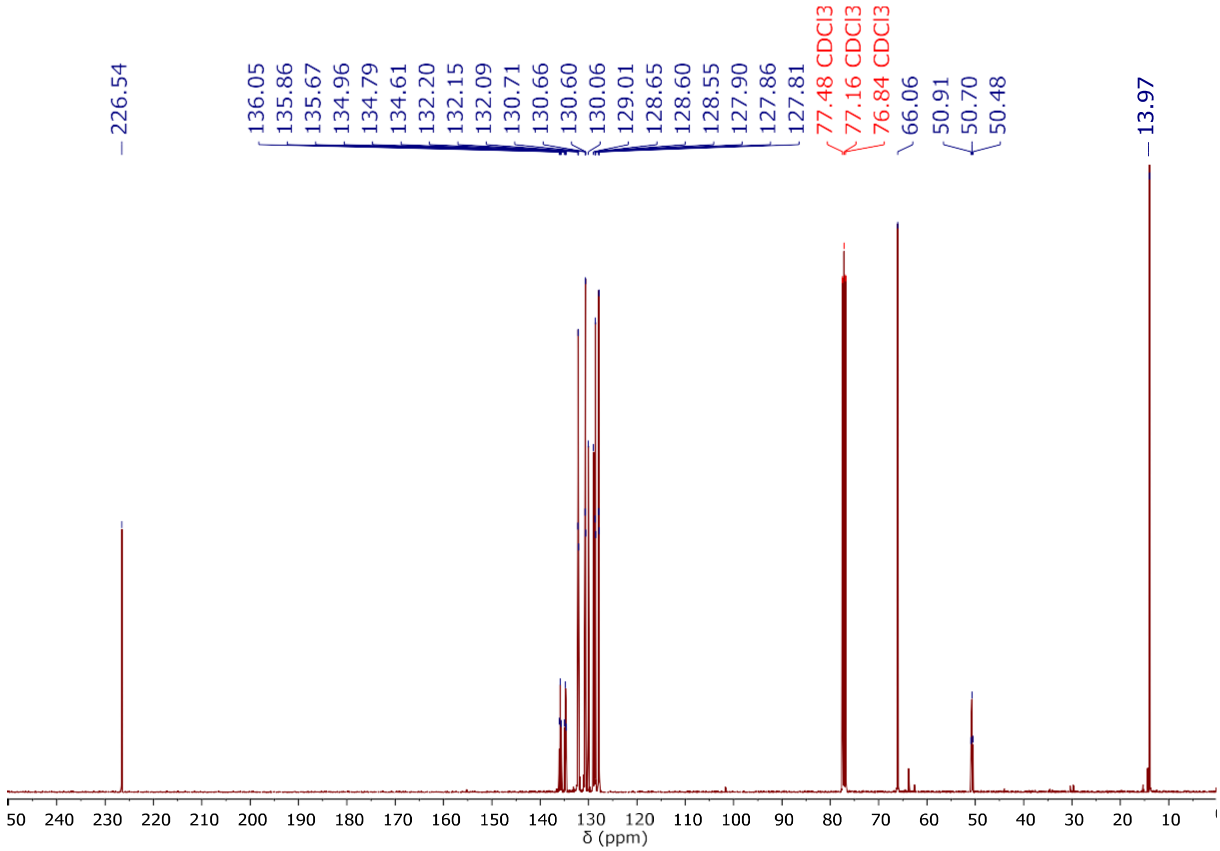

Fig. S3. $^{13}C\{^{1}H\}$ NMR spectrum (101 MHz, $CDCl_3$, 298 K) of [Ru(S_2COEt)$_2$(dppm)] (**1**)

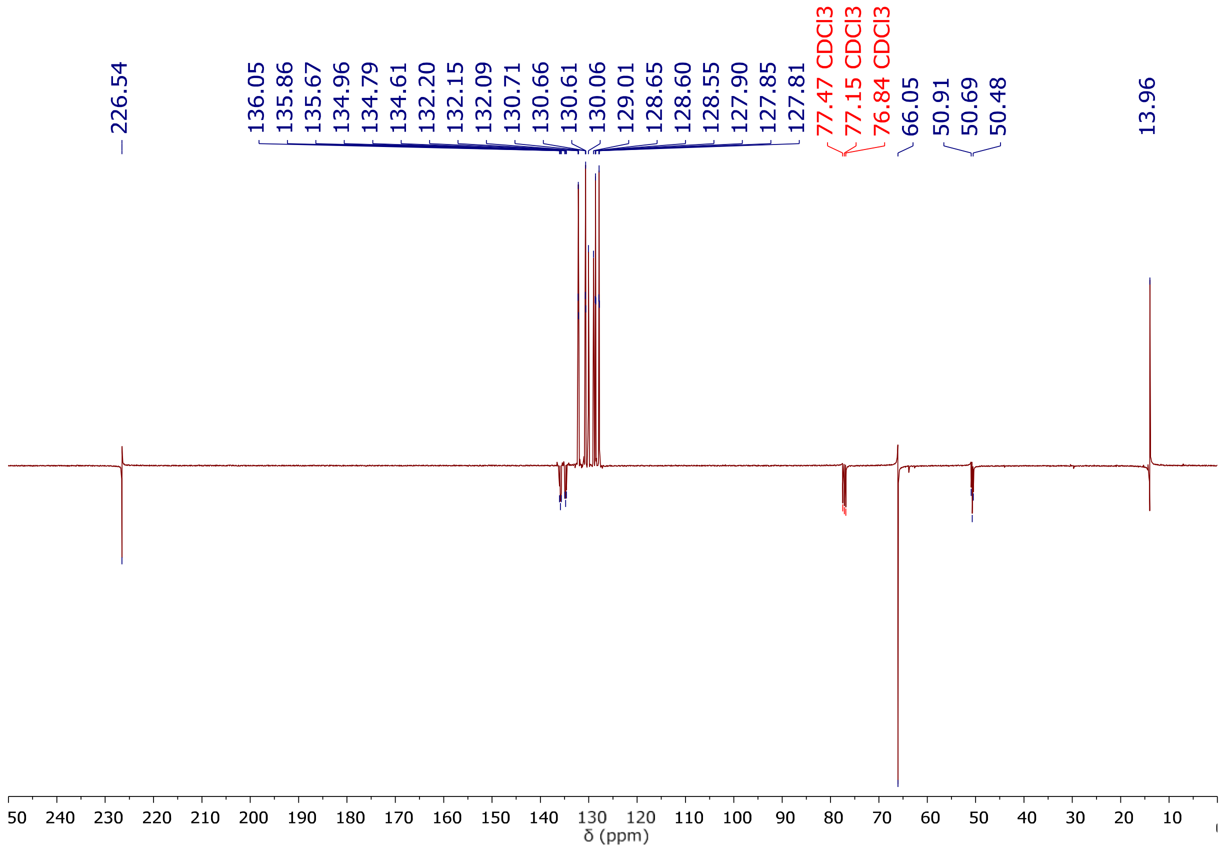

Fig. S4. $^{13}C\{^{1}H\}$ APT NMR spectrum (101 MHz, $CDCl_3$, 298 K) of [Ru(S_2COEt)$_2$(dppm)] (**1**)

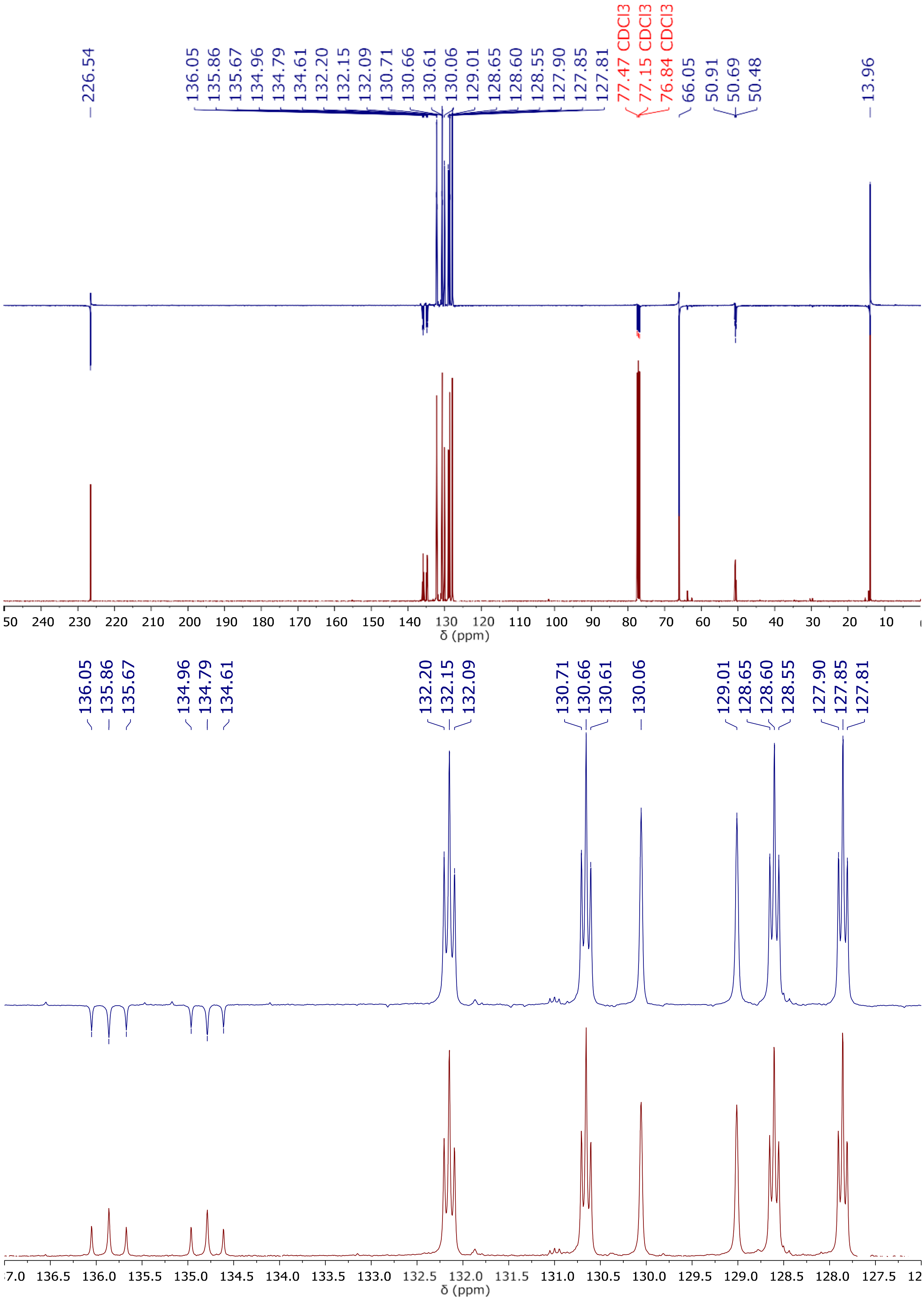

Fig. S5. ^{13}C CPD and APT NMR spectra (101 MHz, $CDCl_3$, 298 K) of [Ru(S_2COEt)$_2$(dppm)] (**1**)

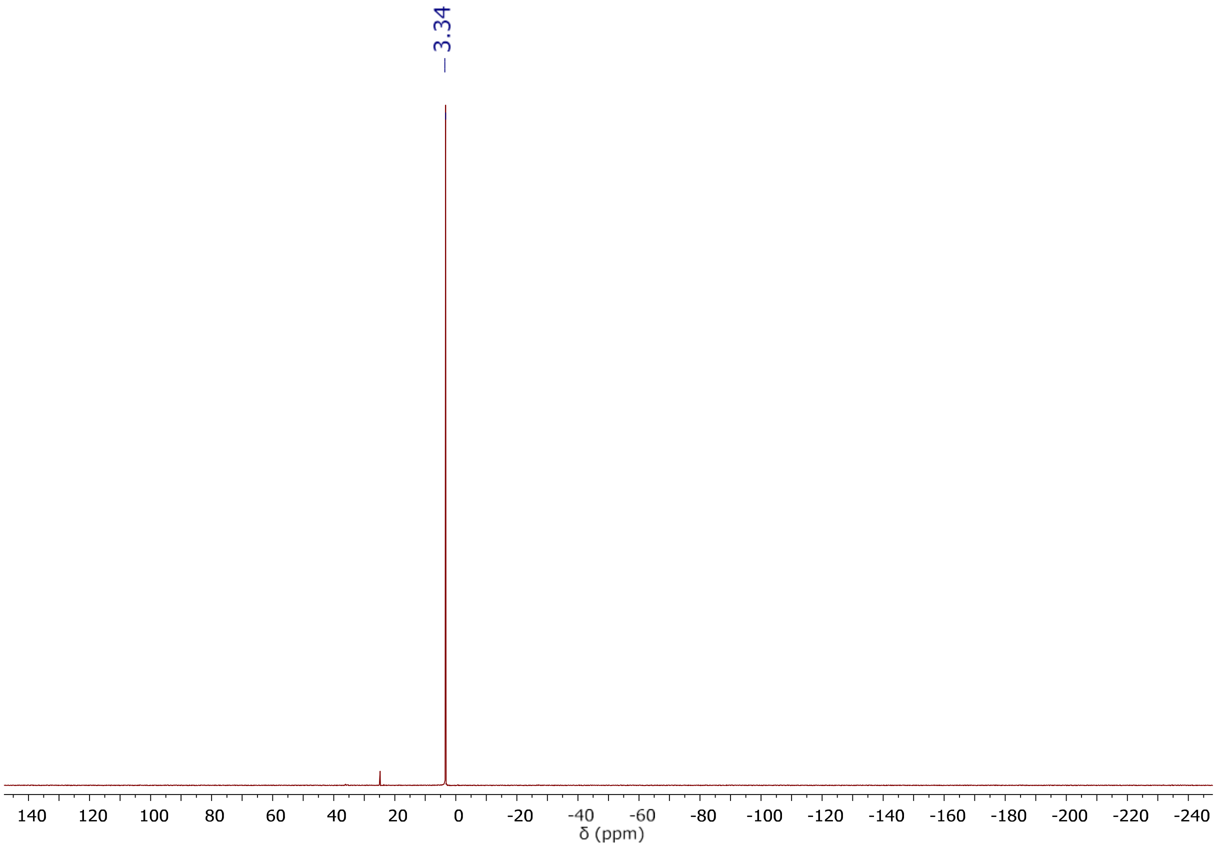

Fig. S6. ^{31}P NMR spectrum (162 MHz, $CDCl_3$, 298 K) of [Ru(S_2COEt)$_2$(dppm)] (**1**)

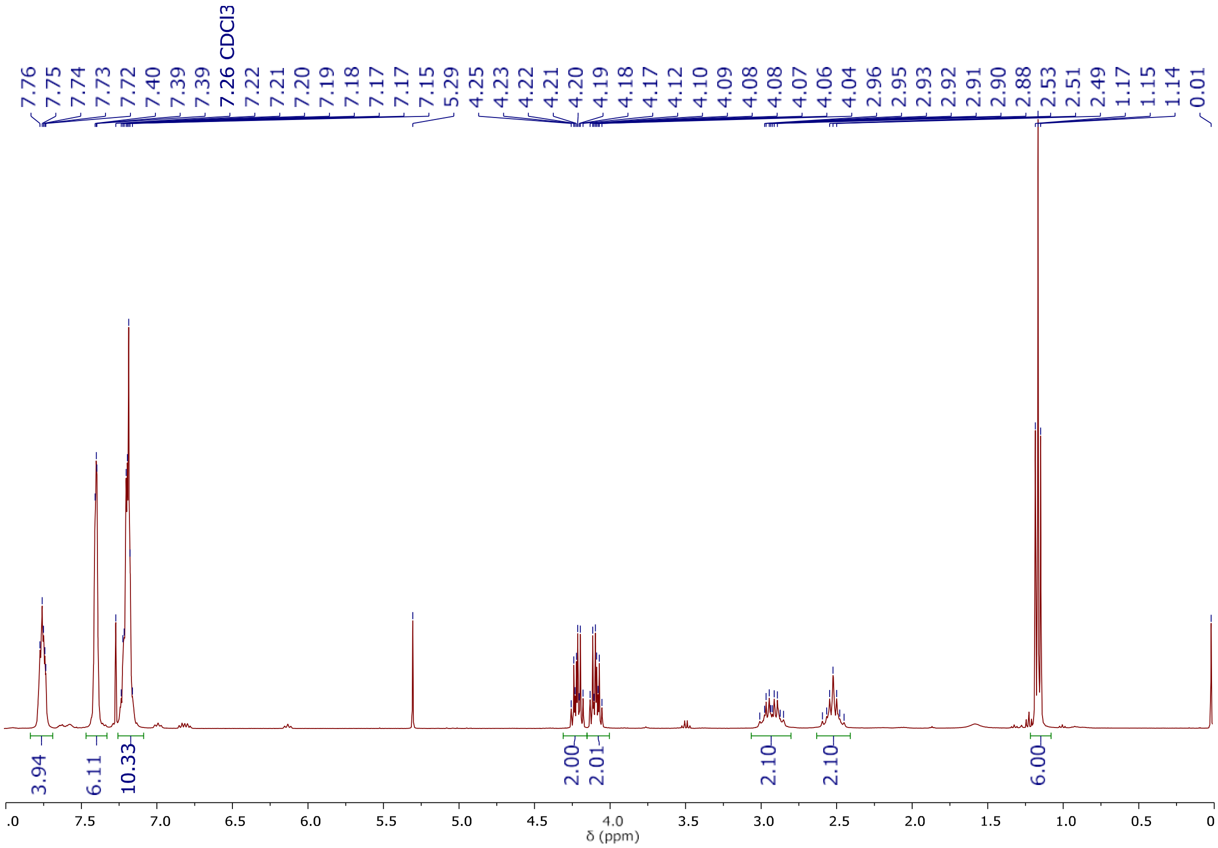

Fig. S7. ^{1}H NMR spectrum (400 MHz, $CDCl_3$, 298 K) of [Ru(S_2COEt)$_2$(dppe)] (**2**)

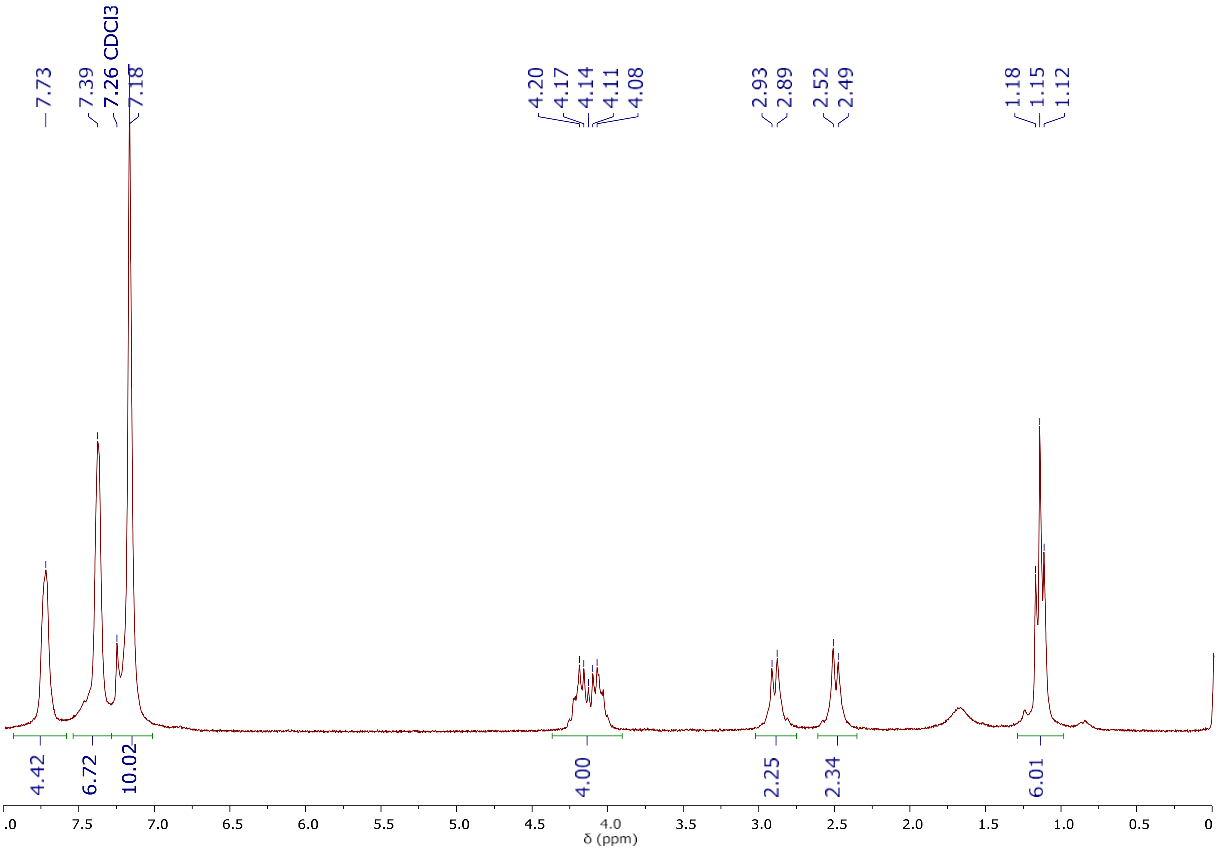

Fig. S8. $^{1}H\{^{31}P\}$ NMR spectrum (250 MHz, $CDCl_3$, 298 K) of $[Ru(S_2COEt)_2(dppe)]$ (**2**)

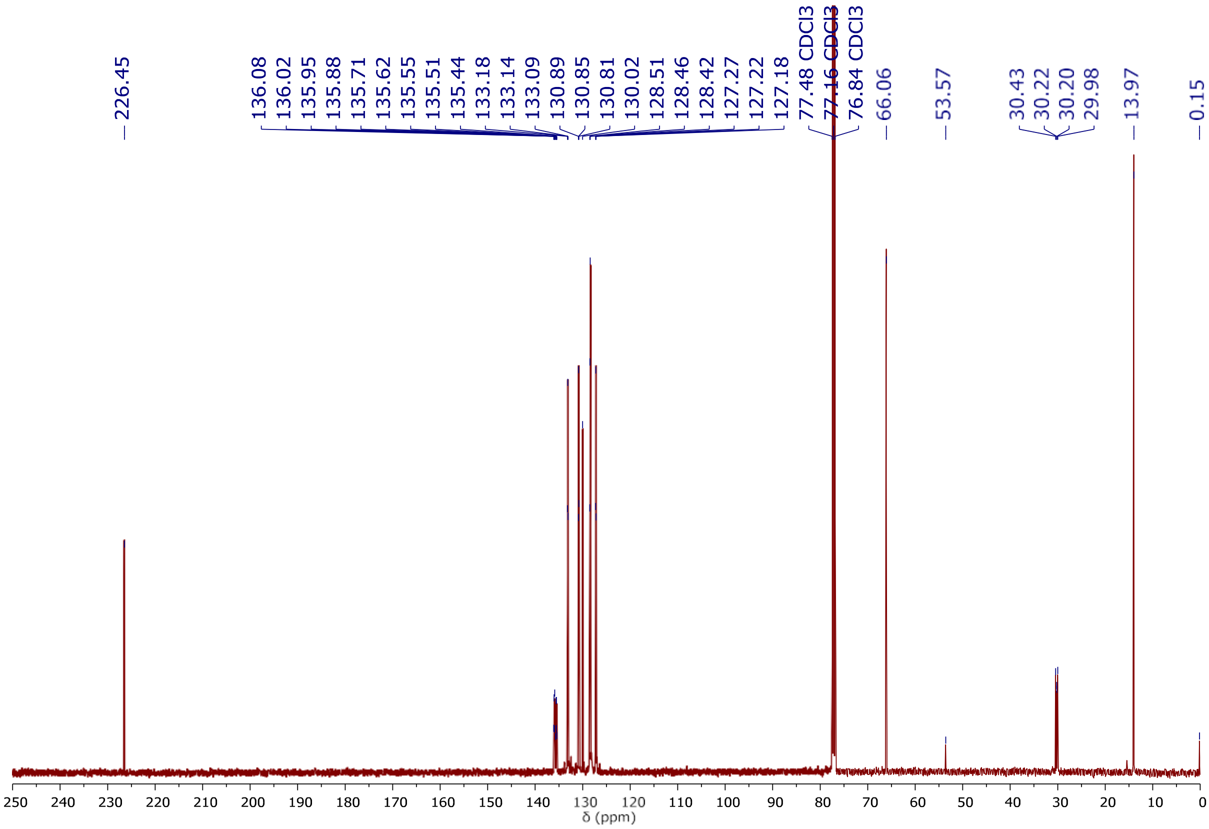

Fig. S9. $^{13}C\{^{1}H\}$ NMR spectrum (101 MHz, $CDCl_3$, 298 K) of $[Ru(S_2COEt)_2(dppe)]$ (**2**)

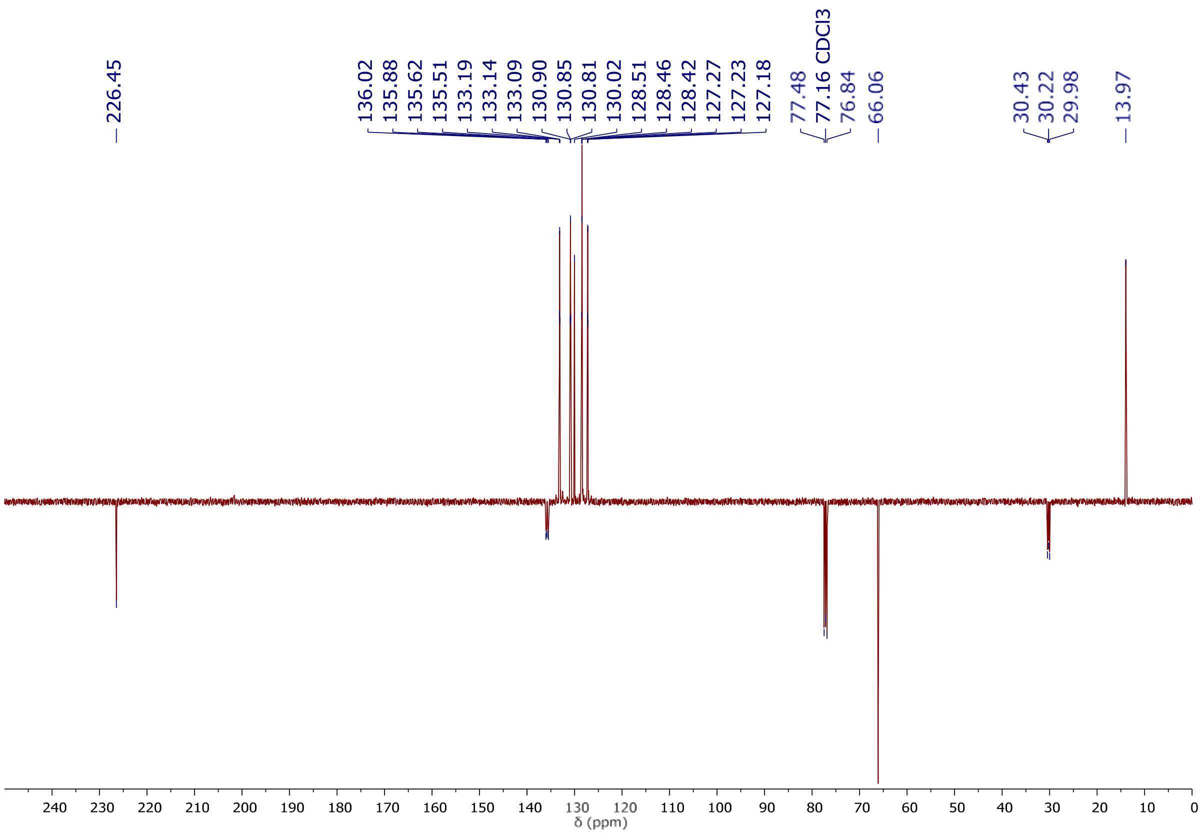

Fig. S10. $^{13}C\{^{1}H\}$ APT NMR spectrum (101 MHz, $CDCl_3$, 298 K) of $[Ru(S_2COEt)_2(dppe)]$ (**2**)

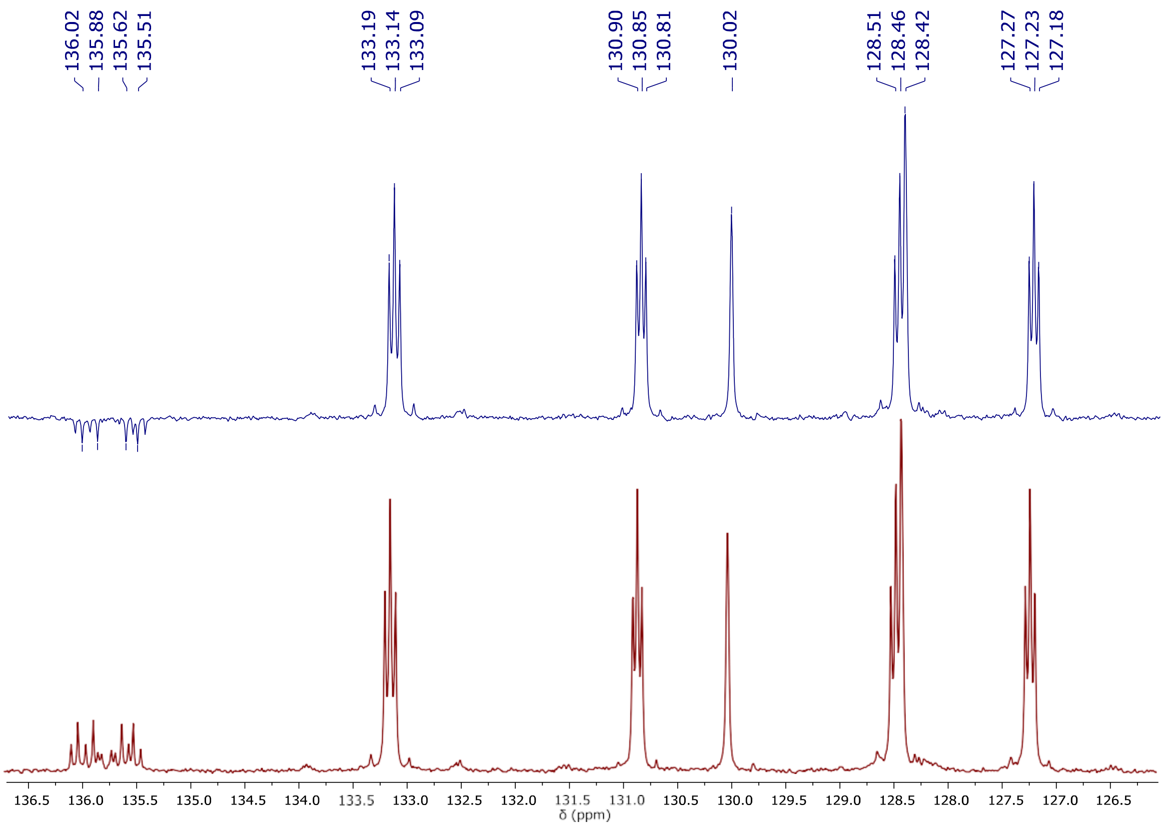

Fig. S11. ^{13}C CPD and APT NMR spectra (101 MHz, $CDCl_3$, 298 K) of $[Ru(S_2COEt)_2(dppe)]$ (**2**)

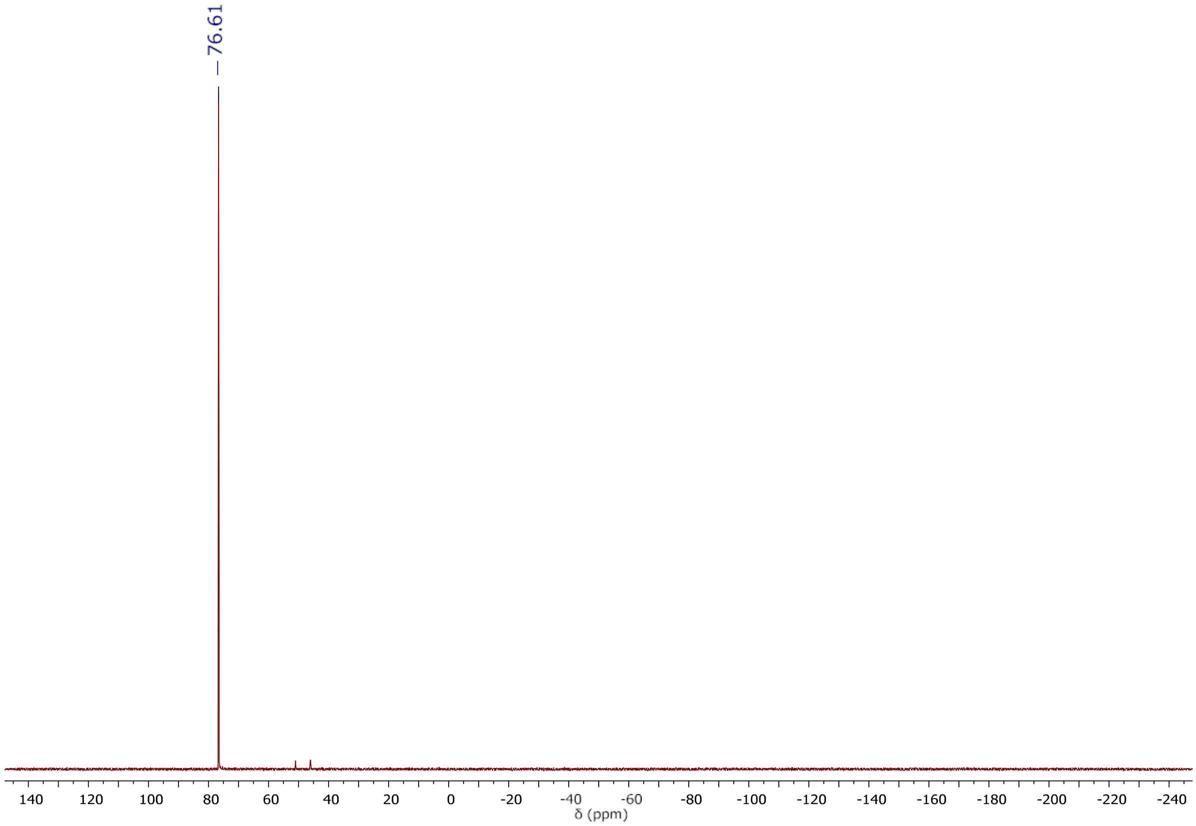

Fig. S12. ^{31}P NMR spectrum (162 MHz, $CDCl_3$, 298 K) of [Ru(S_2COEt)$_2$(dppe)] (**2**)

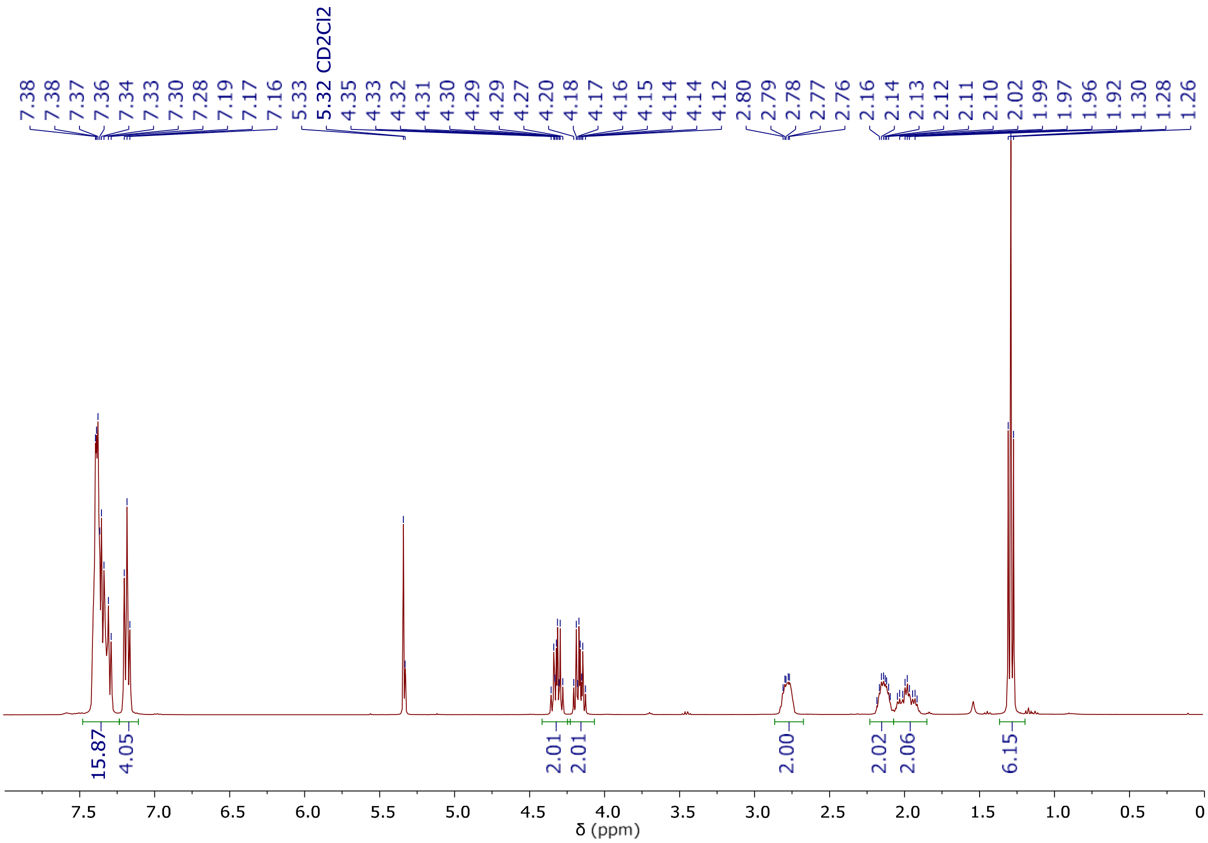

Fig. S13. ^{1}H NMR spectrum (400 MHz, CD_2Cl_2, 298 K) of [Ru(S_2COEt)$_2$(dppp)] (**3**)

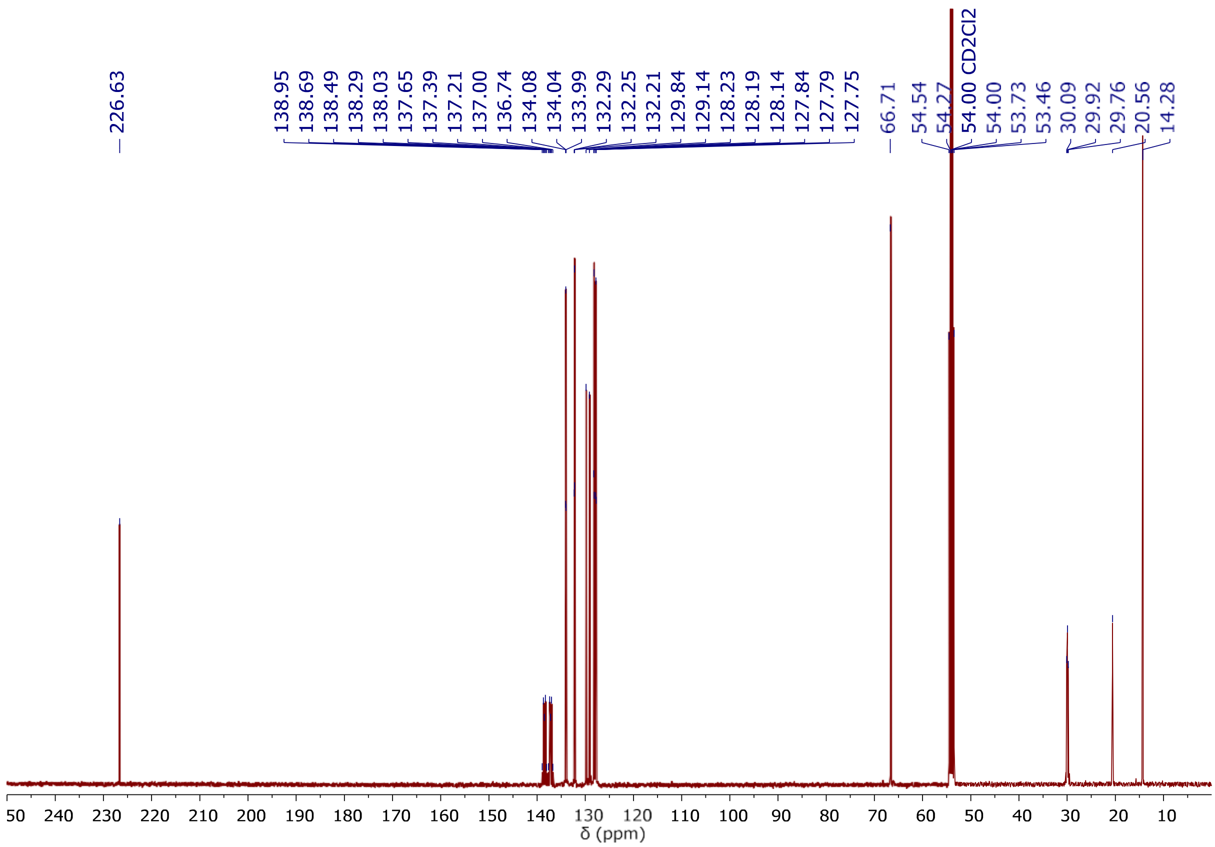

Fig. S14. $^{13}C\{^{1}H\}$ NMR spectrum (101 MHz, CD_2Cl_2, 298 K) of [Ru(S_2COEt)$_2$(dppp)] (**3**)

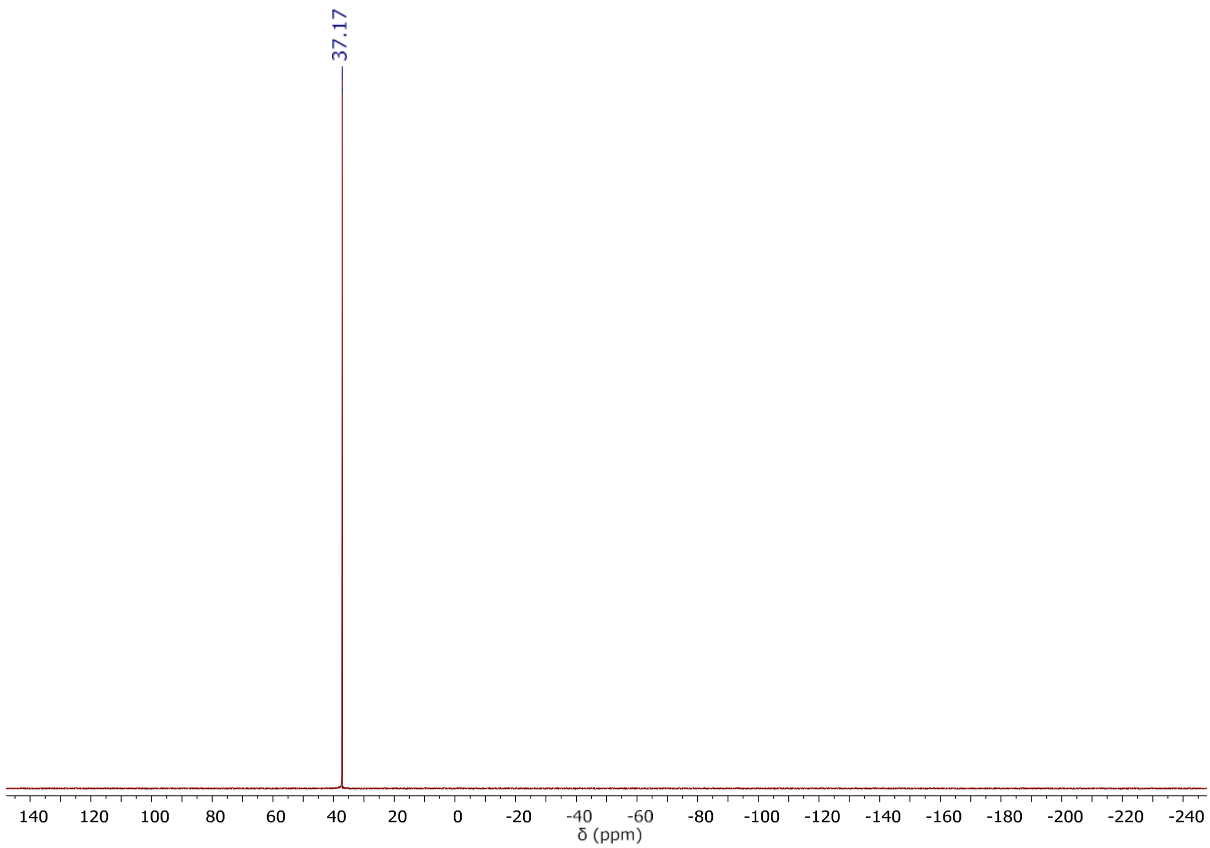

Fig. S15. ^{31}P NMR spectrum (162 MHz, CD_2Cl_2, 298 K) of [Ru(S_2COEt)$_2$(dppp)] (**3**)

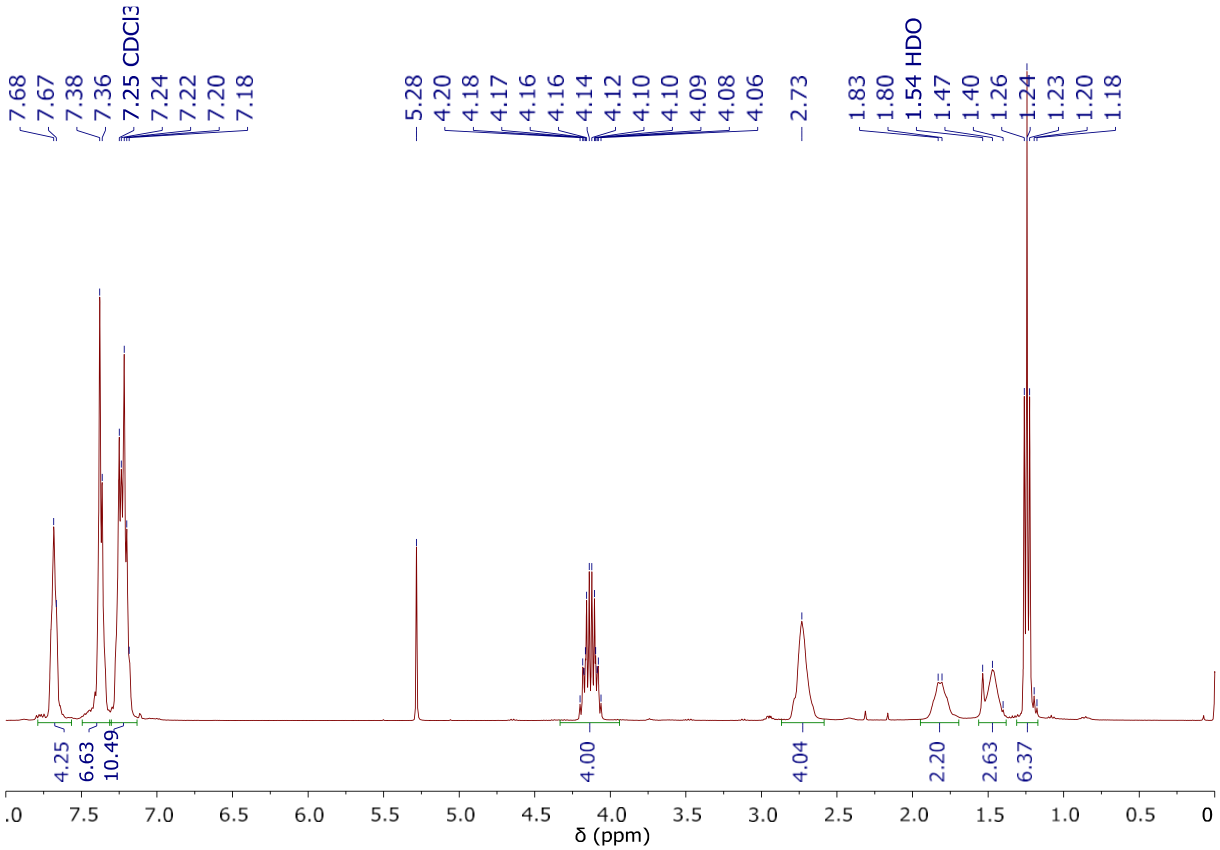

Fig. S16. ^{1}H NMR spectrum (400 MHz, $CDCl_3$, 298 K) of [Ru(S_2COEt)$_2$(dppb)] (**4**)

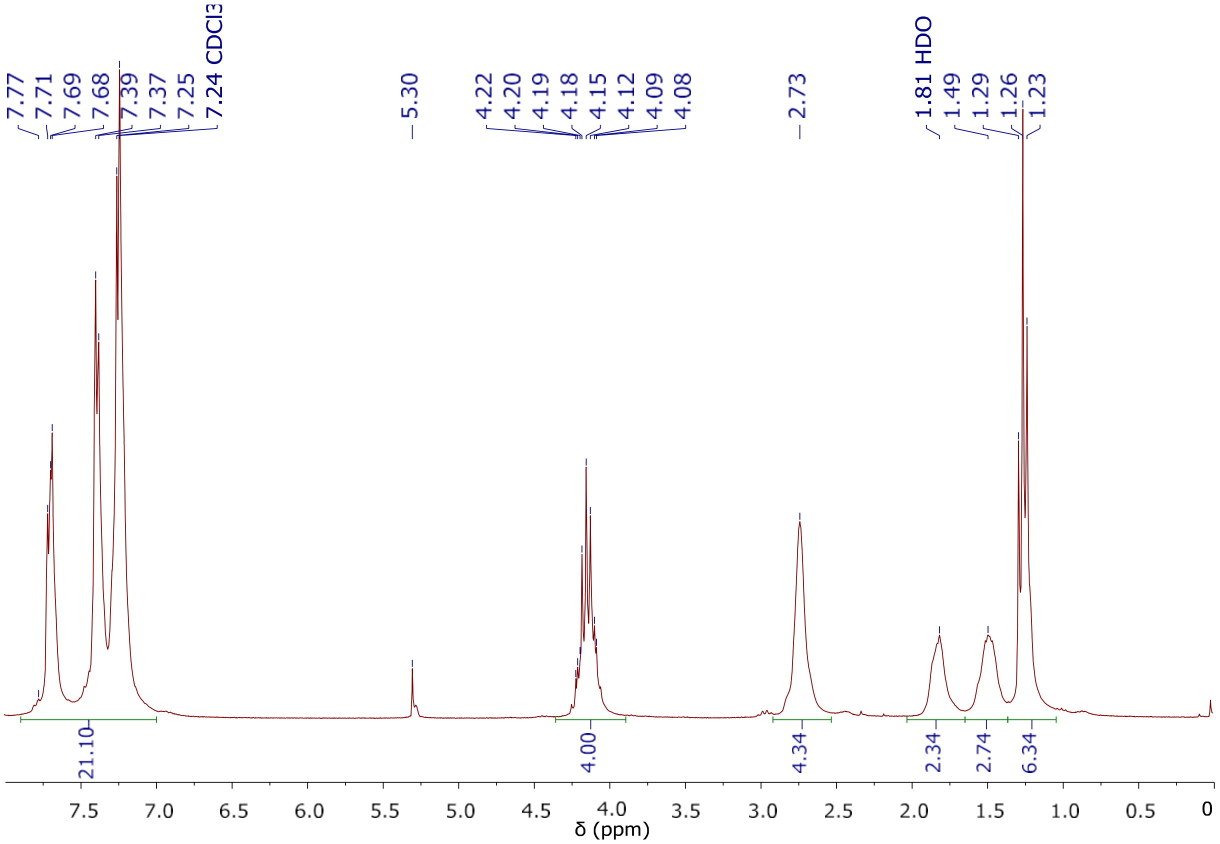

Fig. S17. ^{1}H{^{31}P} NMR spectrum (250 MHz, $CDCl_3$, 298 K) of [Ru(S_2COEt)$_2$(dppb)] (**4**)

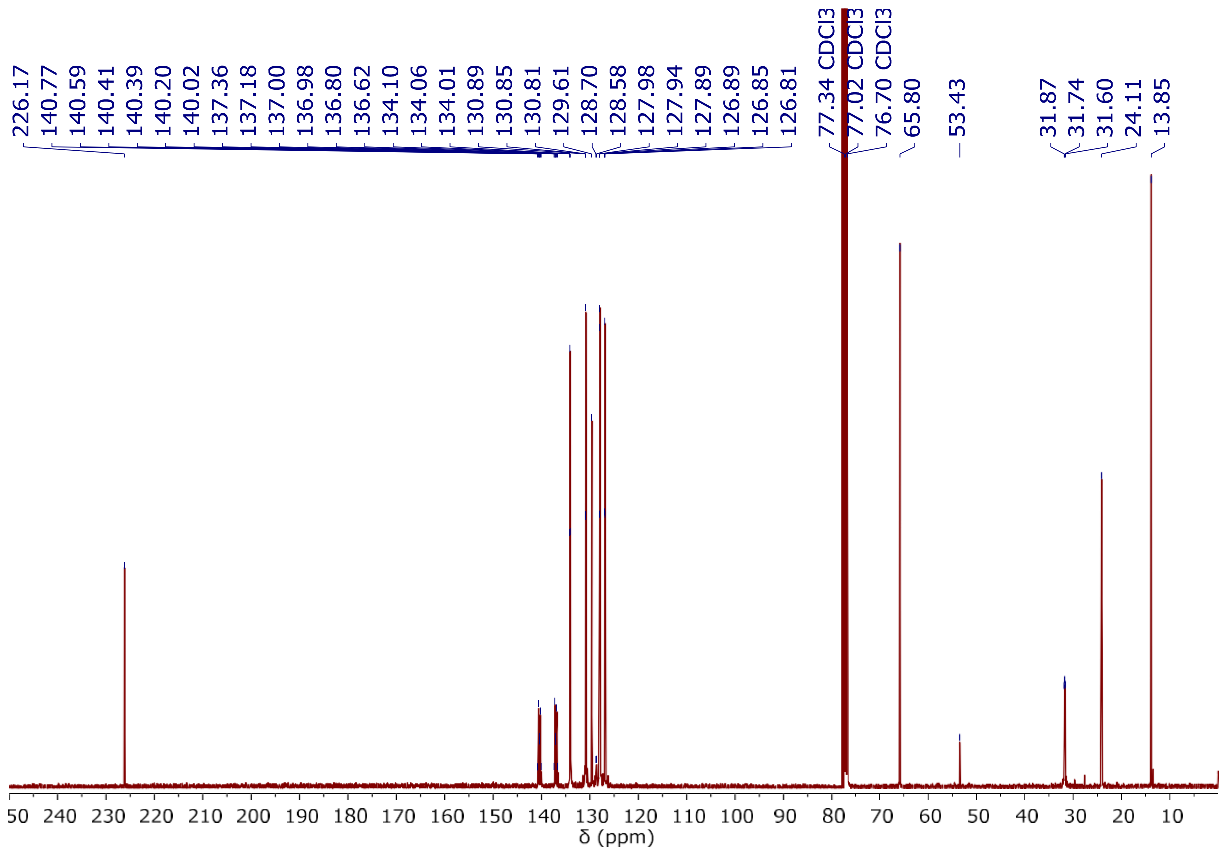

Fig. S18. $^{13}C\{^{1}H\}$ NMR spectrum (101 MHz, $CDCl_3$, 298 K) of $[Ru(S_2COEt)_2(dppb)]$ (**4**)

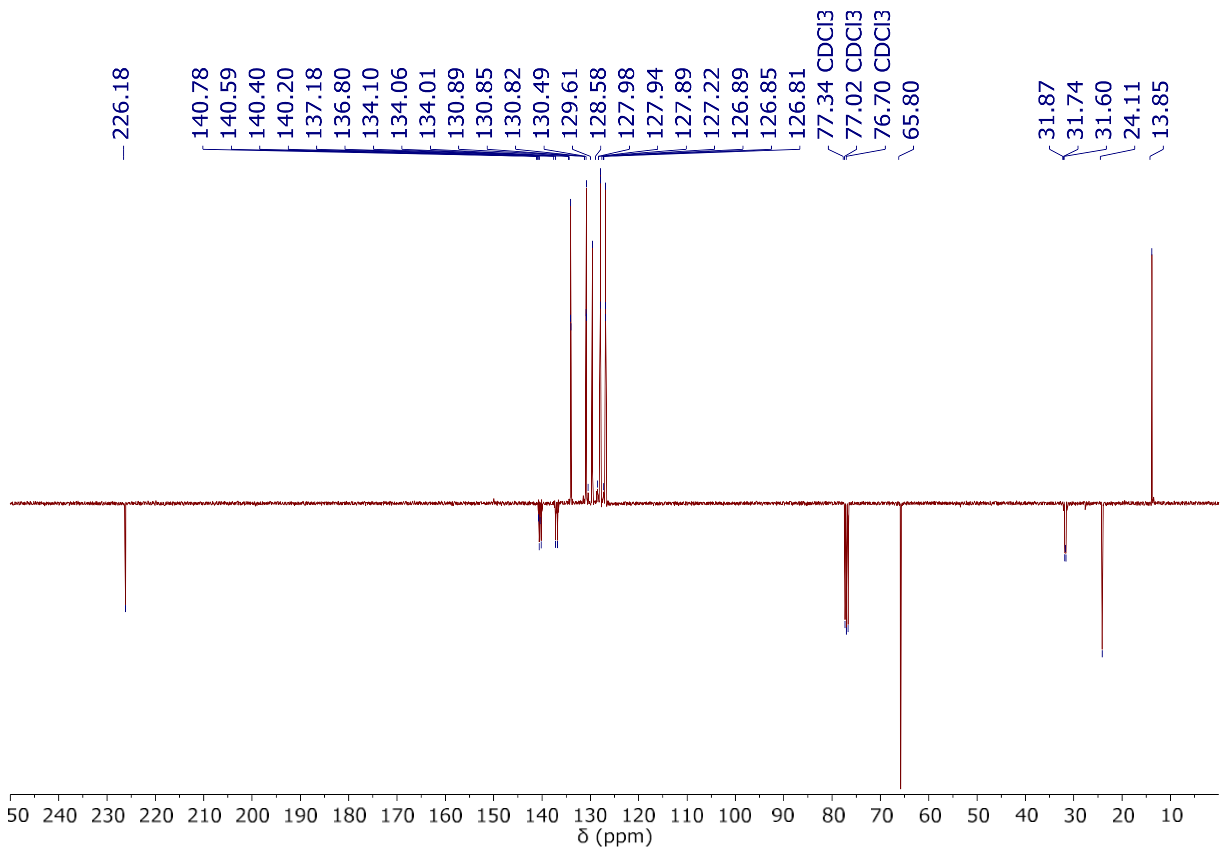

Fig. S19. $^{13}C\{^{1}H\}$ APT NMR spectrum (101 MHz, $CDCl_3$, 298 K) of $[Ru(S_2COEt)_2(dppb)]$ (**4**)

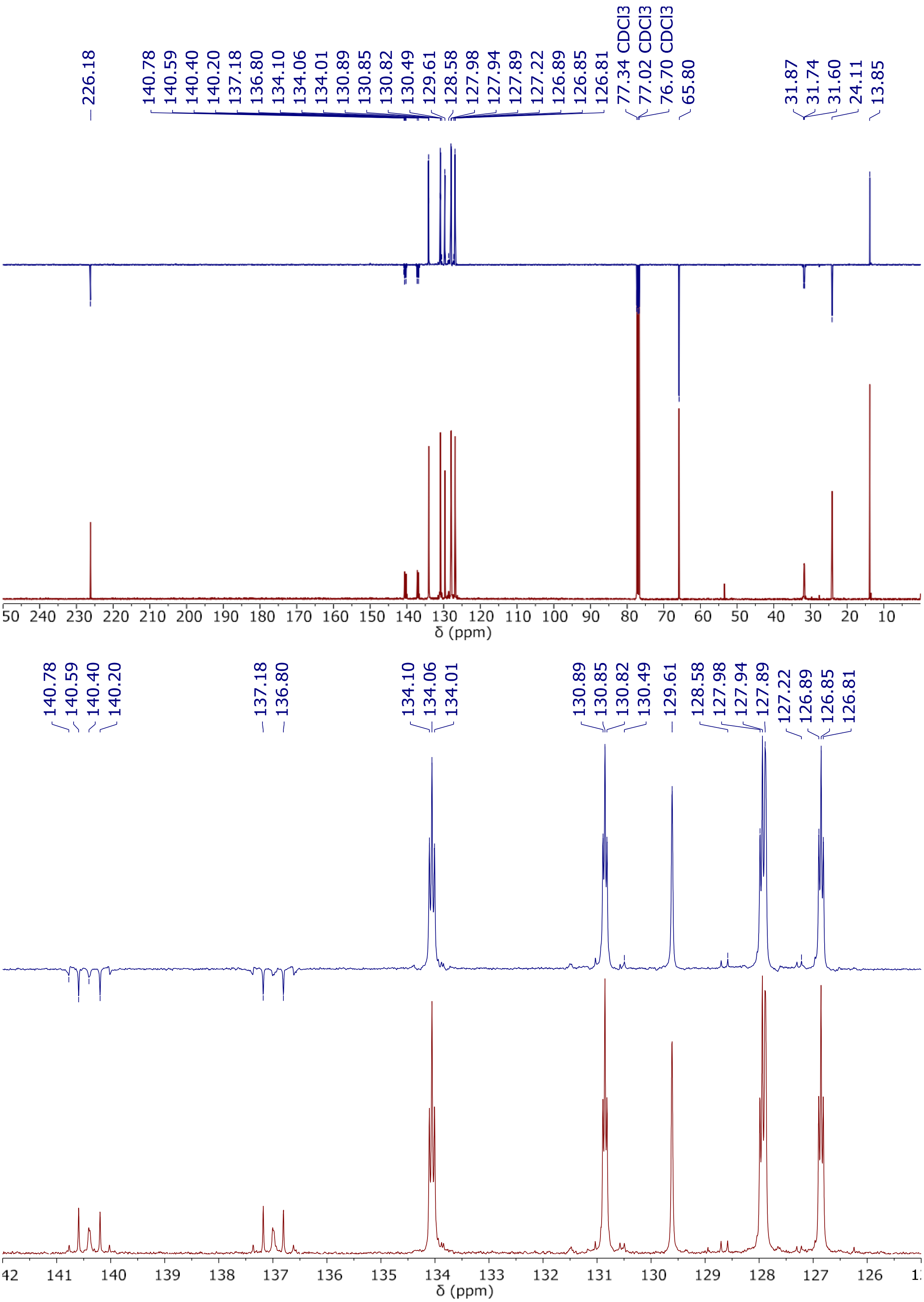

Fig. S20. ^{13}C CPD and APT NMR spectra (101 MHz, $CDCl_3$, 298 K) of [Ru(S_2COEt)$_2$(dppb)] (**4**)

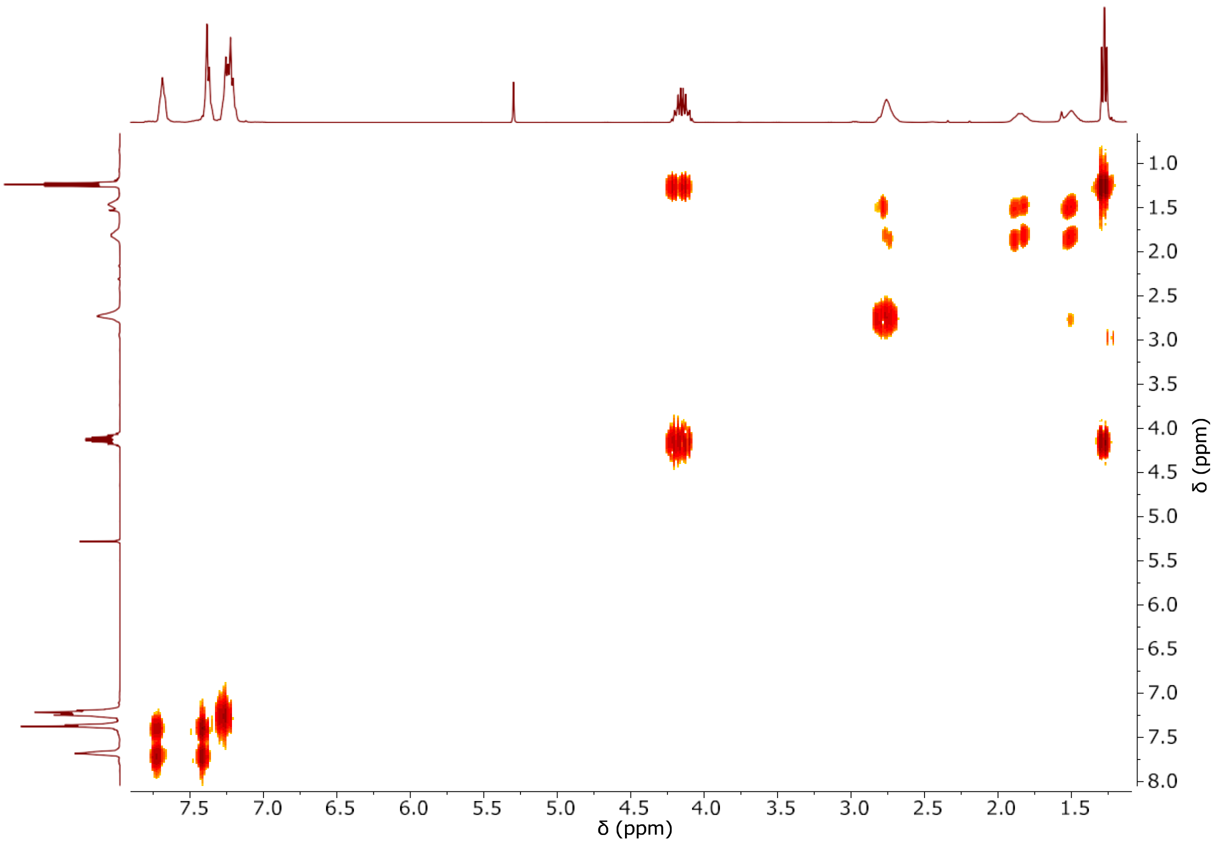

Fig. S21. COSY NMR spectrum (400 MHz, $CDCl_3$, 298 K) of [Ru(S_2COEt)$_2$(dppb)] (**4**)

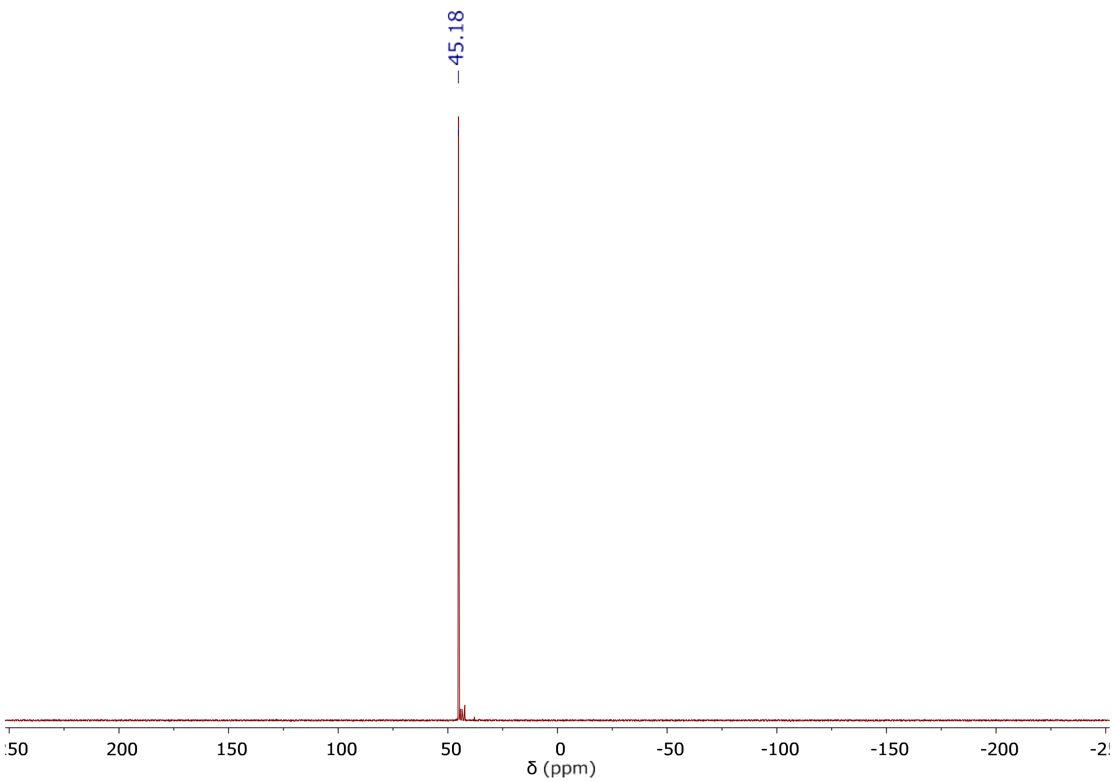

Fig. S22. ^{31}P NMR spectrum (162 MHz, $CDCl_3$, 298 K) of [Ru(S_2COEt)$_2$(dppb)] (**4**)

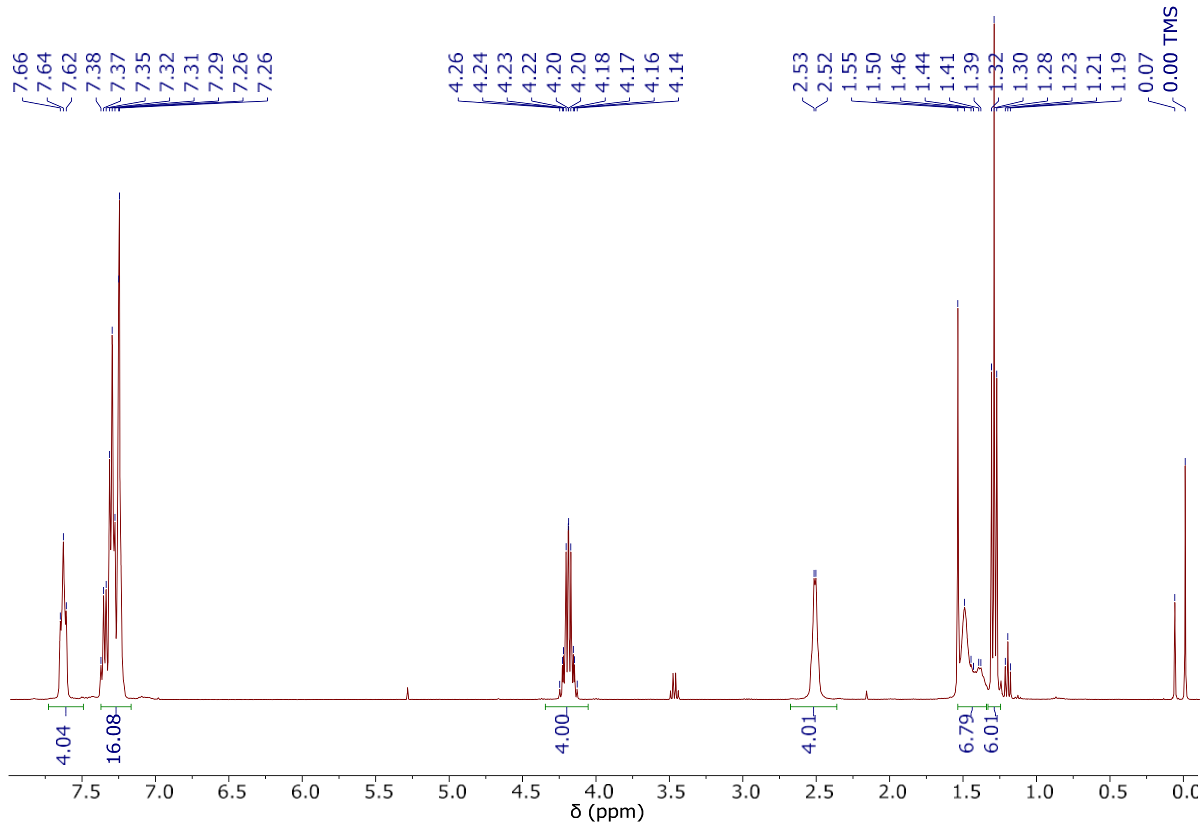

Fig. S23. ^{1}H NMR spectrum (400 MHz, $CDCl_3$, 298 K) of [Ru($S_2COEt)_2$(dpppe)] (**5**)

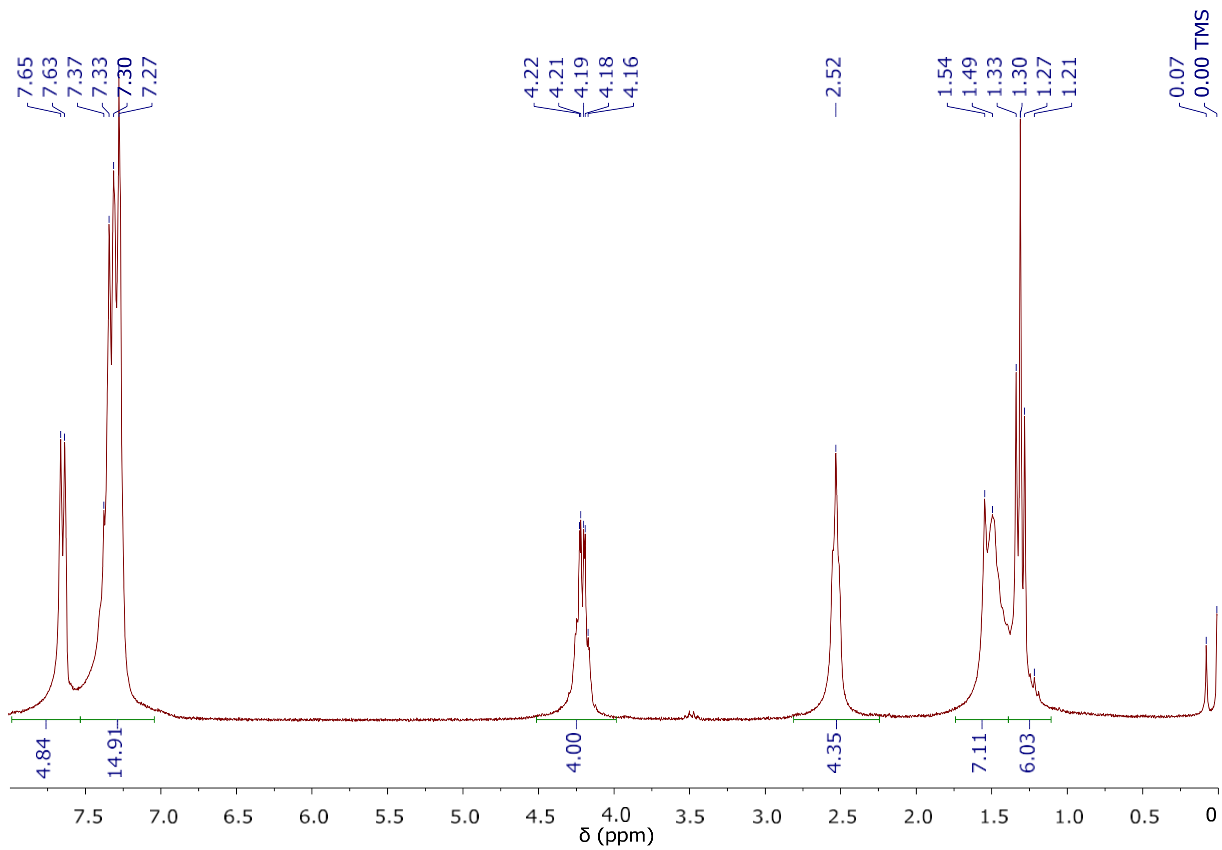

Fig. S24. $^{1}H\{^{31}P\}$ NMR spectrum (250 MHz, $CDCl_3$, 298 K) of [Ru($S_2COEt)_2$(dpppe)] (**5**)

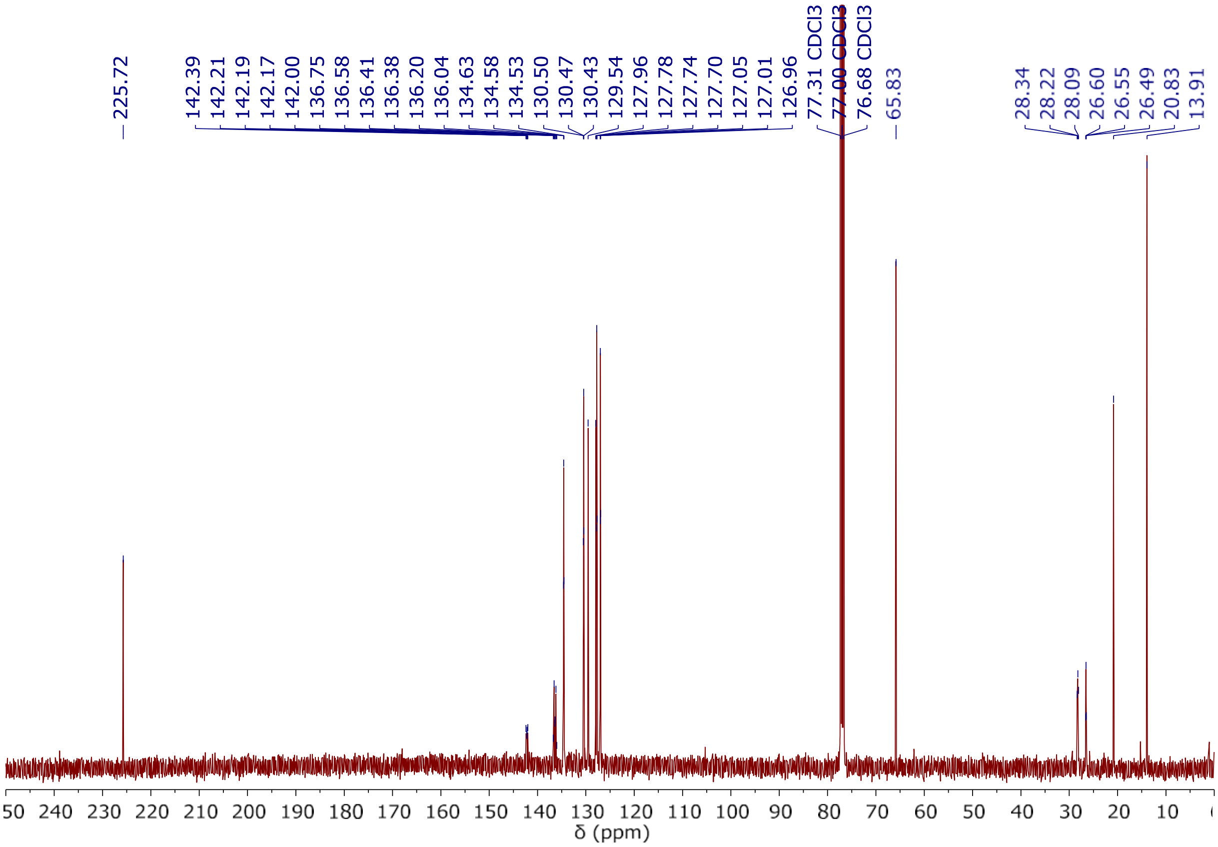

Fig. S25. $^{13}C\{^{1}H\}$ NMR spectrum (101 MHz, $CDCl_3$, 298 K) of [$Ru(S_2COEt)_2$(dpppe)] (**5**)

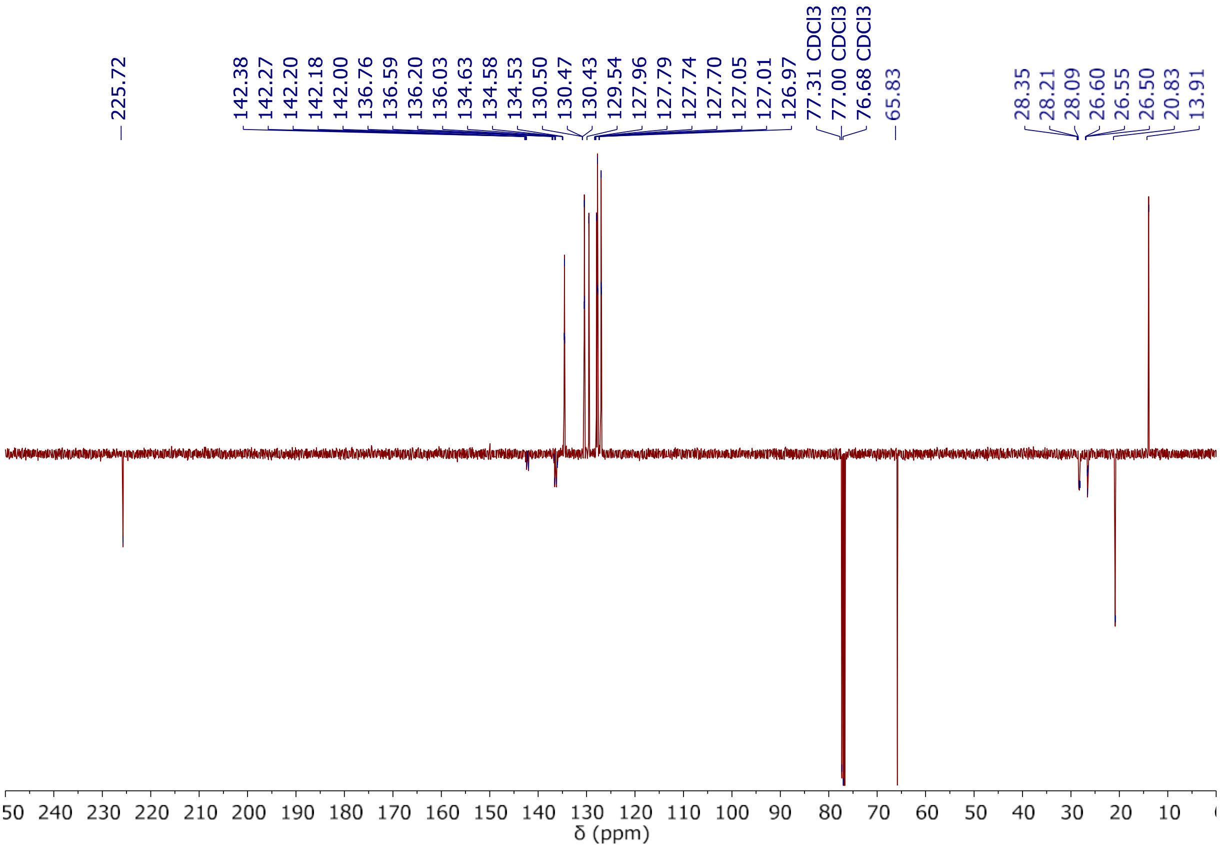

Fig. S26. $^{13}C\{^{1}H\}$ APT NMR spectrum (101 MHz, $CDCl_3$, 298 K) of [$Ru(S_2COEt)_2$(dpppe)] (**5**)

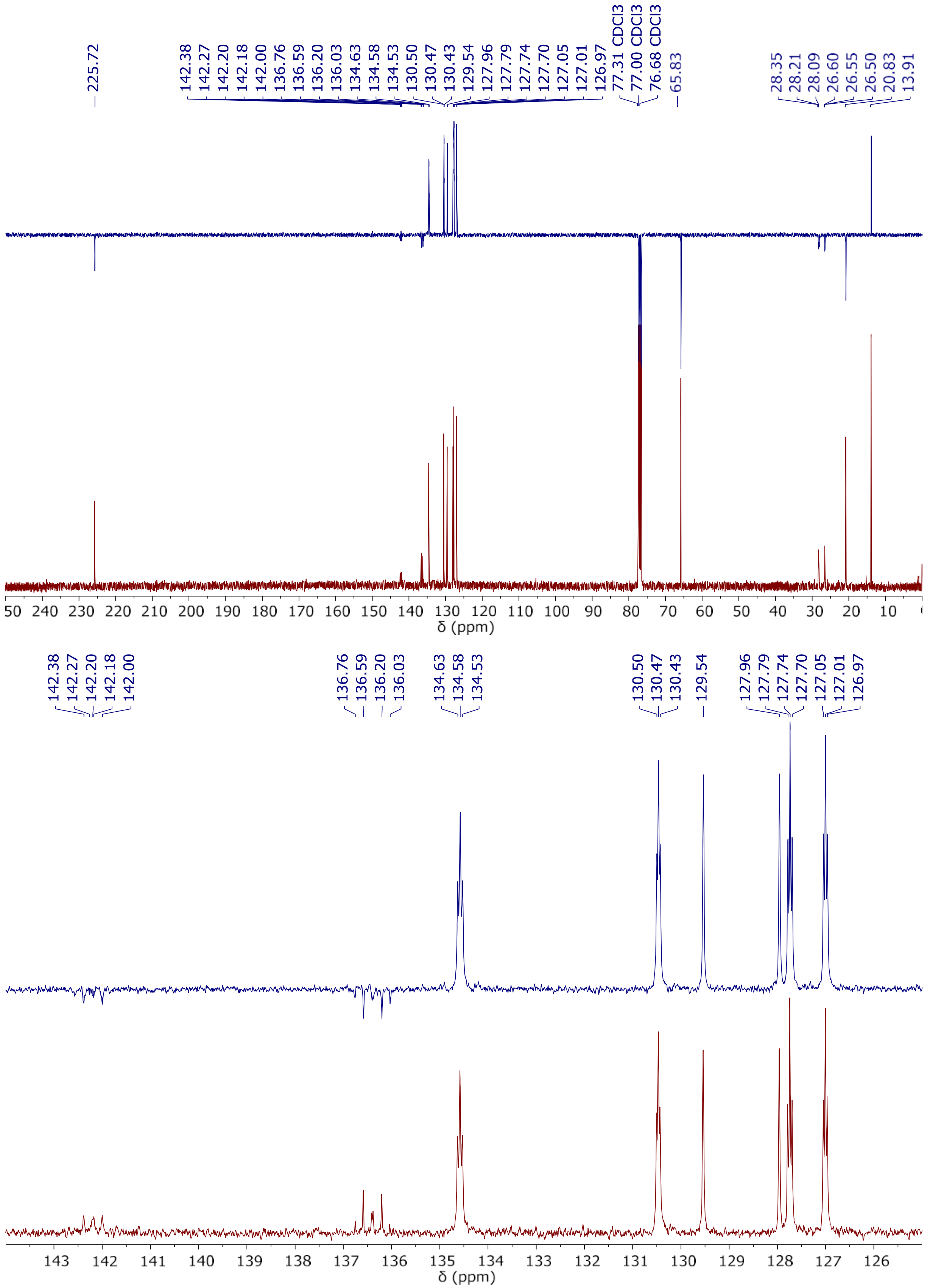

Fig. S27. ^{13}C CPD and APT NMR spectra (101 MHz, $CDCl_3$, 298 K) of [Ru(S_2COEt)$_2$(dpppe)] (**5**)

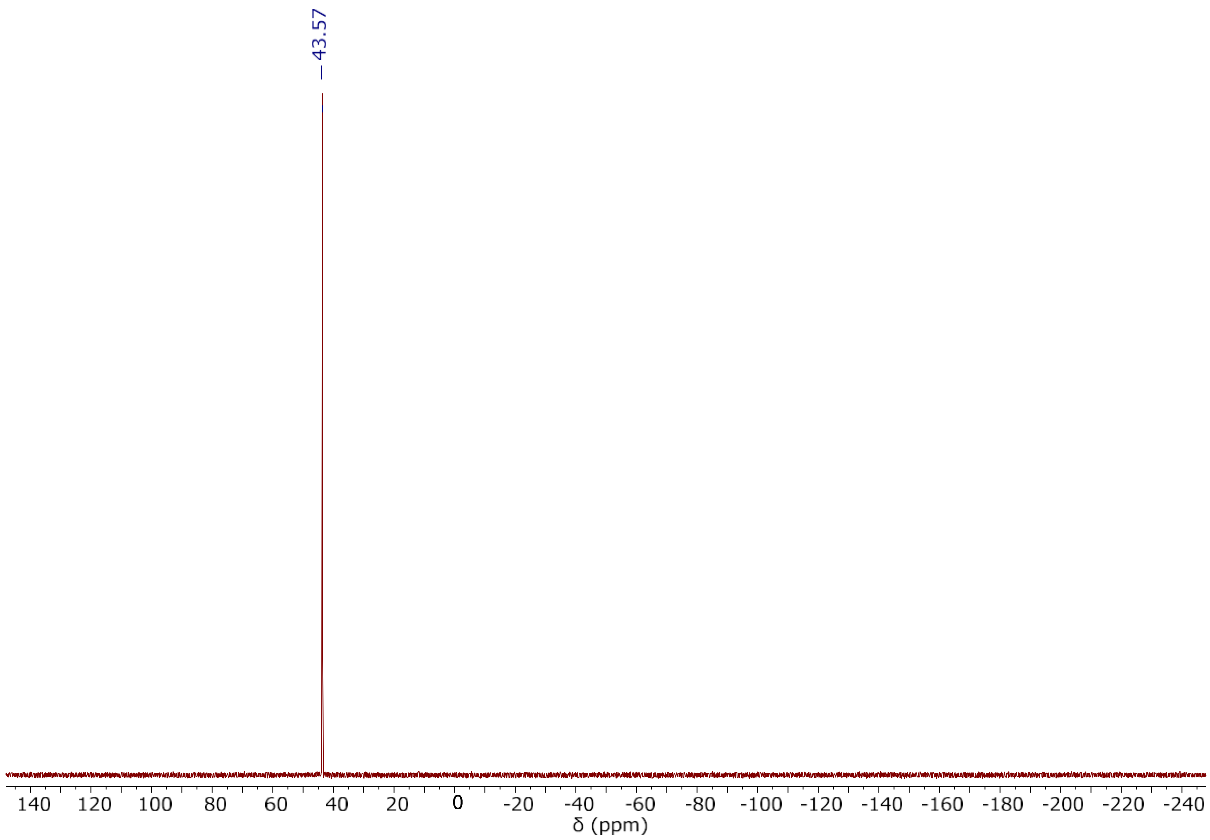

Fig. S28. ^{31}P NMR spectrum (162 MHz, $CDCl_3$, 298 K) of [Ru(S_2COEt)$_2$(dpppe)] (**5**)

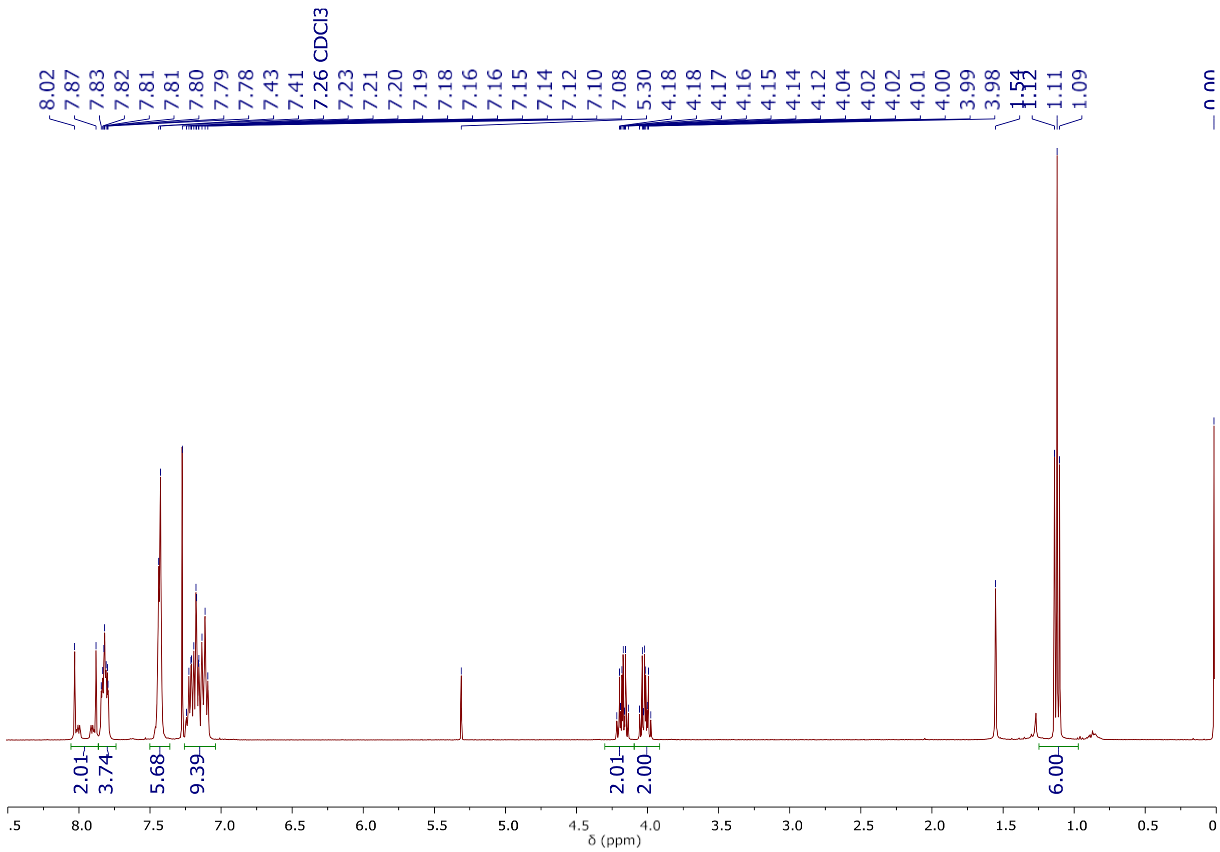

Fig. S29. ^{1}H NMR spectrum (400 MHz, $CDCl_3$, 298 K) of [Ru(S_2COEt)$_2$(dppen)] (**6**)

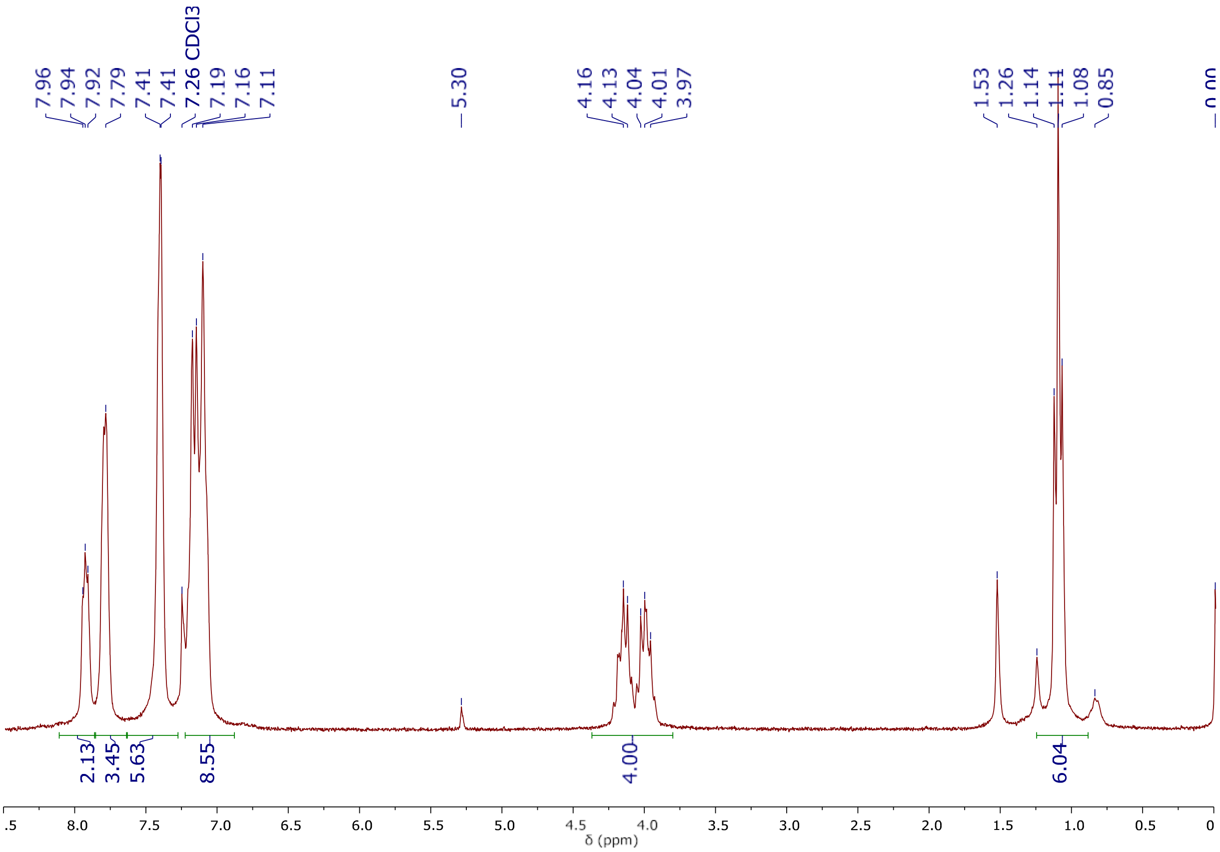

Fig. S30. $^{1}H\{^{31}P\}$ NMR spectrum (250 MHz, $CDCl_3$, 298 K) of [Ru(S_2COEt)$_2$(dppen)] (**6**)

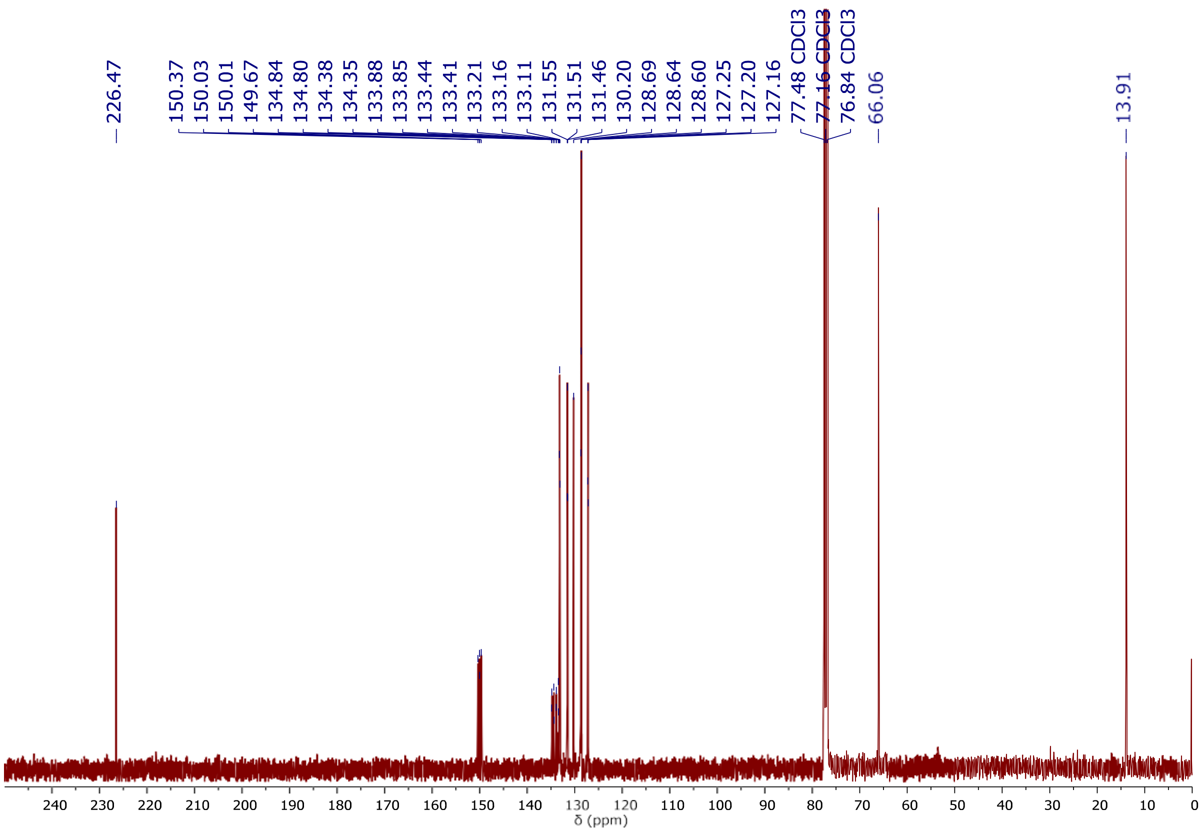

Fig. S31. $^{13}C\{^{1}H\}$ NMR spectrum (101 MHz, $CDCl_3$, 298 K) of [Ru(S_2COEt)$_2$(dppen)] (**6**)

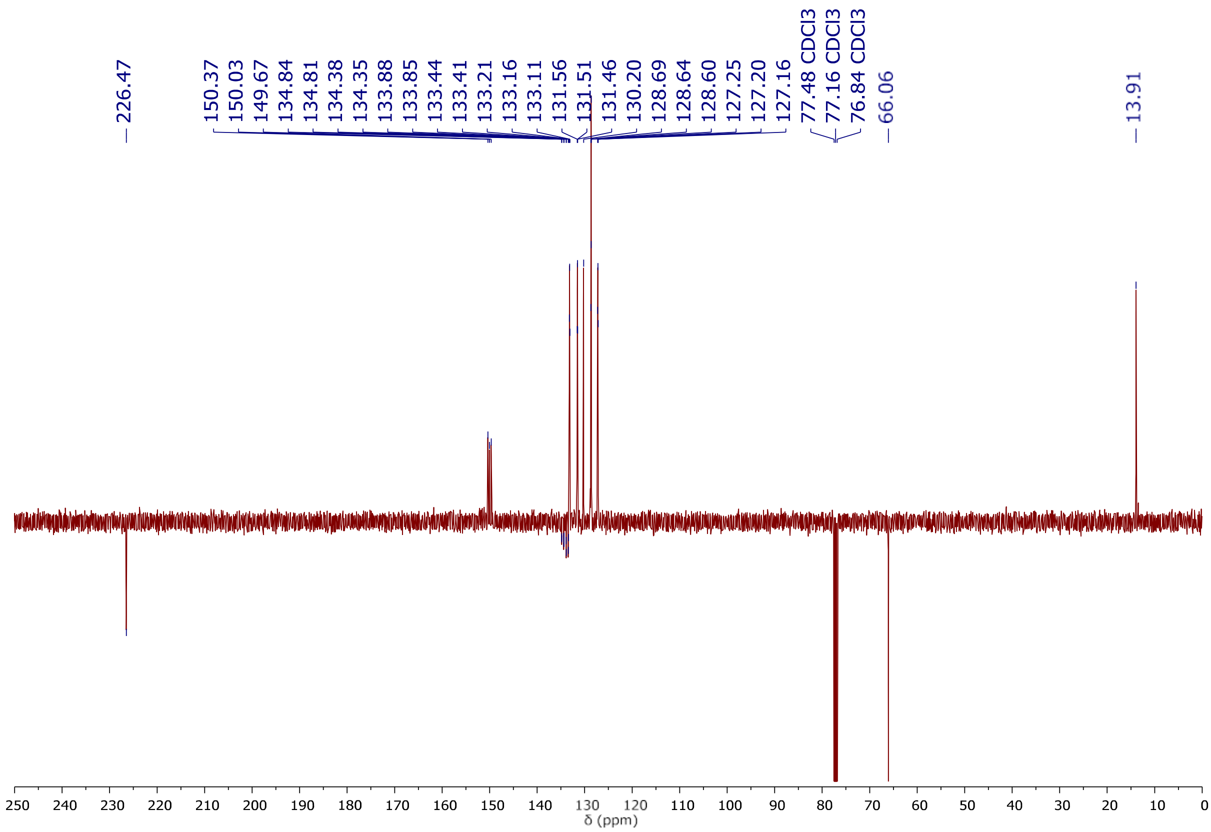

Fig. S32. $^{13}C\{^{1}H\}$ APT NMR spectrum (101 MHz, $CDCl_3$, 298 K) of $[Ru(S_2COEt)_2(dppen)]$ (**6**)

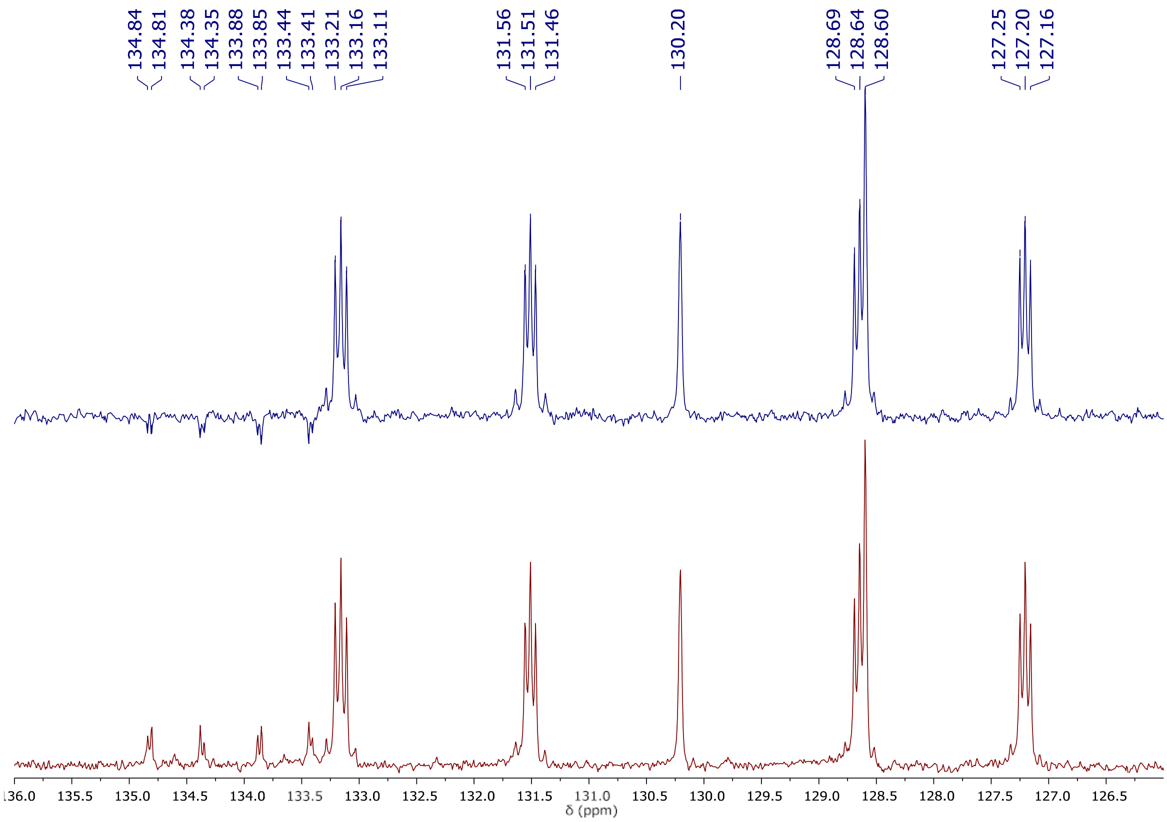

Fig. S33. ^{13}C CPD and APT NMR spectra (101 MHz, $CDCl_3$, 298 K) of $[Ru(S_2COEt)_2(dppen)]$ (**6**)

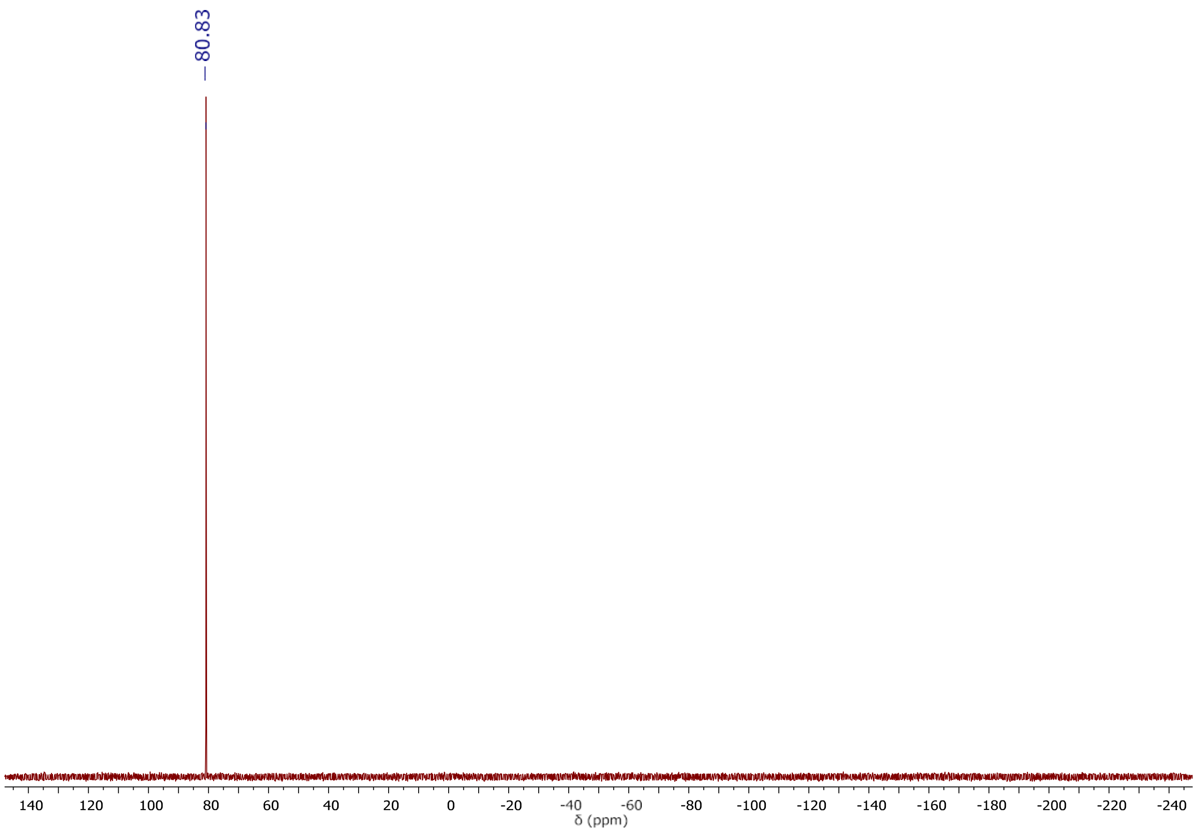

Fig. S34. [31]P NMR spectrum (162 MHz, $CDCl_3$, 298 K) of [Ru(S_2COEt)$_2$(dppen)] (**6**)

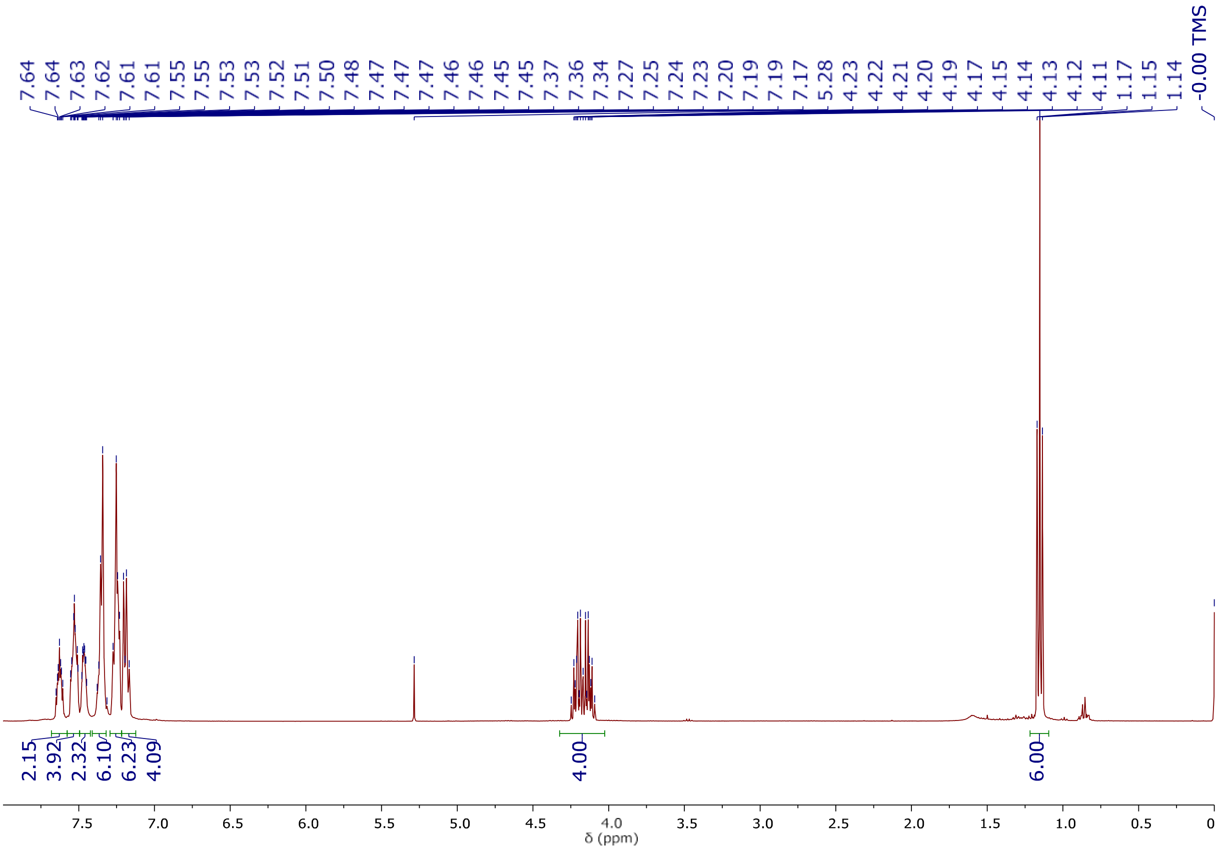

Fig. S35. [1]H NMR spectrum (400 MHz, $CDCl_3$, 298 K) of [Ru(S_2COEt)$_2$(dppbz)] (**7**)

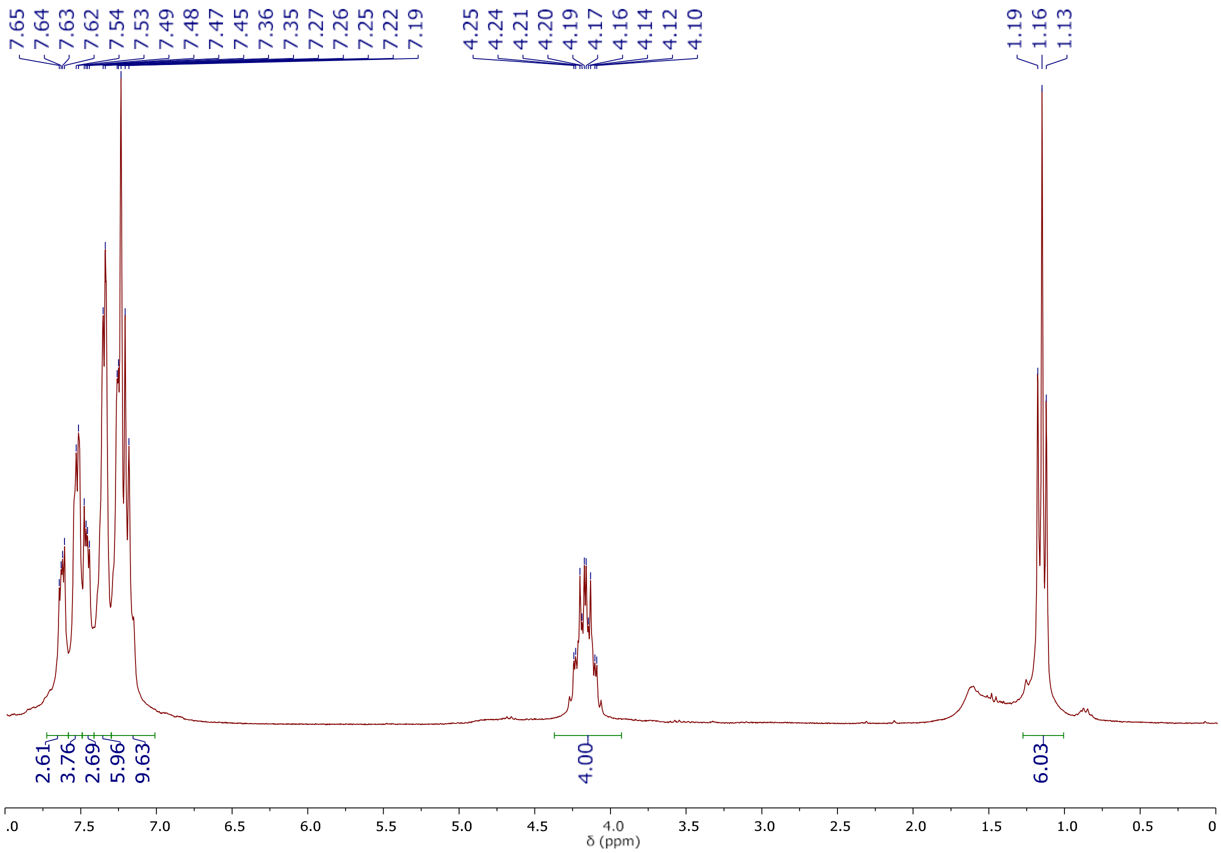

Fig. S36. $^{1}H\{^{31}P\}$ NMR spectrum (250 MHz, $CDCl_3$, 298 K) of $[Ru(S_2COEt)_2(dppbz)]$ (**7**)

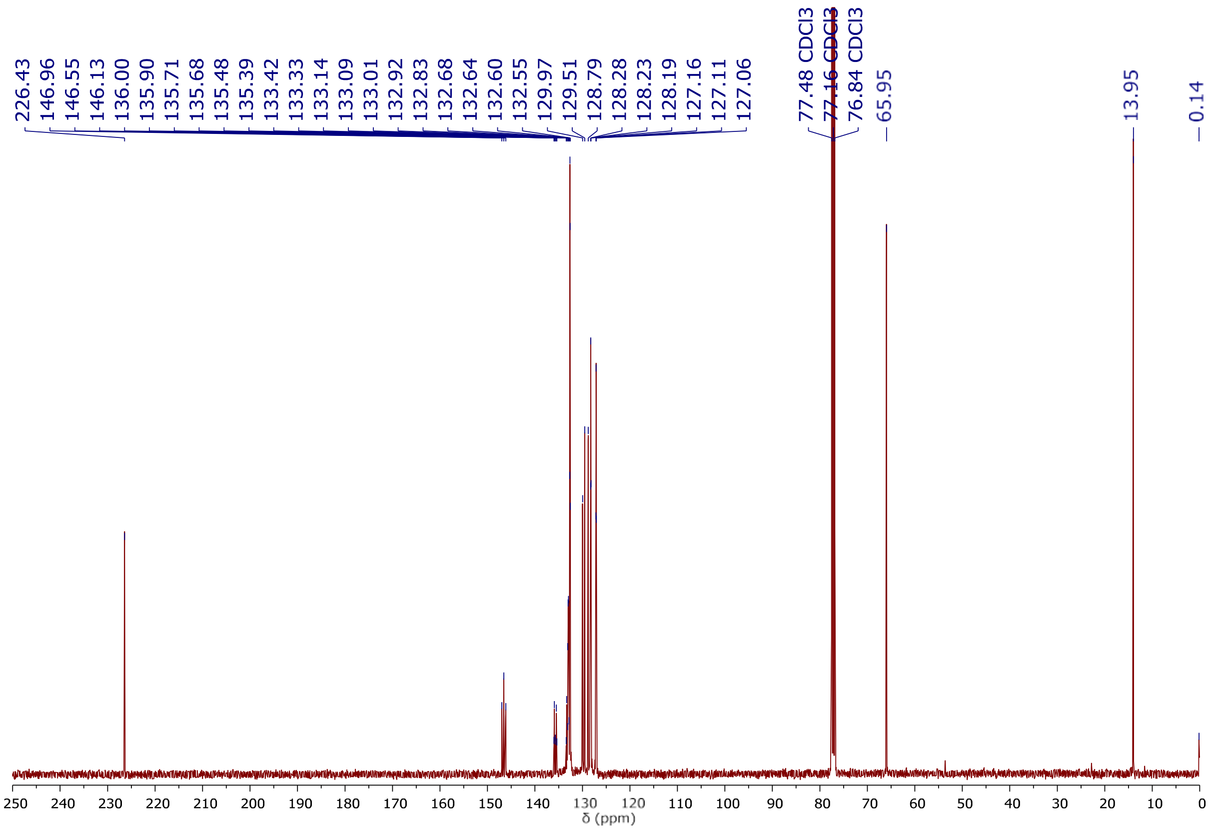

Fig. S37. $^{13}C\{^{1}H\}$ NMR spectrum (101 MHz, $CDCl_3$, 298 K) of $[Ru(S_2COEt)_2(dppbz)]$ (**7**)

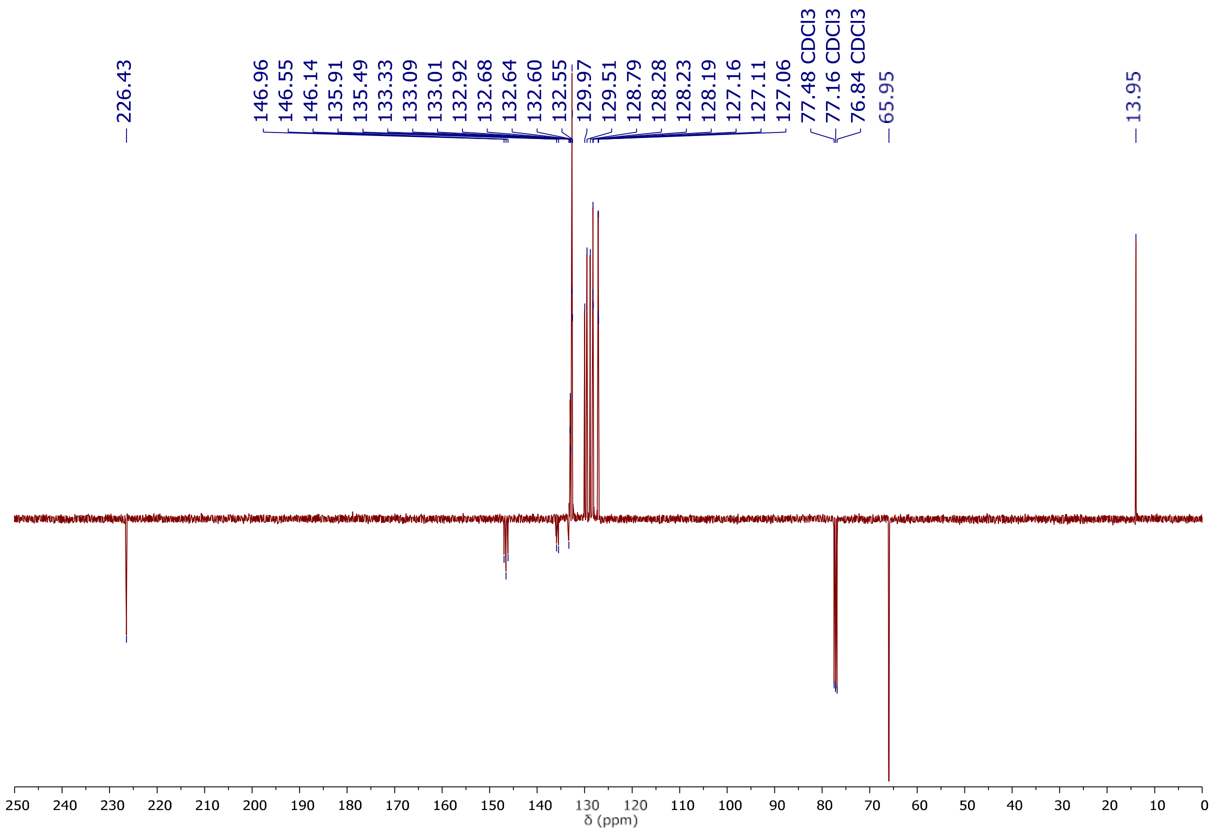

Fig. S38. $^{13}C\{^{1}H\}$ APT NMR spectrum (101 MHz, $CDCl_3$, 298 K) of $[Ru(S_2COEt)_2(dppbz)]$ (**7**)

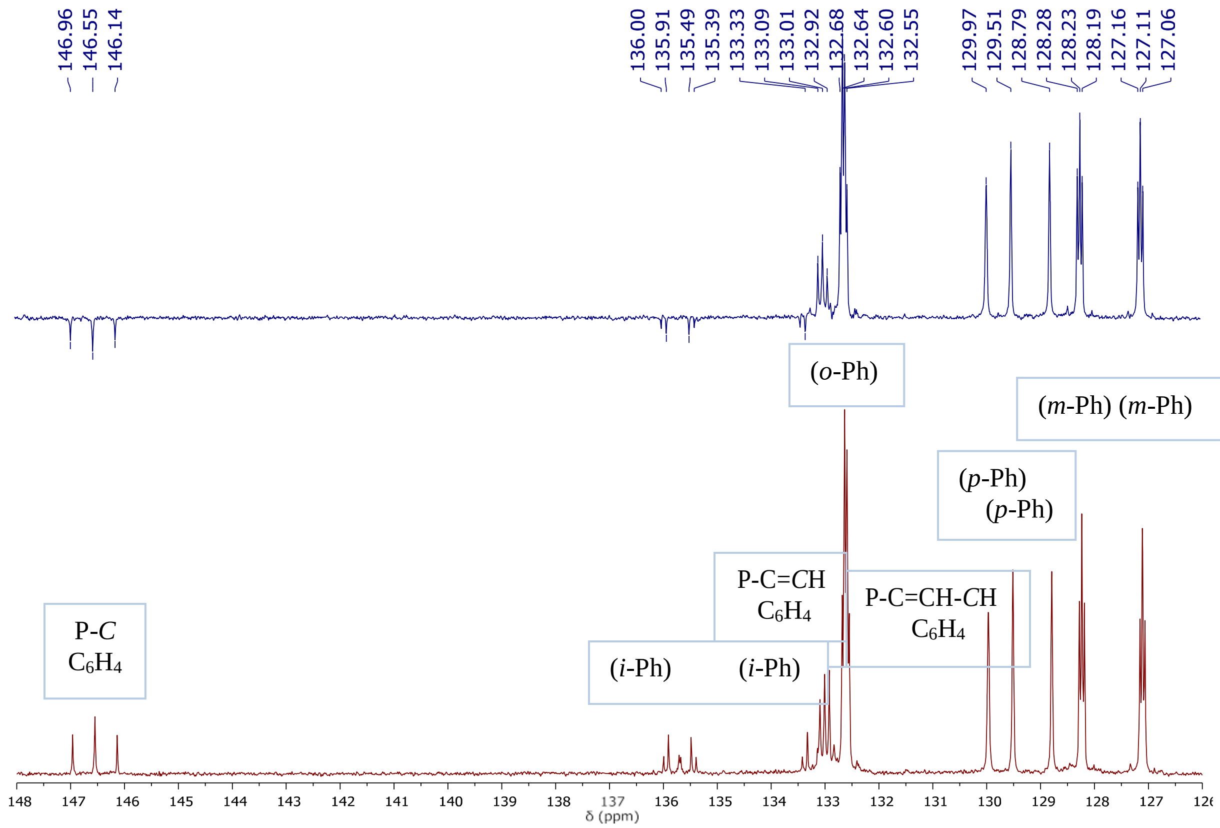

Fig. S39. ^{13}C CPD and APT NMR spectra (101 MHz, $CDCl_3$, 298 K) of $[Ru(S_2COEt)_2(dppbz)]$ (**7**)

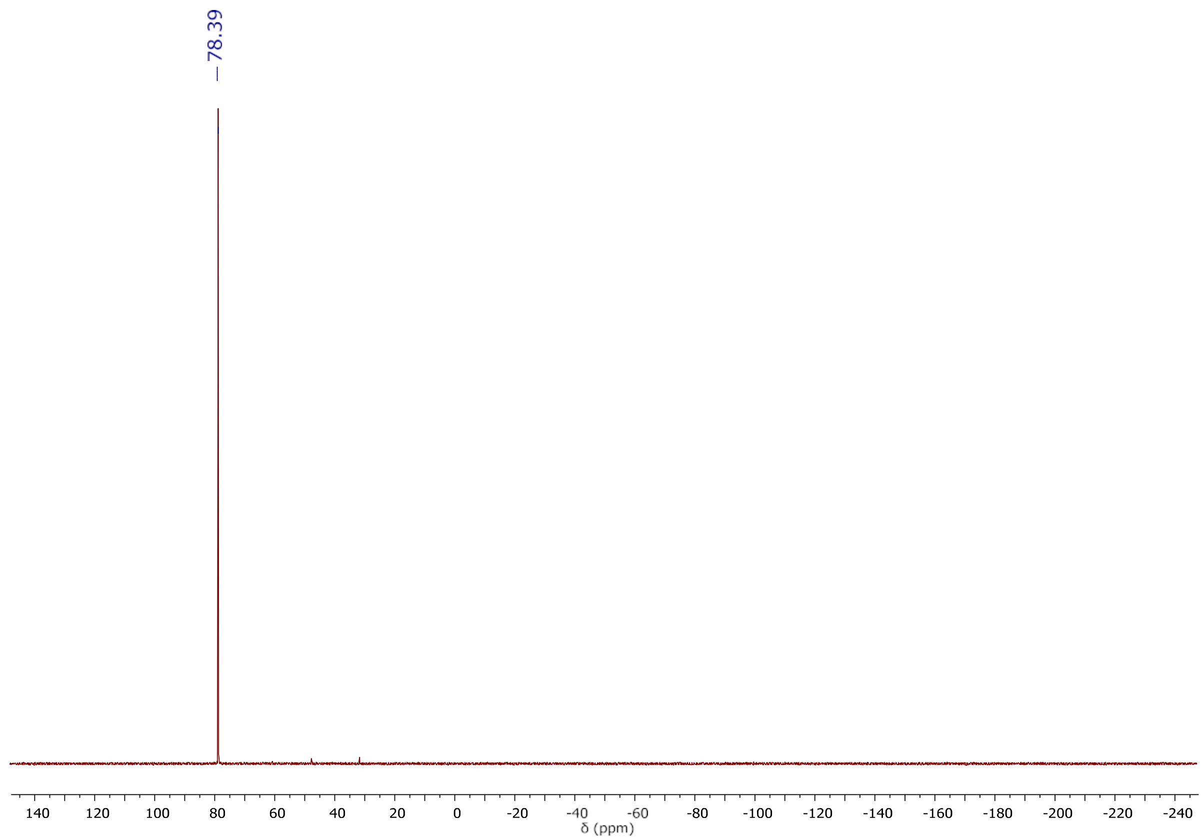

Fig. S40. ^{31}P NMR spectrum (162 MHz, $CDCl_3$, 298 K) of $[Ru(S_2COEt)_2(dppbz)]$ (**7**)

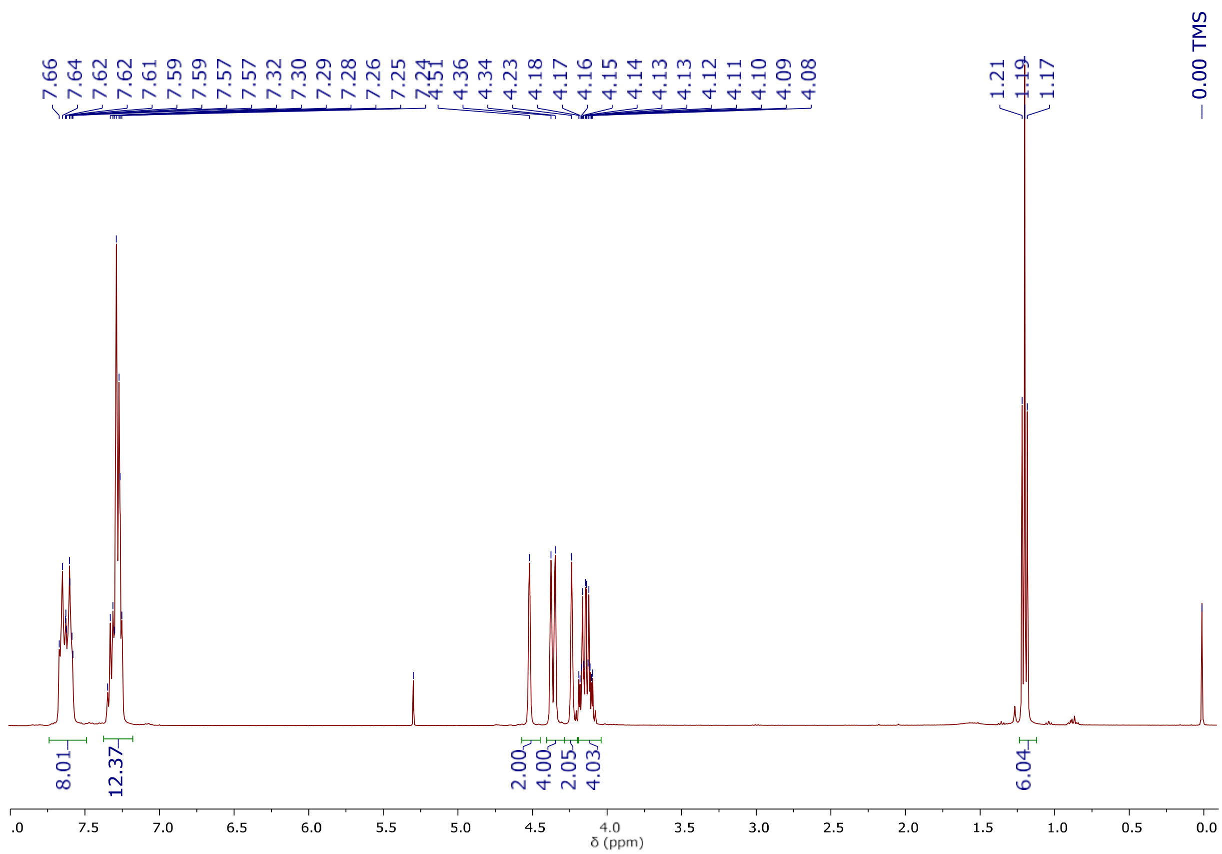

Fig. S41. ^{1}H NMR spectrum (400 MHz, $CDCl_3$, 298 K) of $[Ru(S_2COEt)_2(dppf)]$ (**8**)

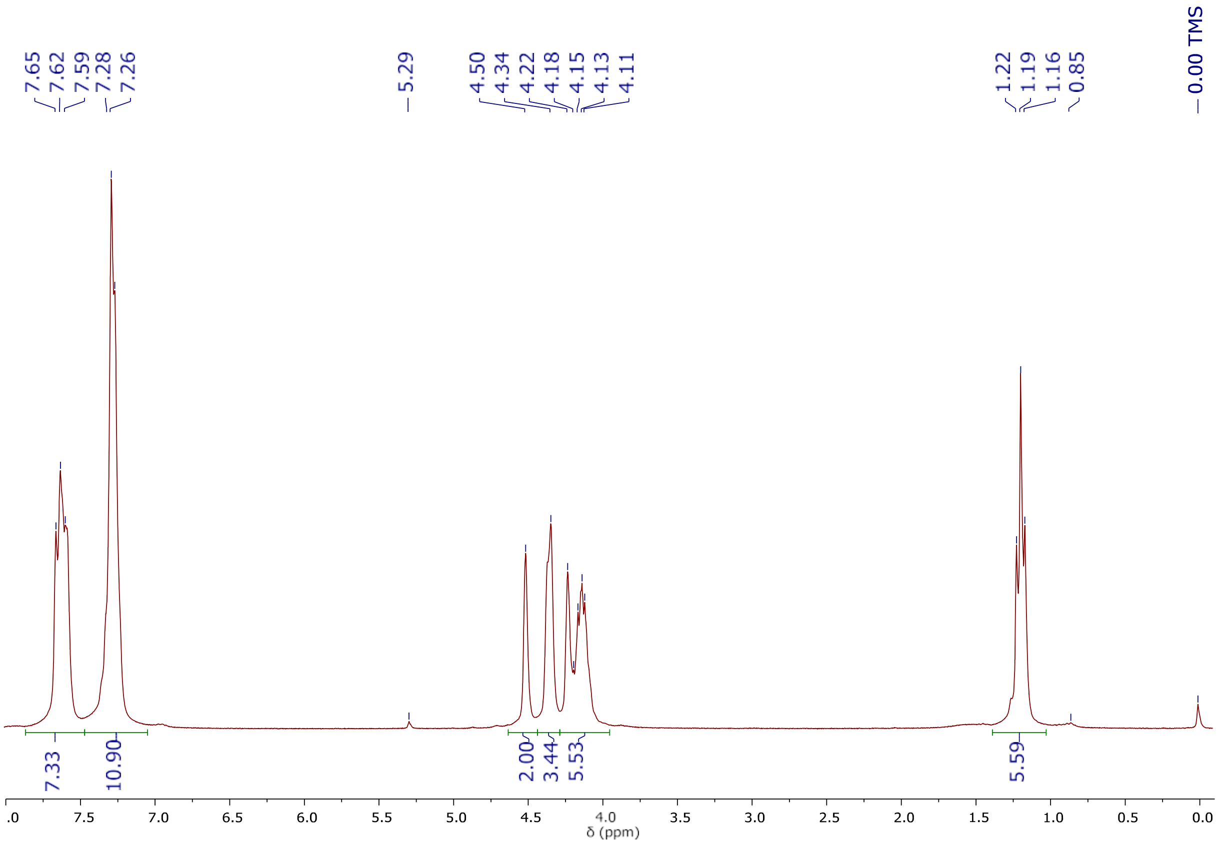

Fig. S42. $^{1}H\{^{31}P\}$ NMR spectrum (250 MHz, $CDCl_3$, 298 K) of $[Ru(S_2COEt)_2(dppf)]$ (**8**)

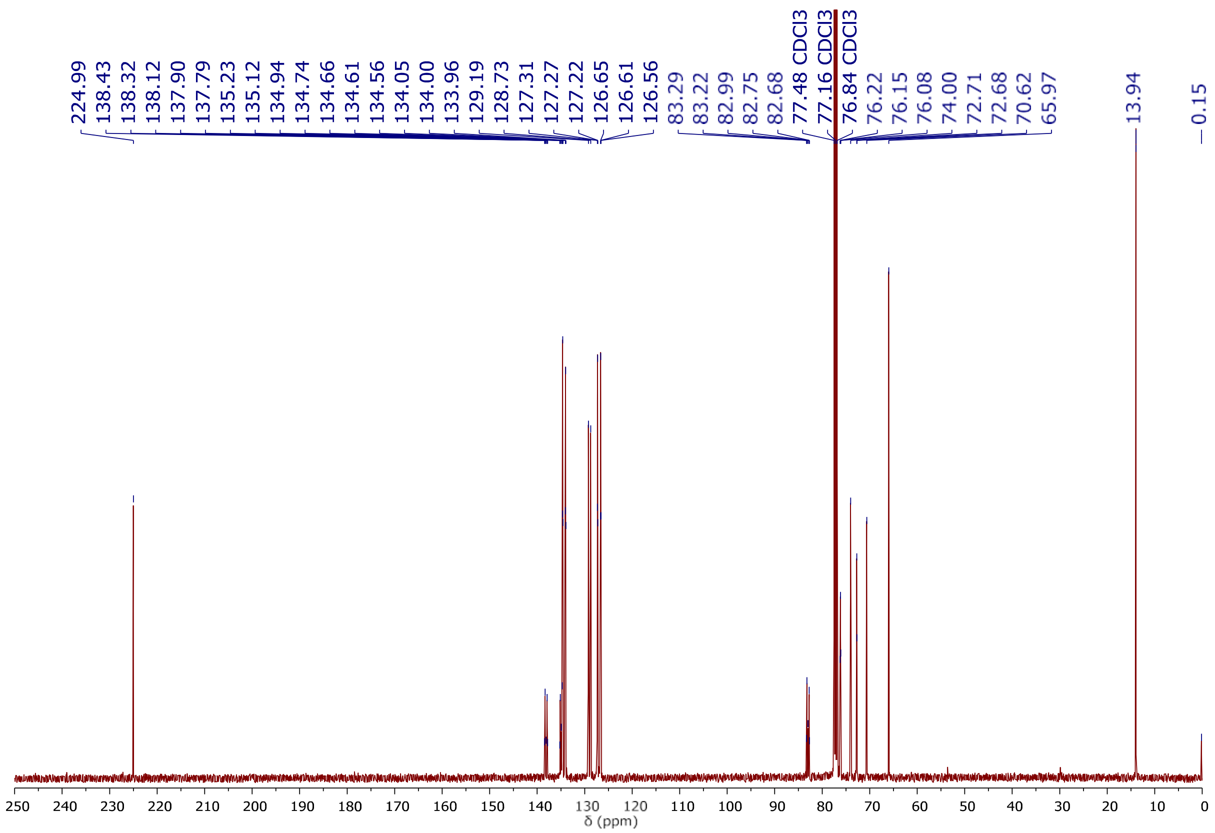

Fig. S43. $^{13}C\{^{1}H\}$ NMR spectrum (101 MHz, $CDCl_3$, 298 K) of $[Ru(S_2COEt)_2(dppf)]$ (**8**)

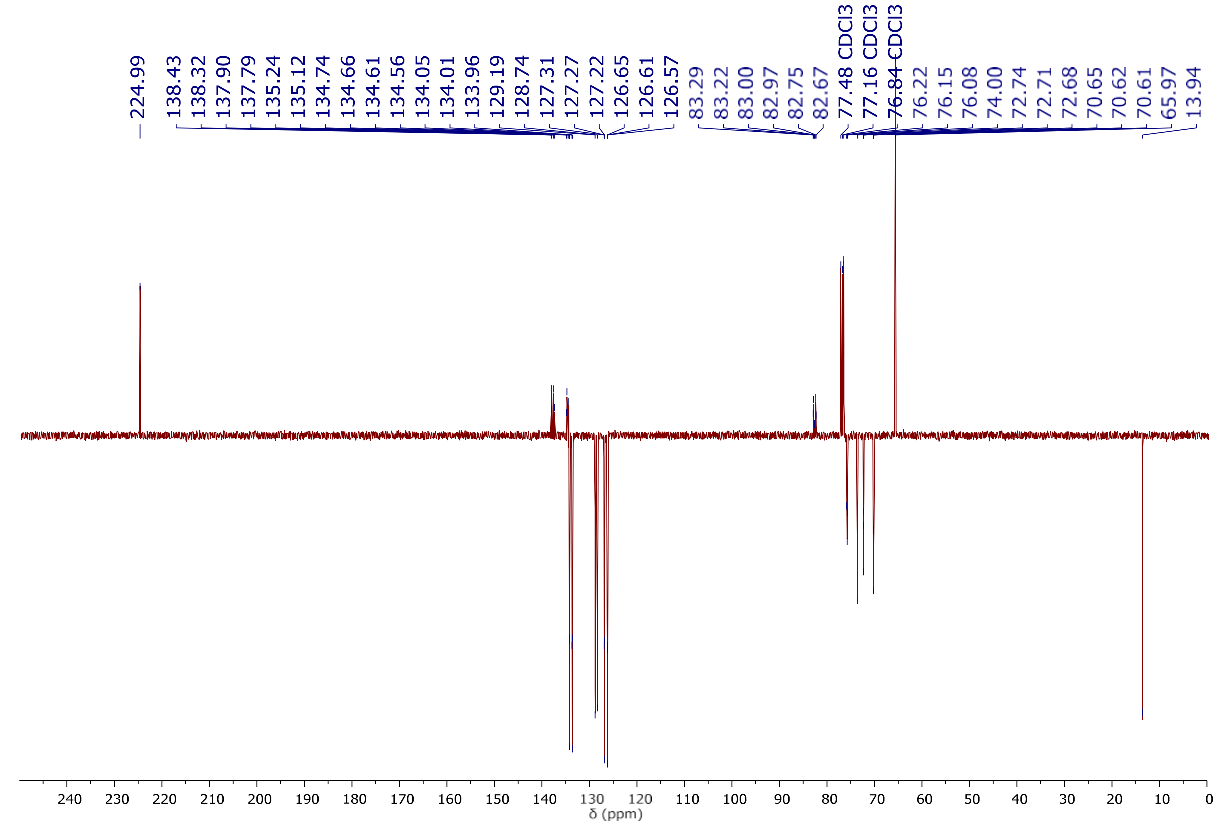

Fig. S44. $^{13}C\{^1H\}$ APT NMR spectrum (101 MHz, $CDCl_3$, 298 K) of [Ru(S_2COEt)$_2$(dppf)] (**8**)

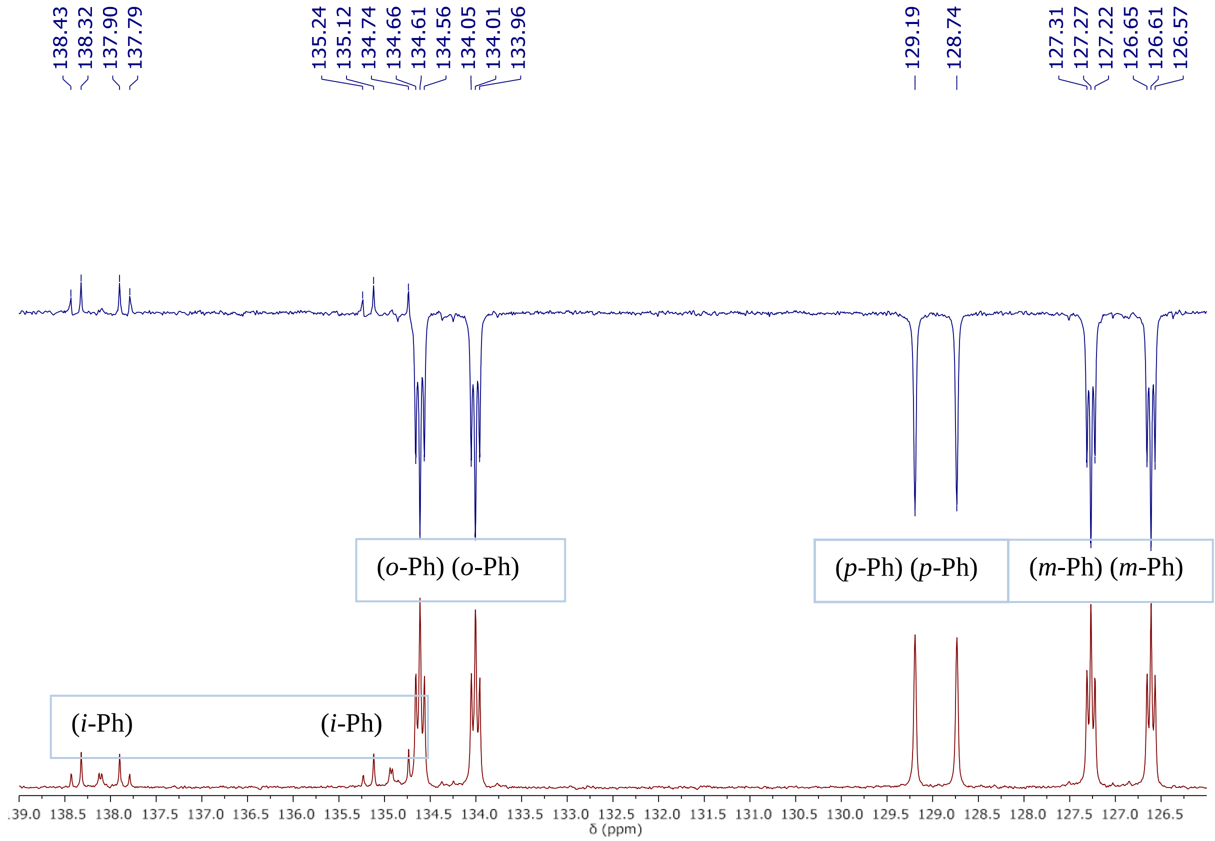

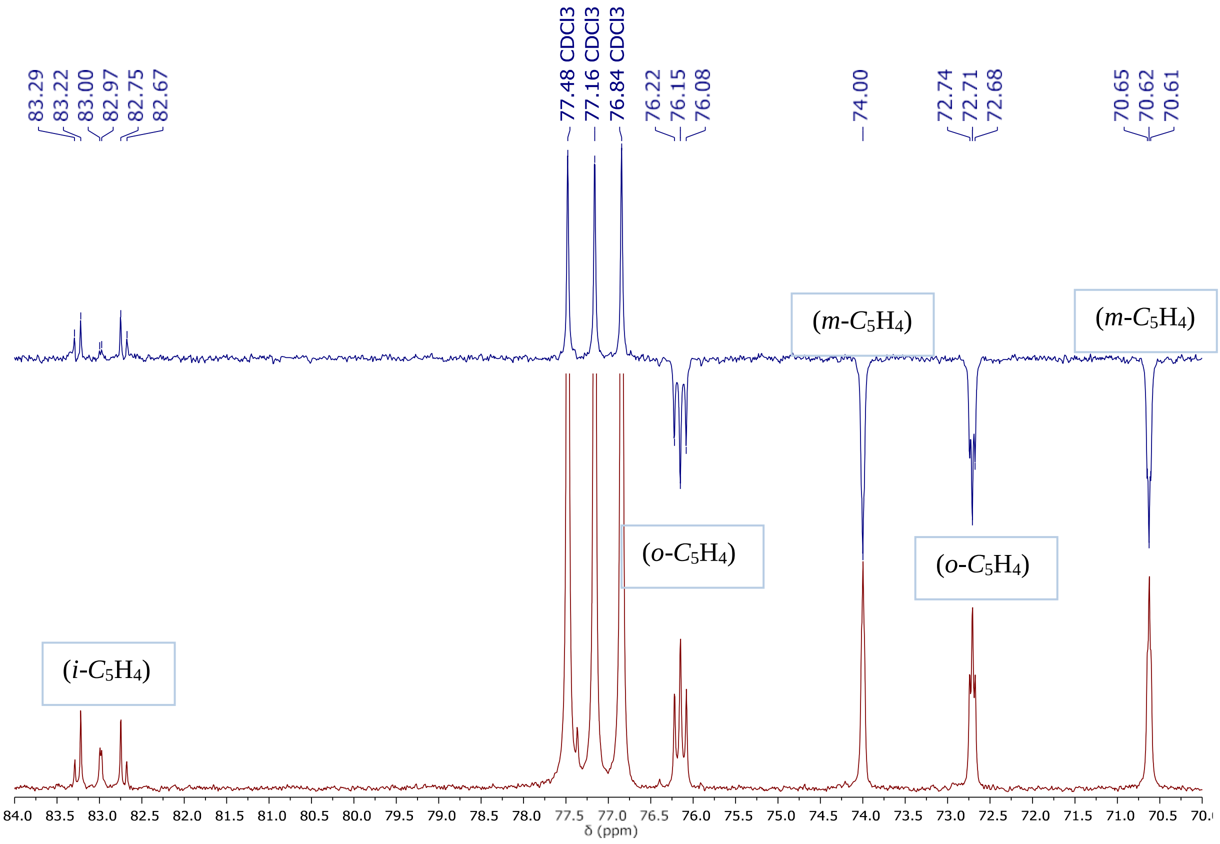

Fig. S45. ^{13}C CPD and APT NMR spectra (101 MHz, $CDCl_3$, 298 K) of [Ru(S_2COEt)$_2$(dppf)] (**8**)

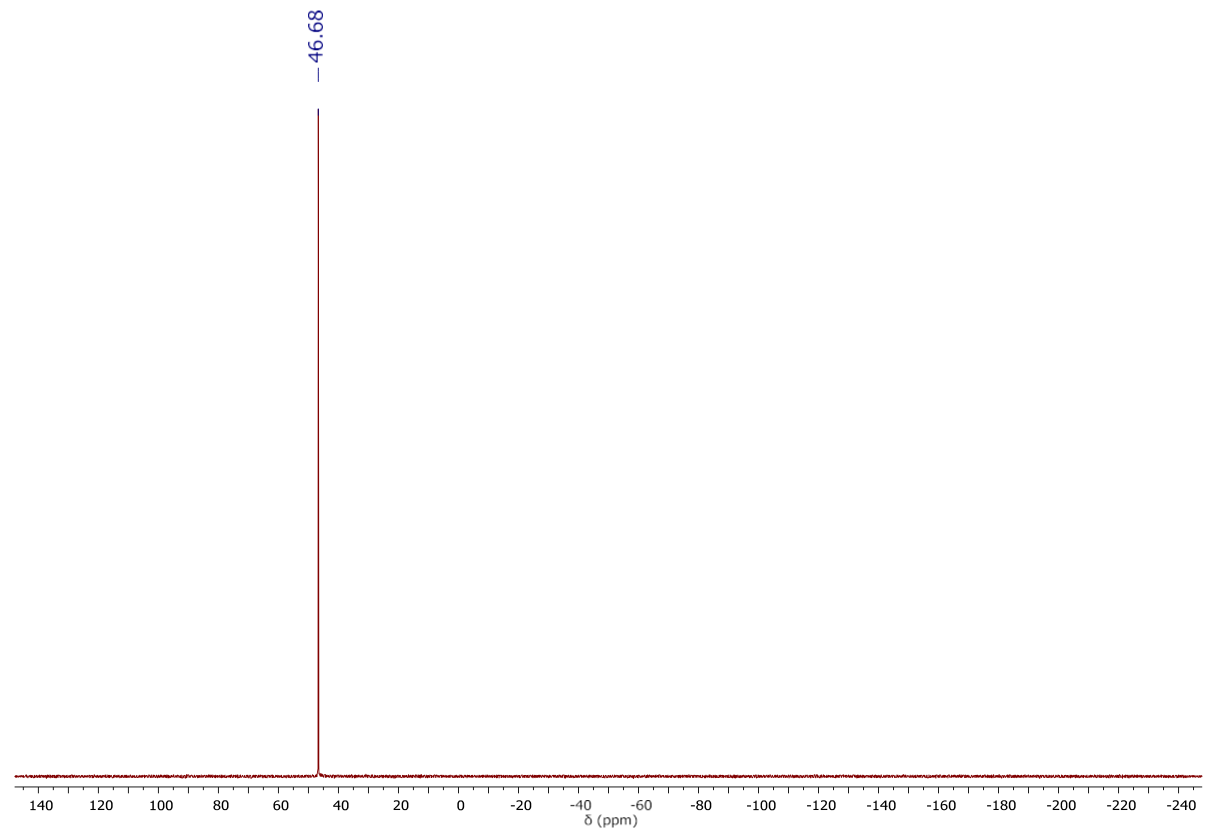

Fig. S46. ^{31}P NMR spectrum (162 MHz, $CDCl_3$, 298 K) of [Ru(S_2COEt)$_2$(dppf)] (**8**)

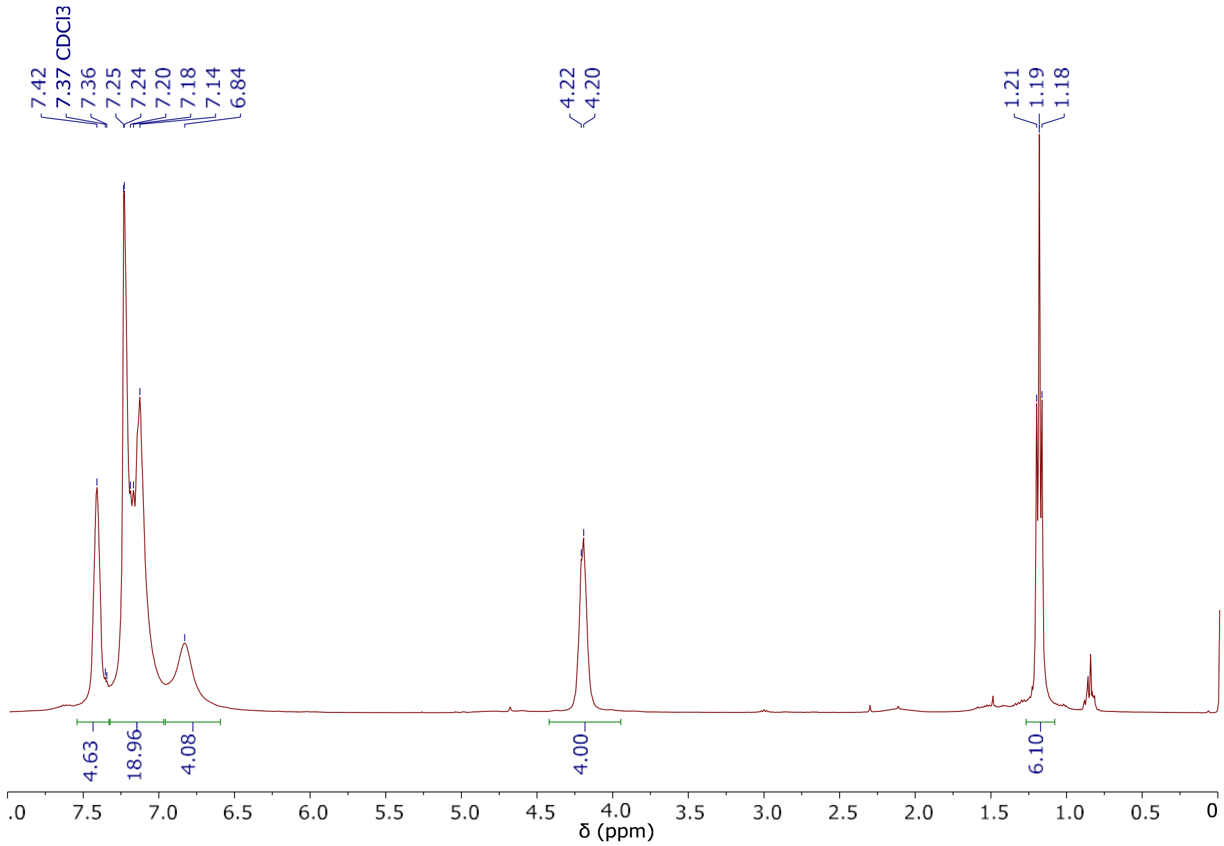

Fig. S47. ^{1}H NMR spectrum (400 MHz, $CDCl_3$, 298 K) of [Ru(S_2COEt)$_2$(DPEphos)] (**9**)

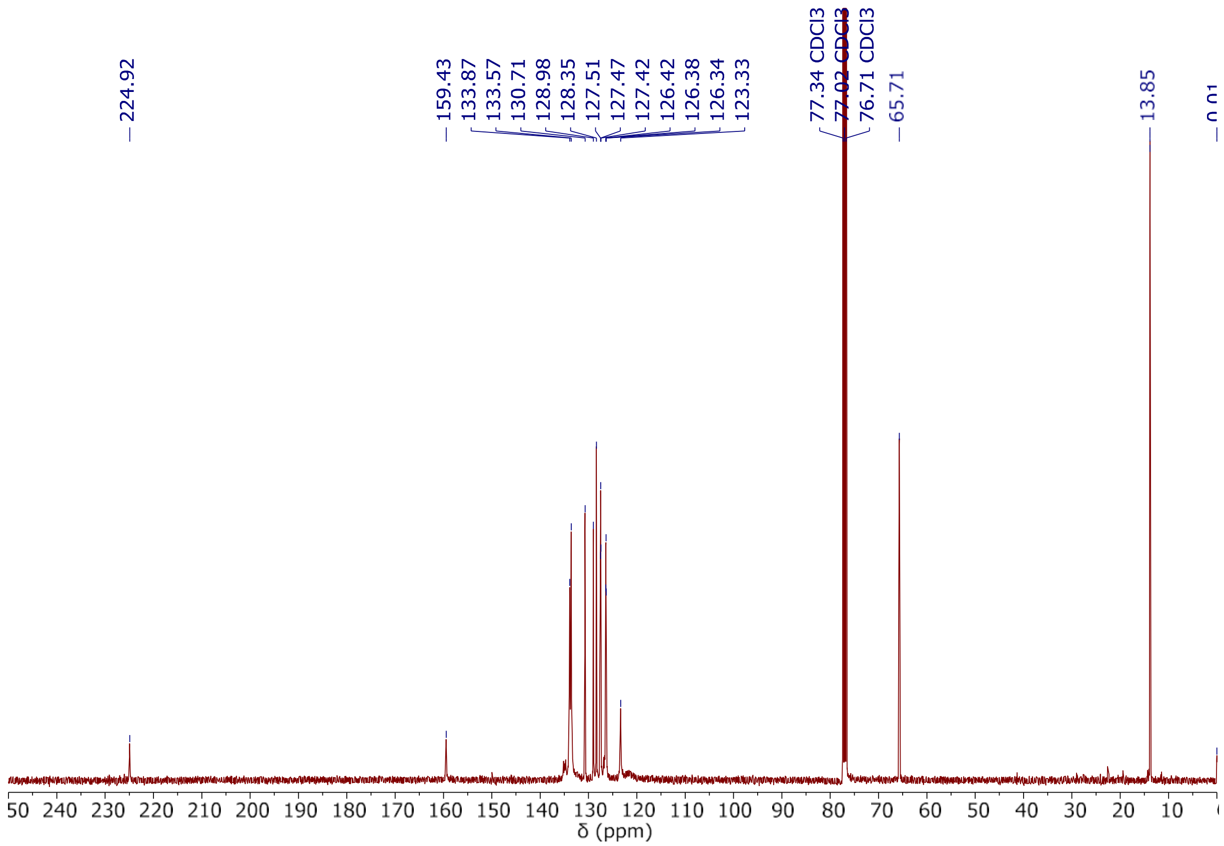

Fig. S48. $^{13}C\{^{1}H\}$ NMR spectrum (101 MHz, $CDCl_3$, 298 K) of [Ru(S_2COEt)$_2$(DPEphos)] (**9**)

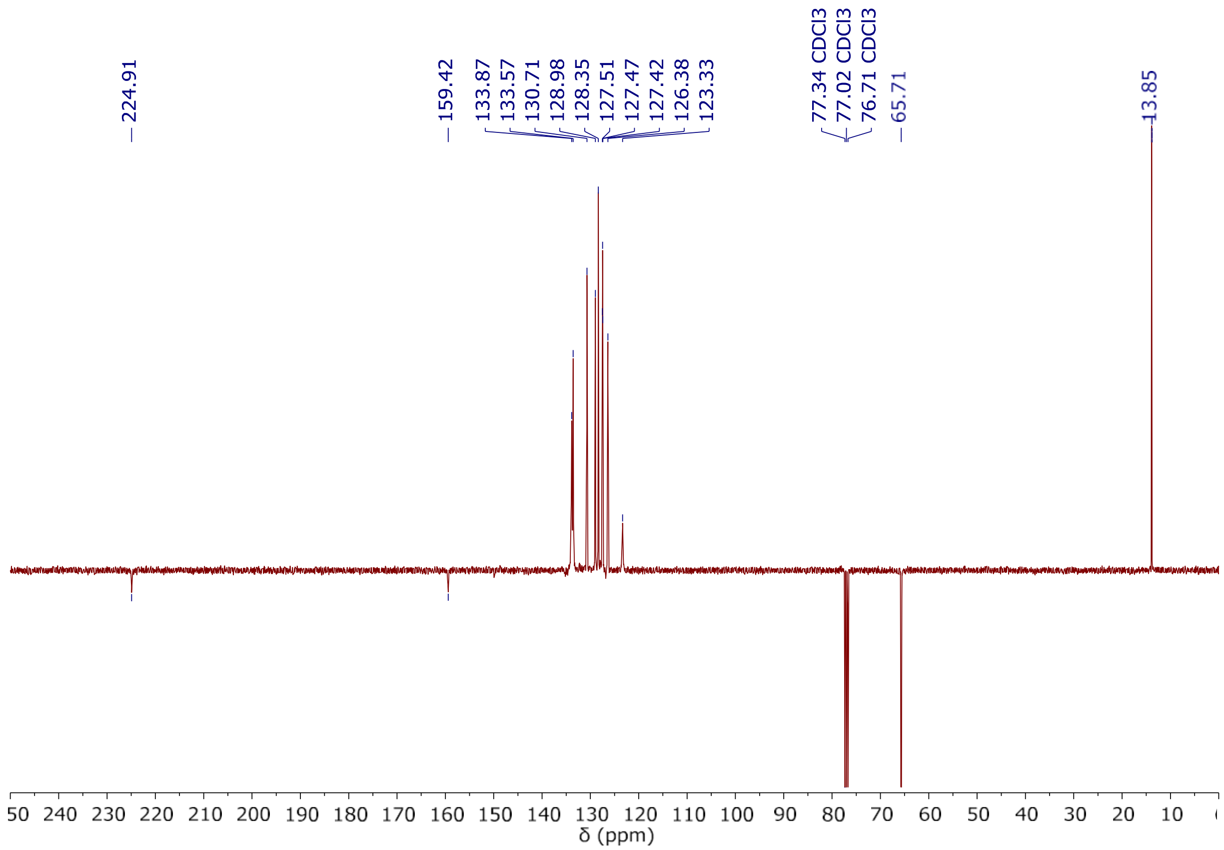

Fig. S49. $^{13}C\{^{1}H\}$ APT NMR spectrum (101 MHz, $CDCl_3$, 298 K) of $[Ru(S_2COEt)_2(DPEphos)]$ (**9**)

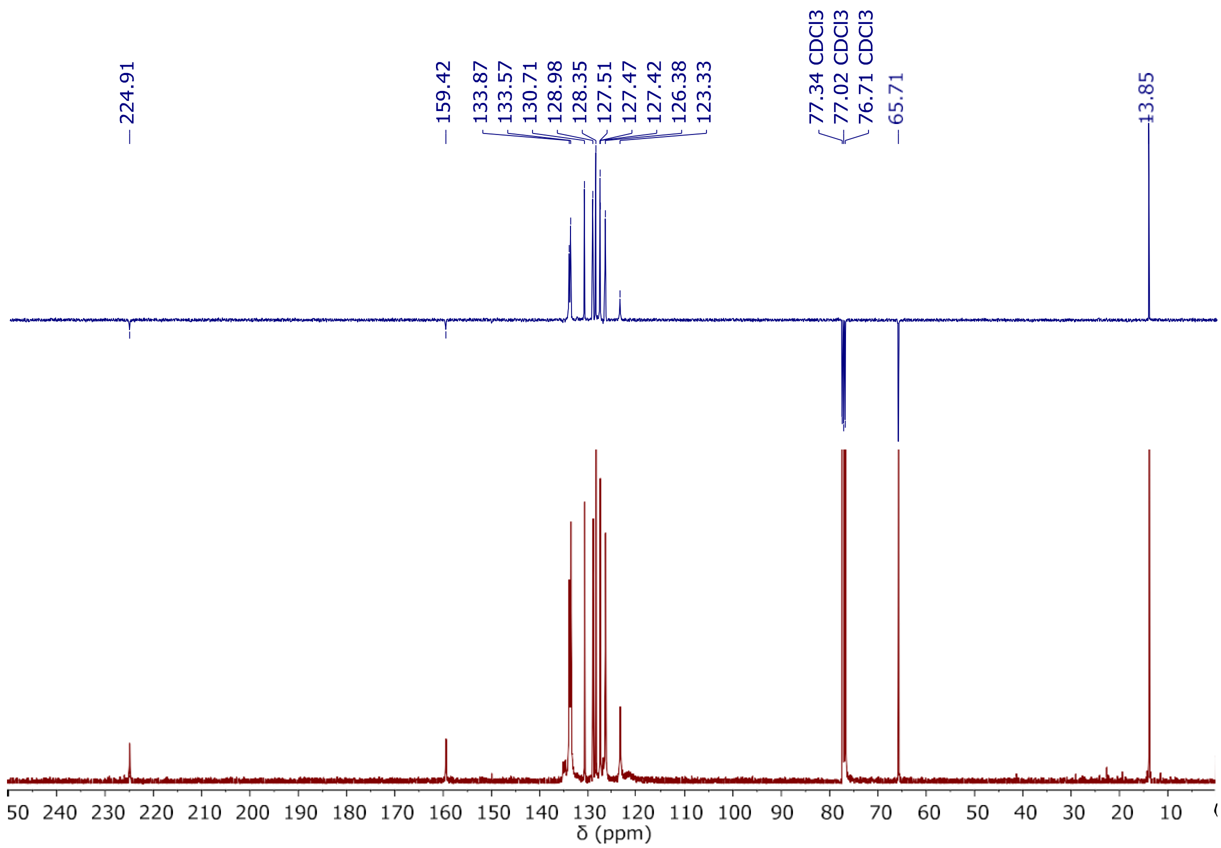

Fig. S50. ^{13}C CPD and APT NMR spectra (101 MHz, $CDCl_3$, 298 K) of $[Ru(S_2COEt)_2(DPEphos)]$ (**9**)

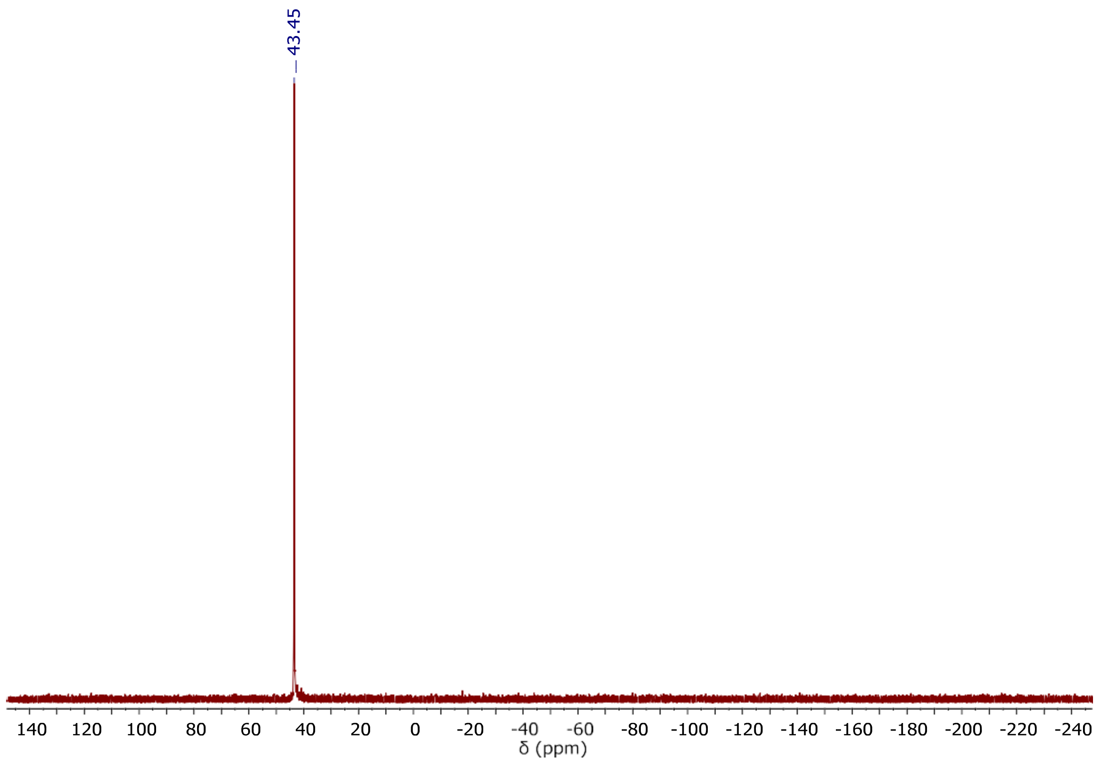

Fig. S51. ^{31}P NMR spectrum (162 MHz, $CDCl_3$, 298 K) of [Ru(S_2COEt)$_2$(DPEphos)] (**9**)

Part 2 – IR spectra

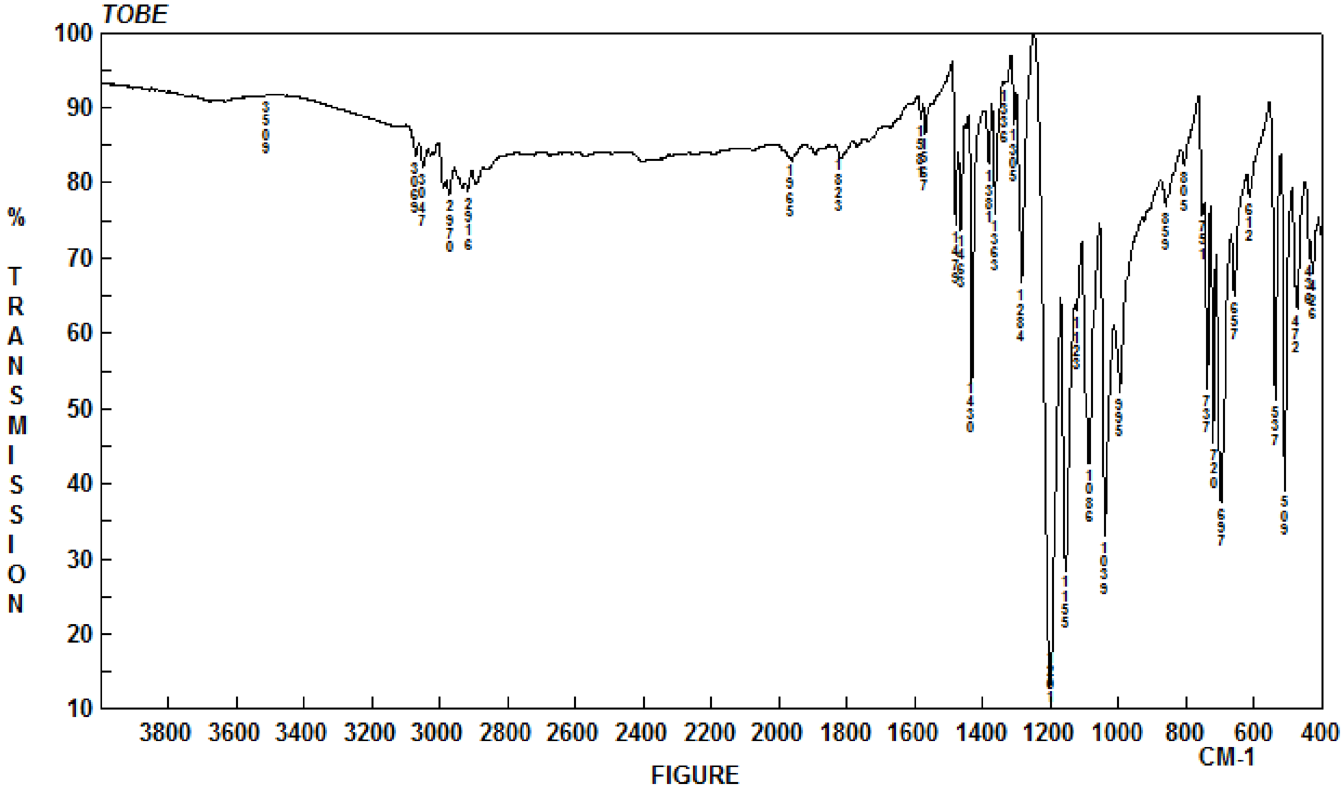

Fig. S52. FT-IR spectrum (KBr) of [Ru($S_2COEt)_2$(dppm)] (**1**)

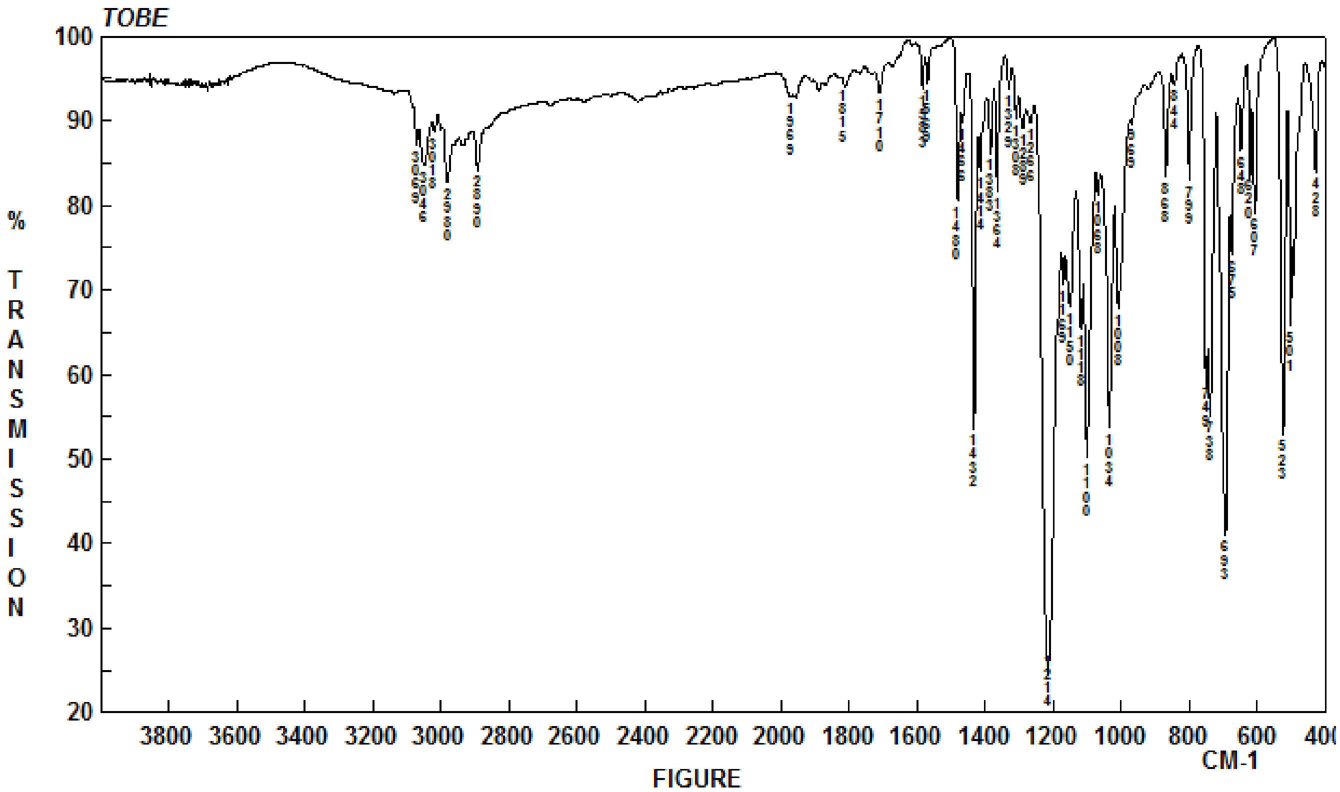

Fig. S53. FT-IR spectrum (KBr) of [Ru($S_2COEt)_2$(dppe)] (**2**)

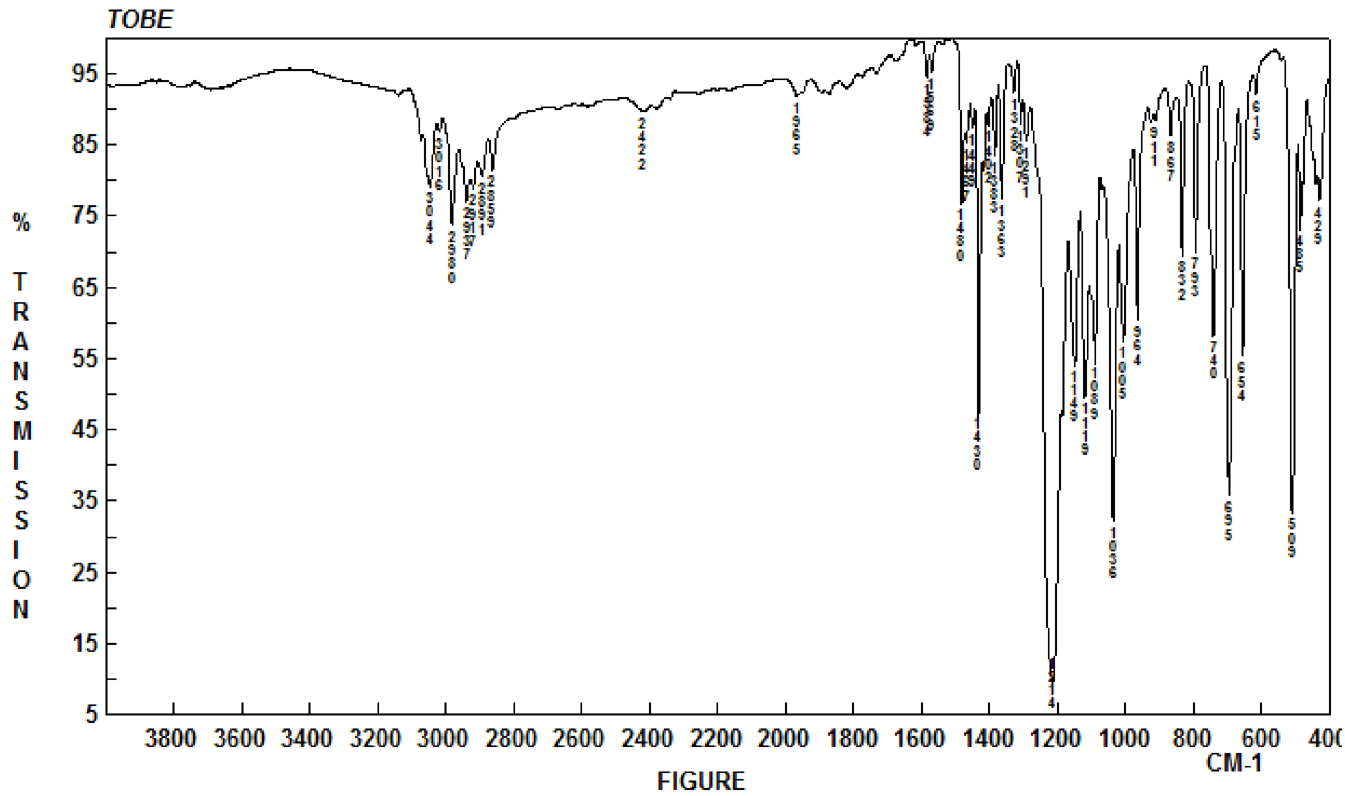

Fig. S54. FT-IR spectrum (KBr) of [Ru(S_2COEt)$_2$(dppp)] (**3**)

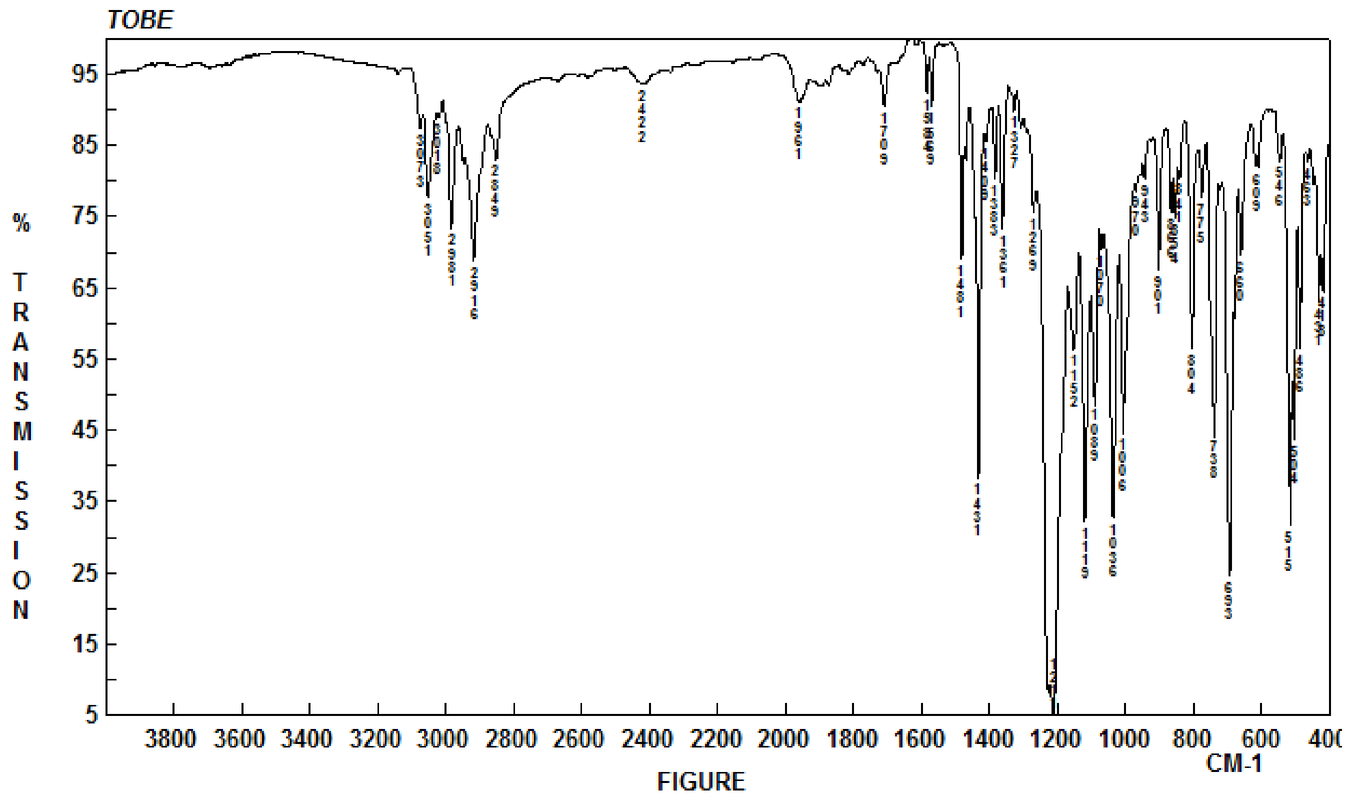

Fig. S55. FT-IR spectrum (KBr) of [Ru(S_2COEt)$_2$(dppb)] (**4**)

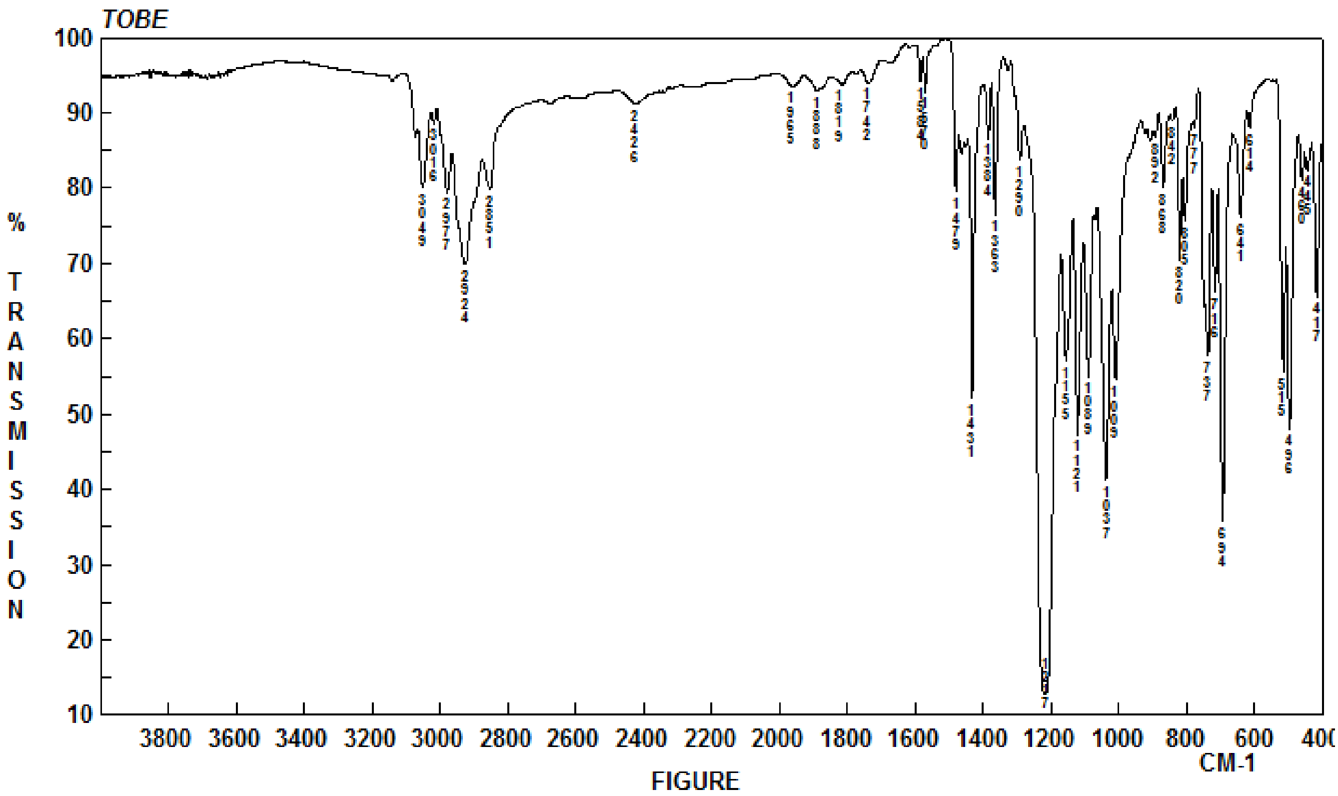

Fig. S56. FT-IR spectrum (KBr) of [Ru(S_2COEt)$_2$(dpppe)] (**5**)

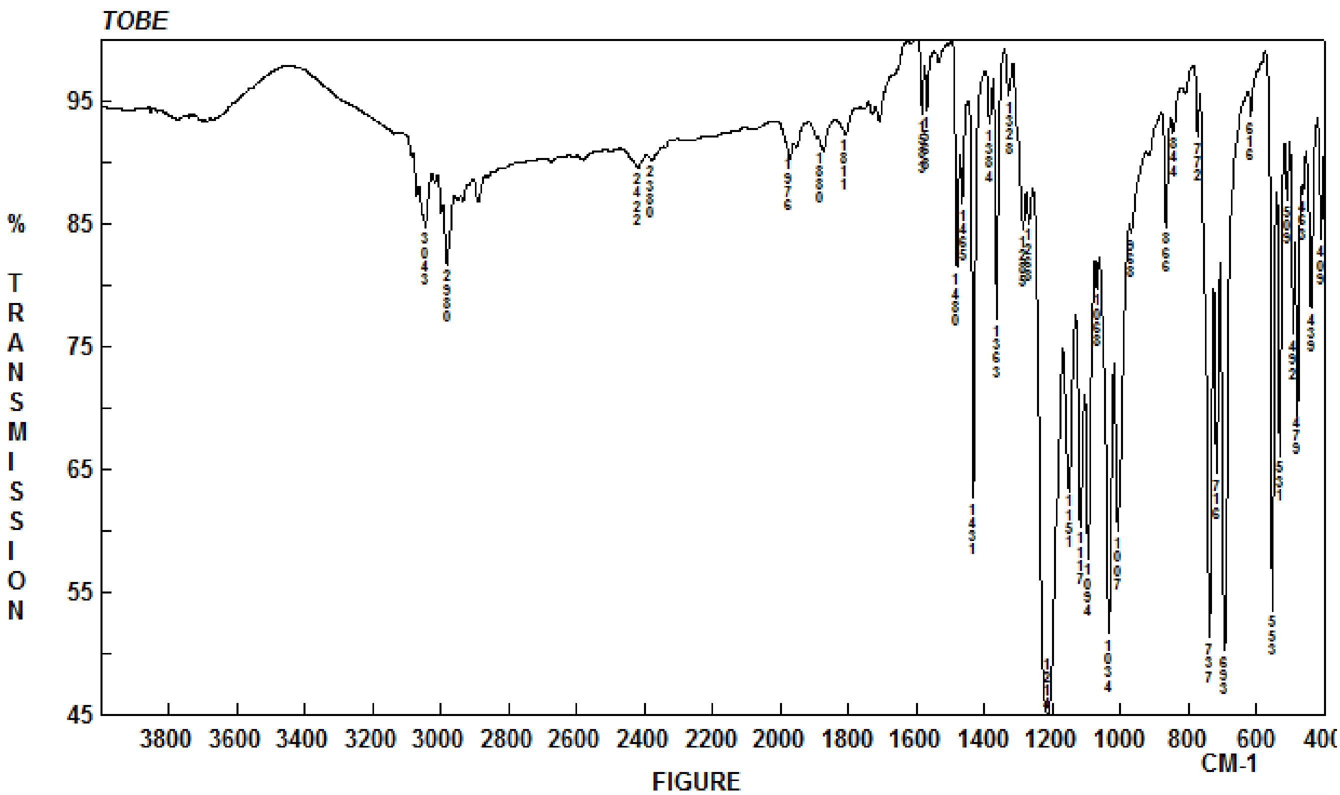

Fig. S57. FT-IR spectrum (KBr) of [Ru(S_2COEt)$_2$(dppen)] (**6**)

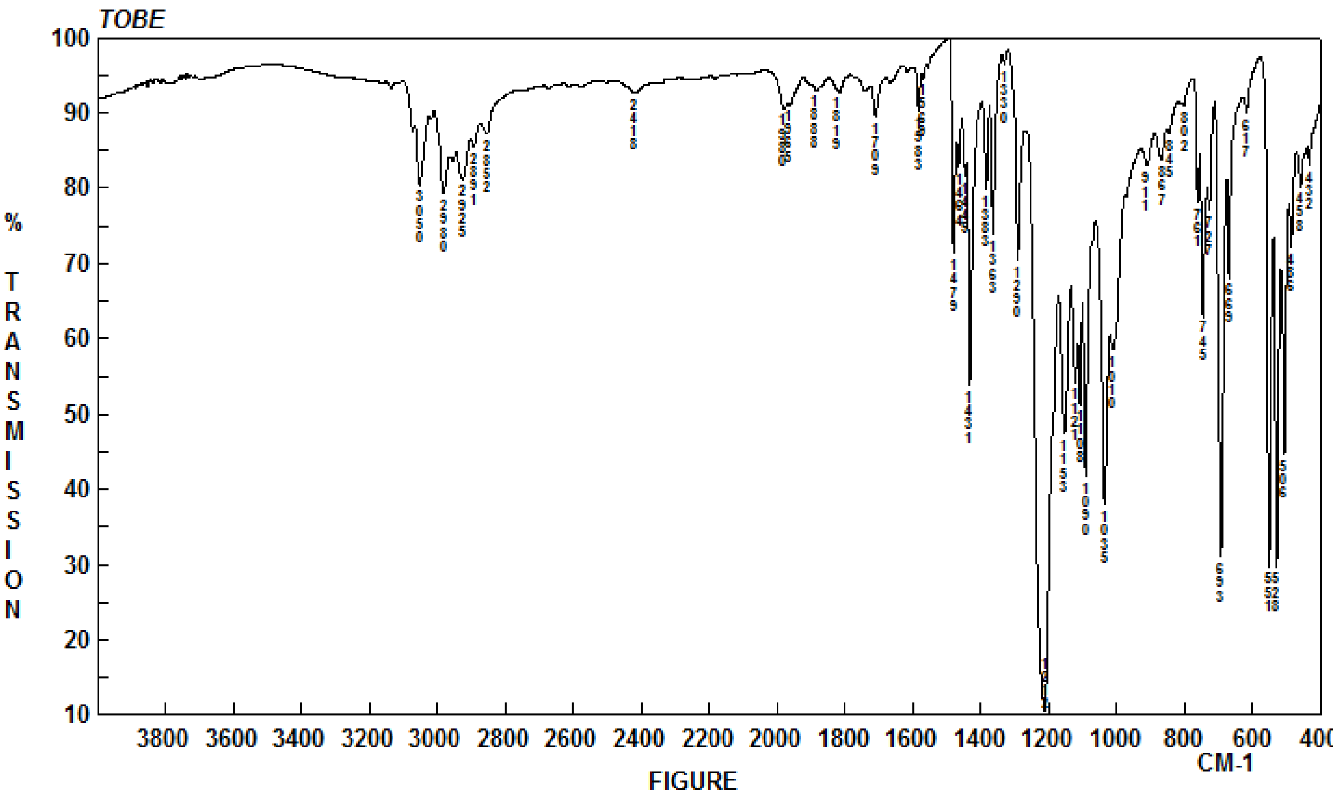

Fig. S58. FT-IR spectrum (KBr) of [Ru(S_2COEt)$_2$(dppbz)] (**7**)

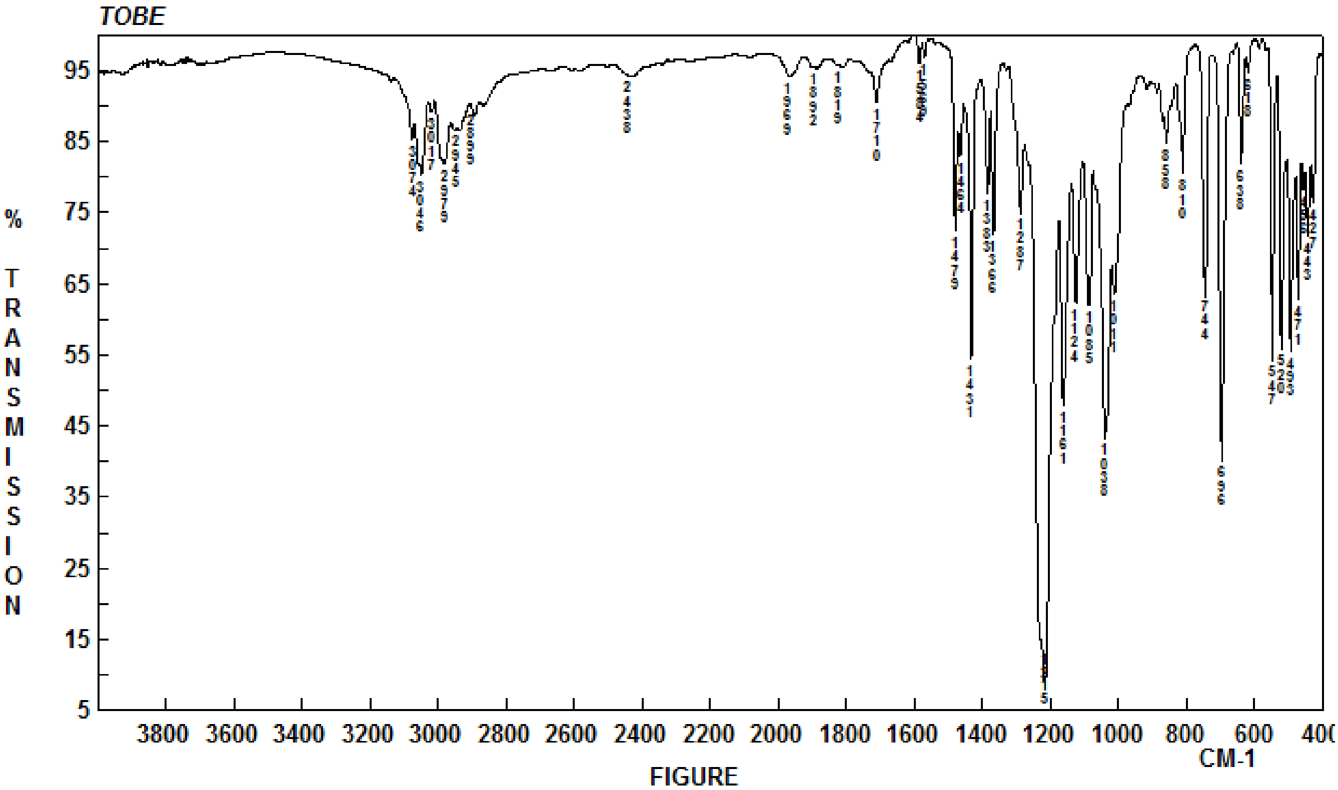

Fig. S59. FT-IR spectrum (KBr) of [Ru(S_2COEt)$_2$(dppf)] (**8**)

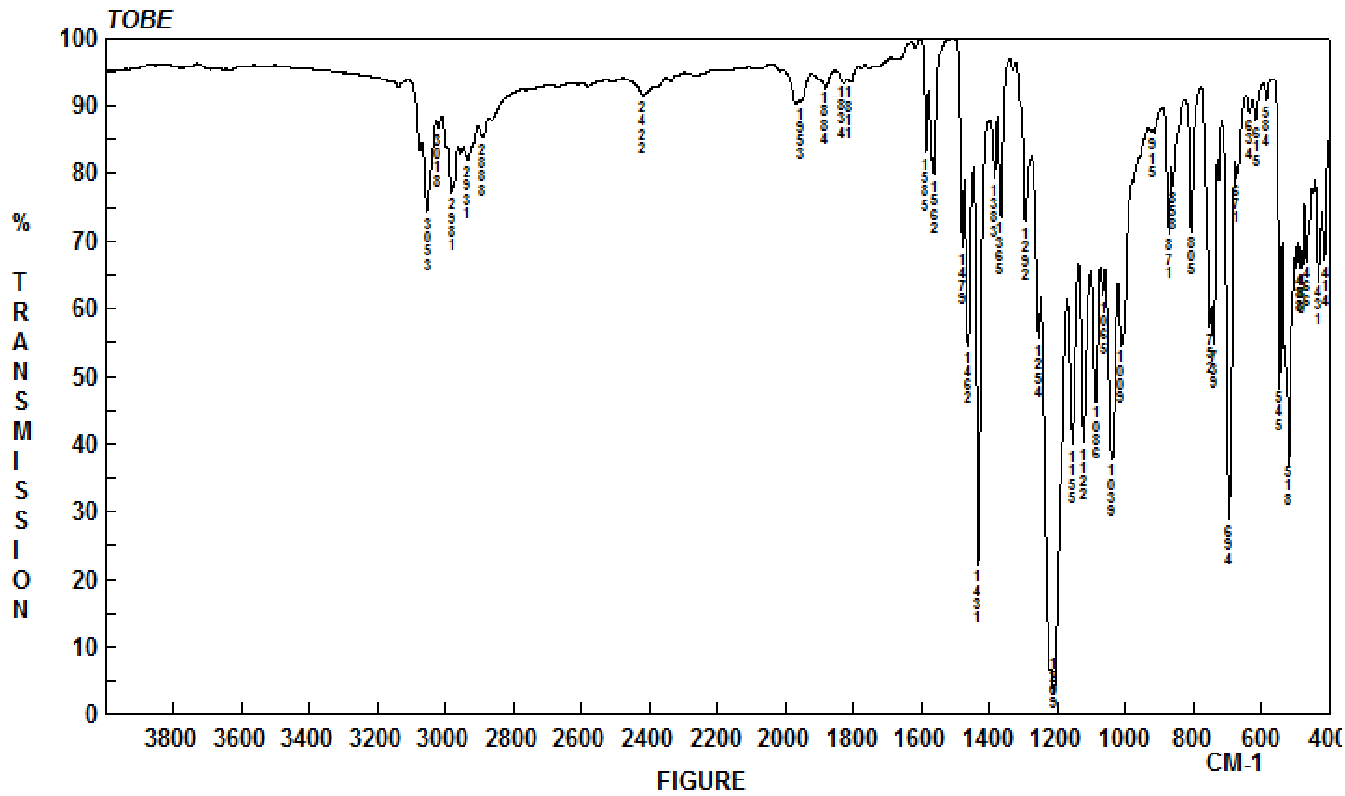

Fig. S60. FT-IR spectrum (KBr) of [Ru(S_2COEt)$_2$(DPEphos)] (**9**)

Part 3 – Mass spectra

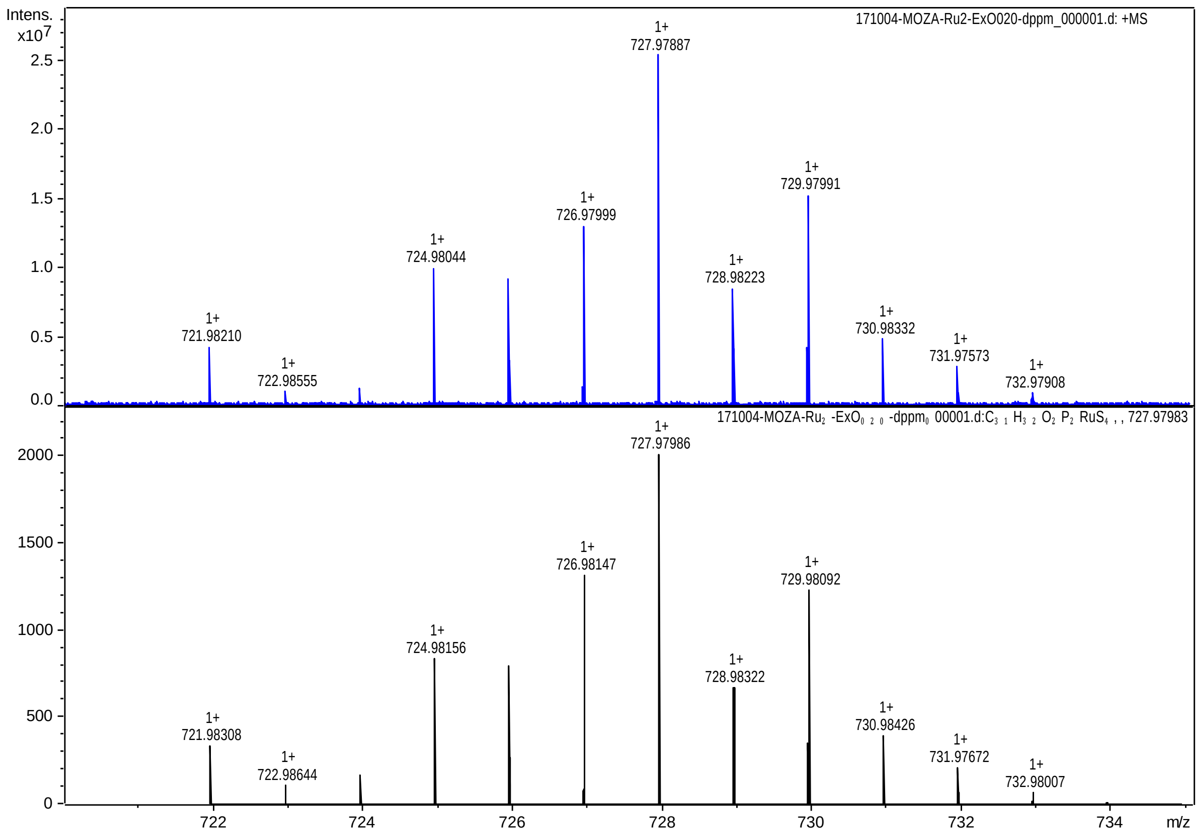

Fig. S61. Isotope profiles of [Ru(S_2COEt)$_2$(dppm)] (**1**) obtained by ESI-MS (in blue) and simulated isotope patterns of the corresponding ion (in black)

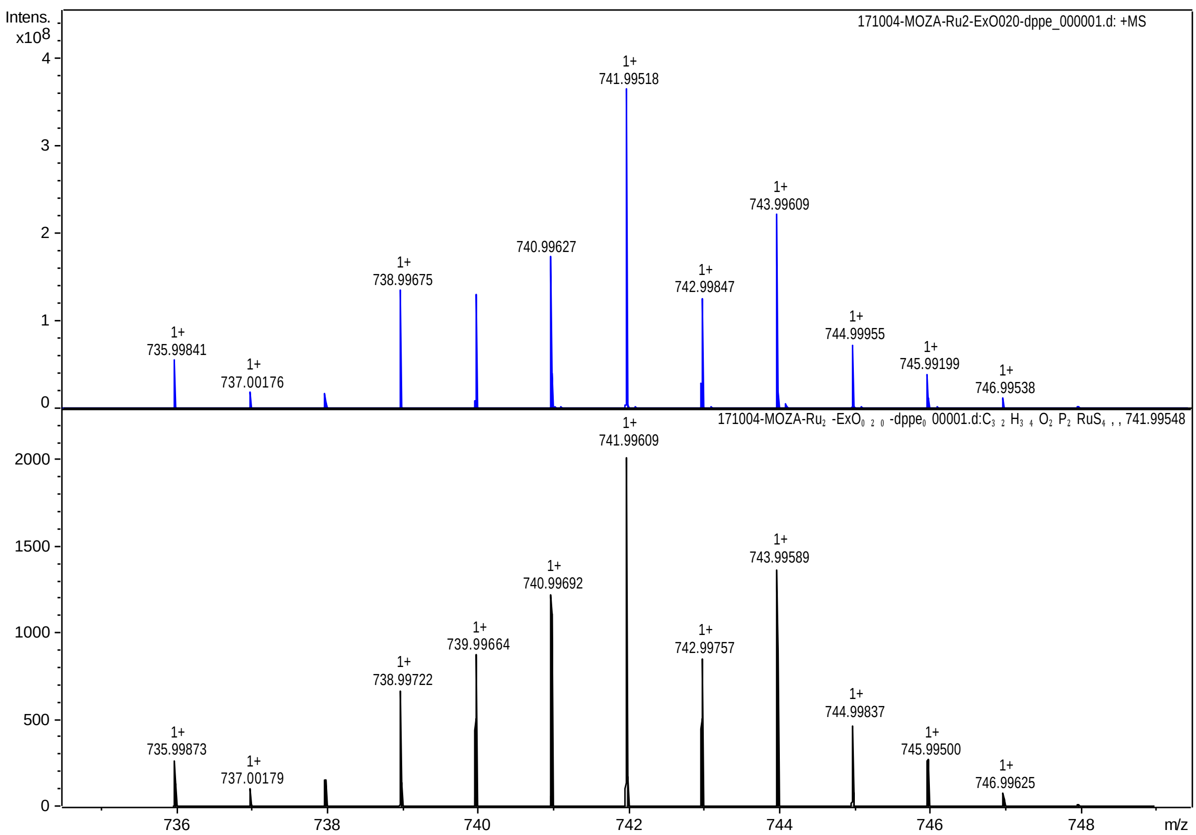

Fig. S62. Isotope profiles of [Ru(S_2COEt)$_2$(dppe)] (**2**) obtained by ESI-MS (in blue) and simulated isotope patterns of the corresponding ion (in black)

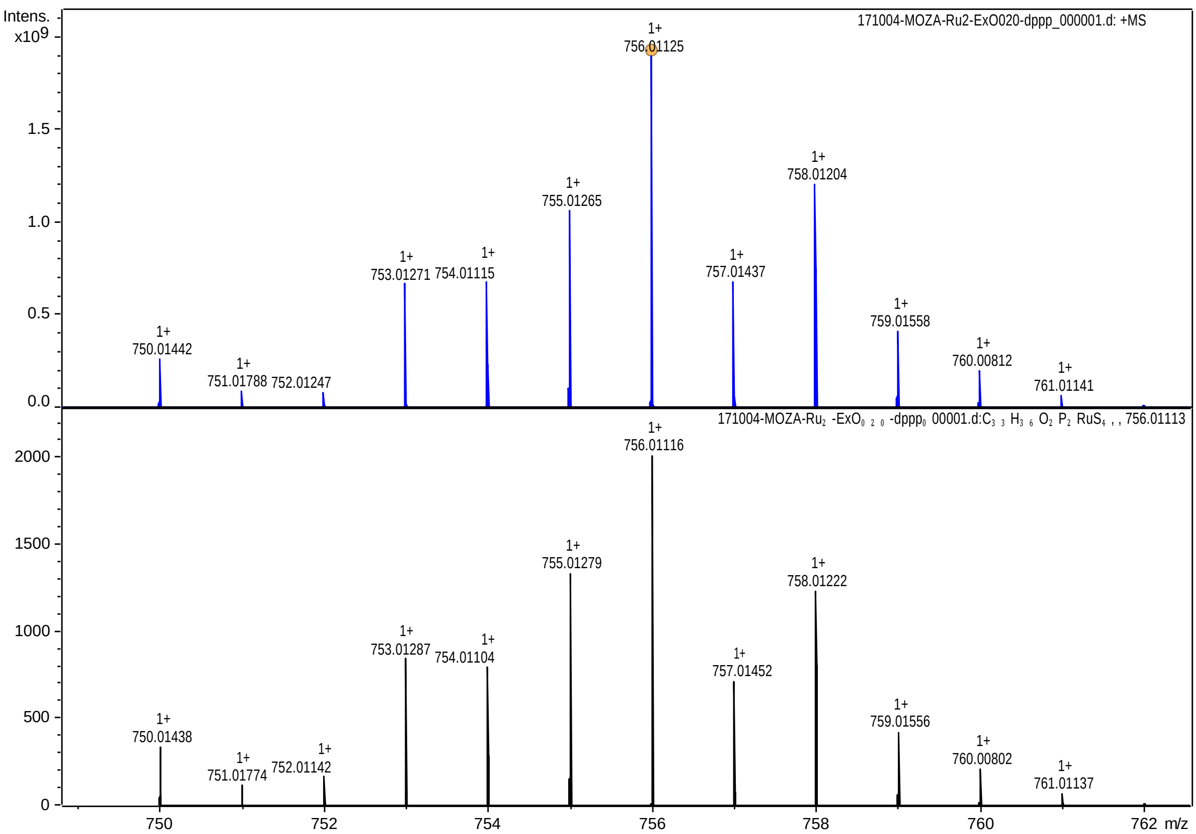

Fig. S63. Isotope profiles of [Ru(S_2COEt)$_2$(dppp)] (**3**) obtained by ESI-MS (in blue) and simulated isotope patterns of the corresponding ion (in black)

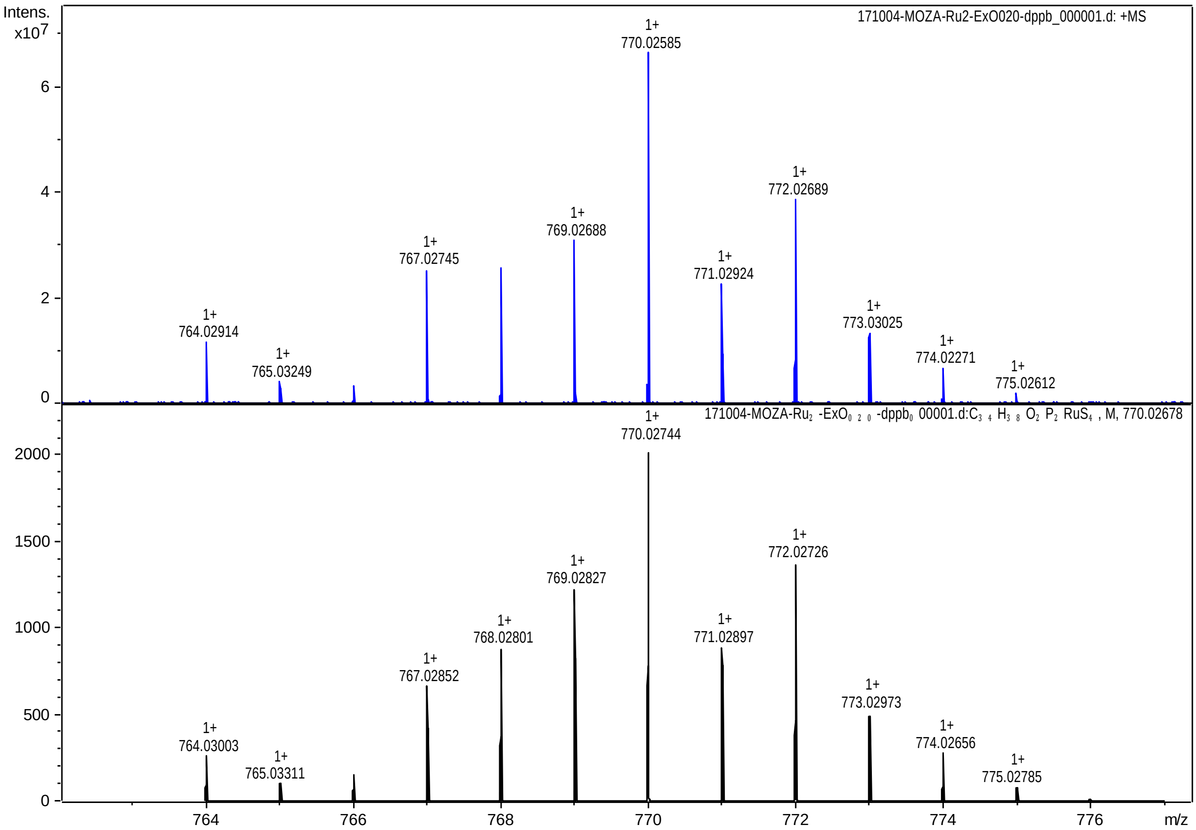

Fig. S64. Isotope profiles of [Ru(S_2COEt)$_2$(dppb)] (**4**) obtained by ESI-MS (in blue) and simulated isotope patterns of the corresponding ion (in black)

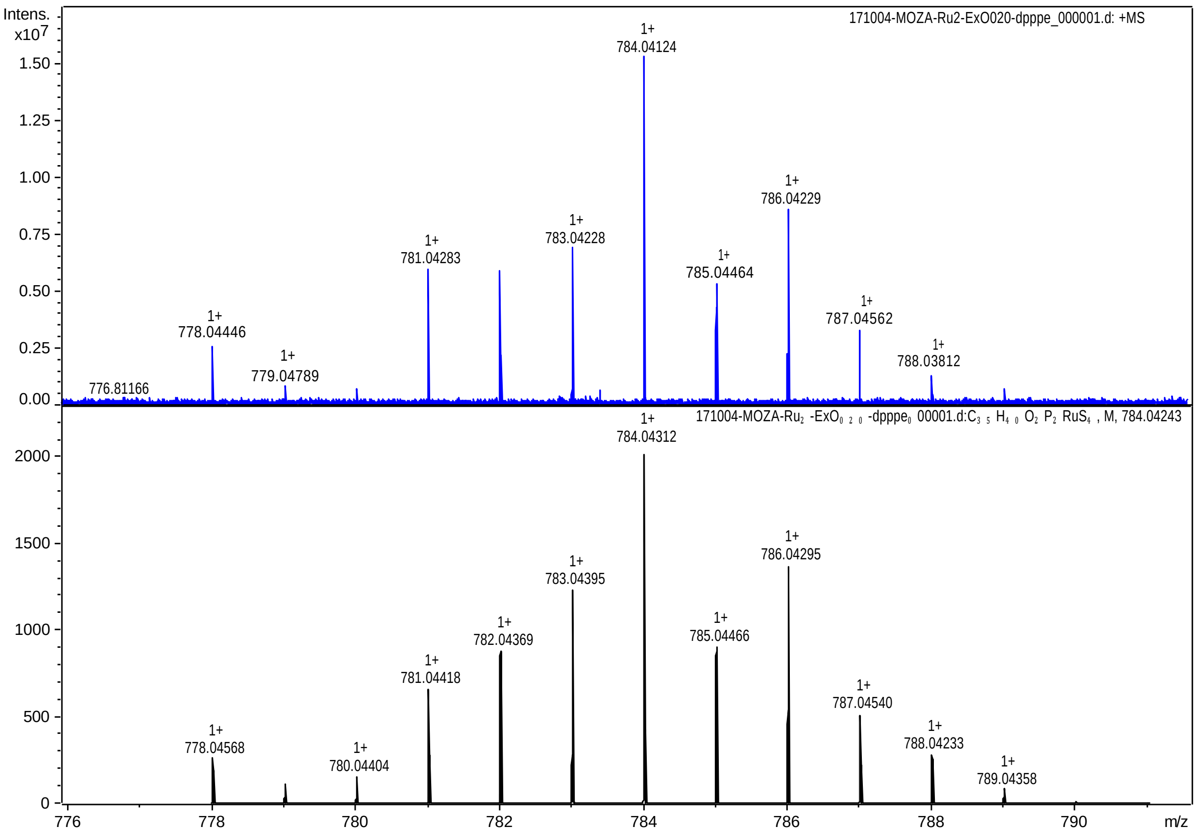

Fig. S65. Isotope profiles of [Ru(S_2COEt)$_2$(dpppe)] (**5**) obtained by ESI-MS (in blue) and simulated isotope patterns of the corresponding ion (in black)

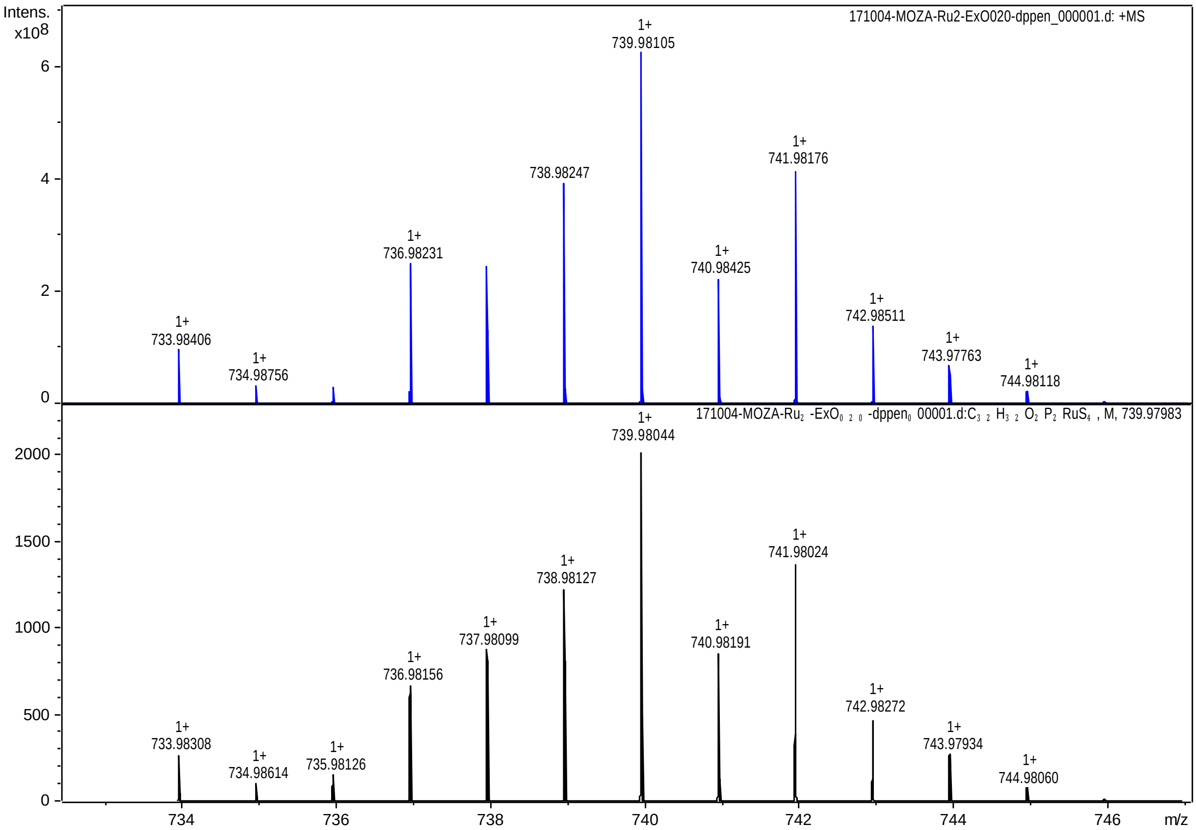

Fig. S66. Isotope profiles of [Ru(S_2COEt)$_2$(dppen)] (**6**) obtained by ESI-MS (in blue) and simulated isotope patterns of the corresponding ion (in black)

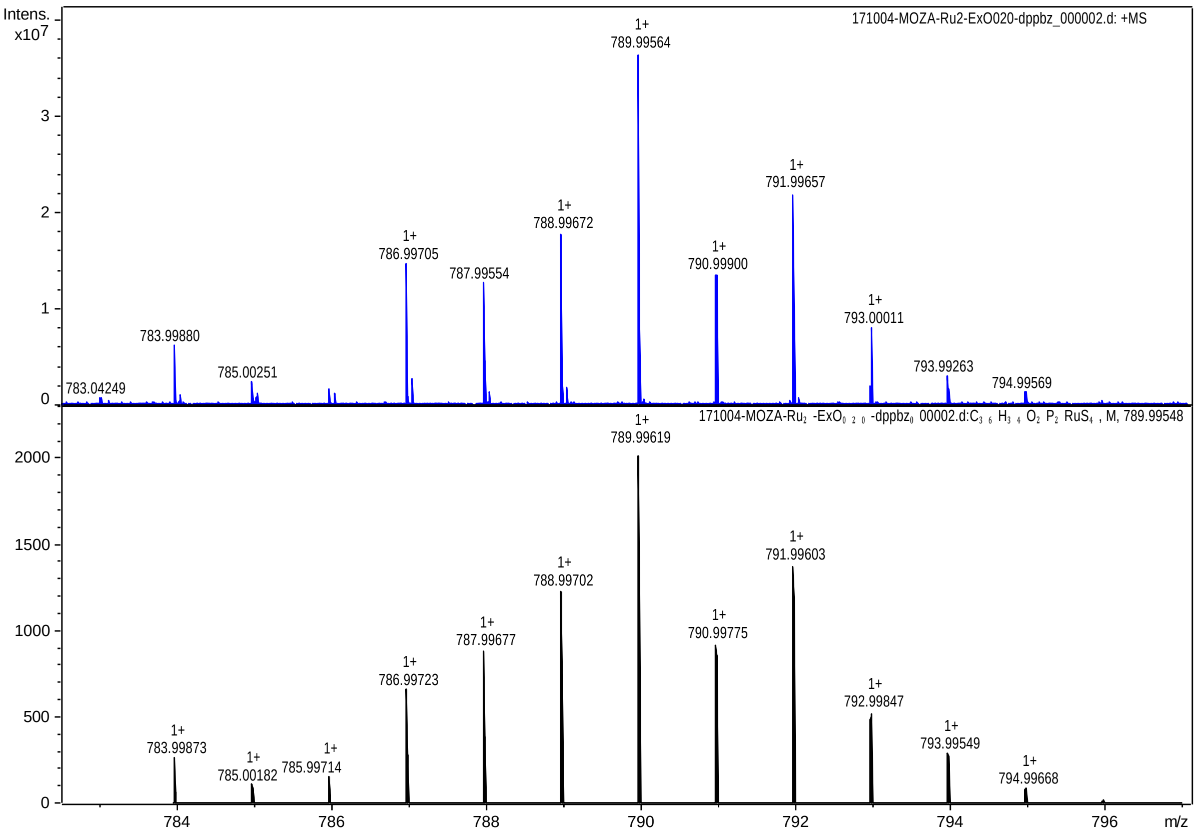

Fig. S67. Isotope profiles of [Ru(S_2COEt)$_2$(dppbz)] (**7**) obtained by ESI-MS (in blue) and simulated isotope patterns of the corresponding ion (in black)

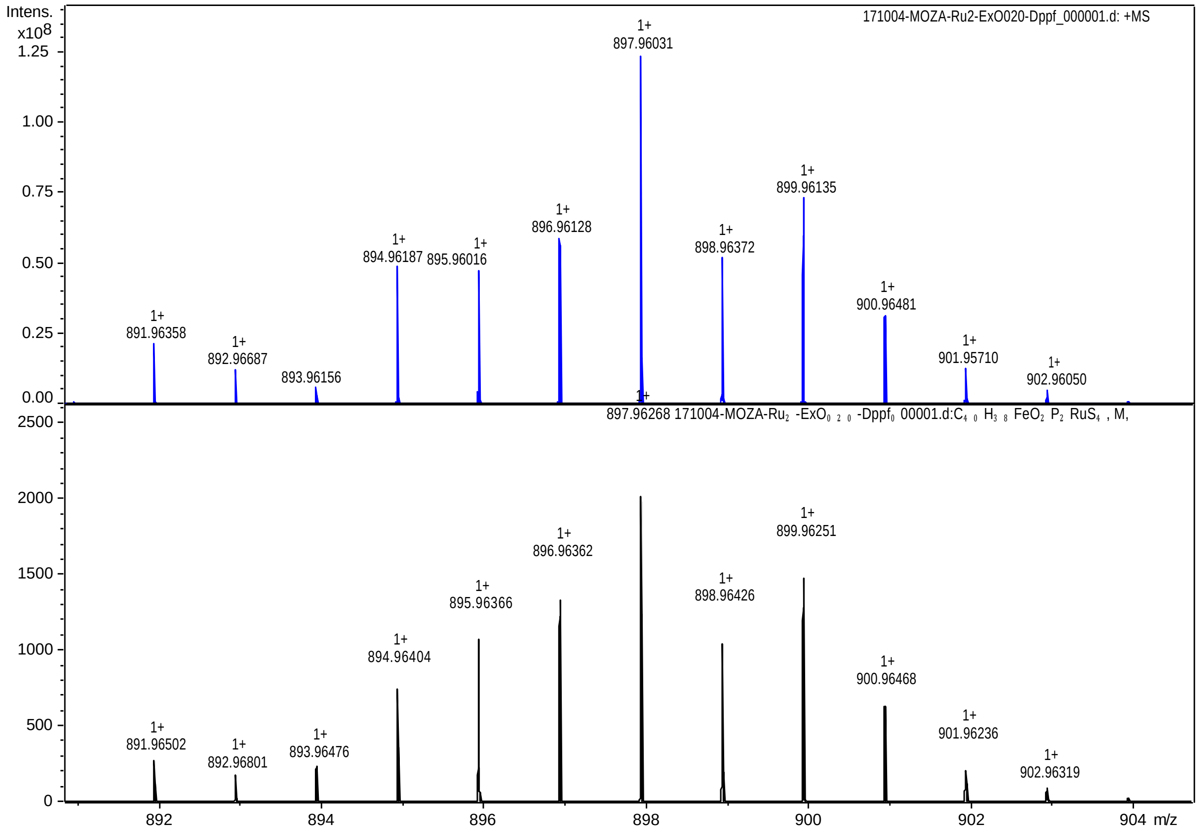

Fig. S68. Isotope profiles of [Ru(S_2COEt)$_2$(dppf)] (**8**) obtained by ESI-MS (in blue) and simulated isotope patterns of the corresponding ion (in black)

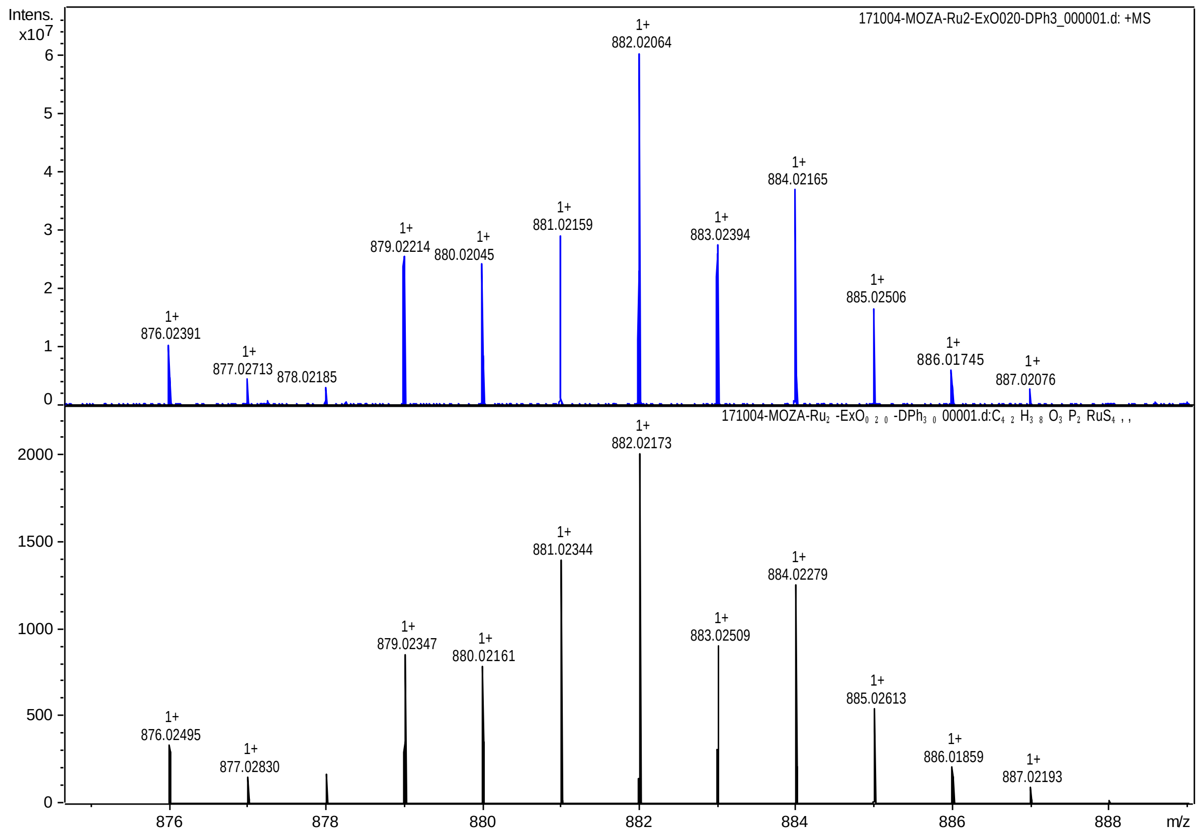

Fig. S69. Isotope profiles of [Ru(S_2COEt)$_2$(DPEphos)] (**9**) obtained by ESI-MS (in blue) and simulated isotope patterns of the corresponding ion (in black)

Part 4 – Crystallography

Table S1. Crystal data and structure refinement parameters for compounds **1−9**

Complex	**1**	**2**	**3**	**4**	**5**
Chemical formula	$C_{31}H_{32}O_2P_2RuS_4$	$C_{32}H_{34}O_2P_2RuS_4$	$2(C_{33}H_{36}O_2P_2RuS_4)\cdot CH_2Cl_2$	$C_{34}H_{38}O_2P_2RuS_4$	$C_{35}H_{40}O_2P_2RuS_4$
M (g mol^{-1})	727.81	741.84	1596.66	769.89	783.92
Crystal system	Triclinic	Orthorhombic	Orthorhombic	Monoclinic	Triclinic
Space group	P–1	$P2_12_12_1$	$Aba2$	$P2_1/n$	P–1
a (Å)	9.0261(7)	11.1196(6)	20.1261(7)	12.8809(10)	11.3144(3)
b (Å)	11.1233(9)	14.0834(10)	21.5909(8)	16.5329(11)	11.4472(3)
c (Å)	16.9387(14)	20.6451(12)	16.4408(7)	16.3601(9)	13.6613(4)
α (°)	72.137(4)	90	90	90	94.926(2)
β (°)	80.855(4)	90	90	105.668(3)	93.661(2)
γ (°)	73.704(5)	90	90	90	97.305(2)
V (Å^3)	1548.7(2)	3233.1(3)	7144.2(5)	3354.6(4)	1743.53(8)
Z	2	4	4	4	2
D_x (g cm^{-3})	1.561	1.524	1.484	1.524	1.493
μ(Mo Kα) (mm^{-1})	0.908	0.871	0.867	0.843	0.812
Reflns collected	58899	51408	36877	41282	19804
Indpndt reflns	7671	9865	6994	8244	6359
R_{int}	0.055	0.098	0.095	0.048	0.055
$R_1{}^a$ (all data)	0.038	0.057	0.069	0.040	0.075
$wR_2{}^b$ (all data)	0.059	0.073	0.103	0.068	0.086
GOF^c on F^2	1.059	0.996	1.012	1.046	0.994

Complex	**6**	**7**	**8**	**9**
Chemical formula	$C_{32}H_{32}O_2P_2RuS_4$	$C_{36}H_{34}O_2P_2RuS_4$	$C_{40}H_{38}FeO_2P_2RuS_4$	$C_{42}H_{38}O_3P_2RuS_4$
M (g mol^{-1})	739.82	789.88	897.8	881.97
Crystal system	Orthorhombic	Triclinic	Monoclinic	Triclinic
Space group	$P2_12_12_1$	P–1	$P2_1/n$	P–1
a (Å)	11.301(2)	11.3572(7)	19.1300(9)	10.8511(6)
b (Å)	13.968(3)	11.7146(10)	9.7269(3)	11.1779(7)
c (Å)	20.344(3)	13.7193(12)	22.0104(10)	17.2515(10)
α (°)	90	95.488(6)	90	82.595(4)
β (°)	90	105.893(5)	115.313(2)	73.977(3)
γ (°)	90	96.247(5)	90	73.322(3)
V (Å^3)	3211.4(10)	1730.0(2)	3702.4(3)	1923.7(2)
Z	4	2	4	2
D_x (g cm^{-3})	1.53	1.516	1.611	1.523
μ(Mo Kα) (mm^{-1})	0.877	0.819	1.148	0.748
Reflns collected	30577	32670	56273	35910
Indpndt reflns	7935	8558	7566	9179
R_{int}	0.093	0.083	0.108	0.047
$R_1{}^a$ (all data)	0.069	0.072	0.065	0.050
$wR_2{}^b$ (all data)	0.078	0.093	0.083	0.077
GOF^c on F^2	0.98	0.989	1.017	1.067

^{a} $R_1 = \sum||F_o| - |F_c||/\sum|F_o|$. ^{b} $wR_2 = [(\sum w(F_o{}^2 - F_c{}^2)^2/\sum|F_o|^2)]^{1/2}$. ^{c} GOF $= [\sum[w(F_o{}^2 - F_c{}^2)^2]/(N_o - N_v)]^{1/2}$ (N_o = number of observations; N_v = number of variables).

Part 5 – Cyclic voltammetry

Table S2. Electrochemical data obtained from cyclic voltammetry experiments for compounds **1**–**9**[a]

Complex	$I_{p,ox}$ (mA/cm²)	$I_{p,red}$ (mA/cm²)	$E_{p,ox}$ (V)	$E_{p,red}$ (V)	$E_{1/2}$ (V)[b]
1 (dppm)	0.192	–0.097	0.785	0.551	0.668
2 (dppe)	0.140	–0.107	0.861	0.676	0.769
3 (dppp)	0.183	–0.124	0.857	0.661	0.759
4 (dppb)	0.232	–0.190	0.841	0.645	0.743
5 (dpppe)	0.275	–0.215	0.824	0.655	0.740
6 (dppen)	0.305	–0.227	0.890	0.710	0.800
7 (dppbz)	0.224	–0.174	0.861	0.684	0.773
8 (dppf)	0.121	–0.113	0.764	0.525	0.645
9 (DPEphos)	0.276	–0.238	0.754	0.590	0.672

[a] Peak current densities (I_p) and peak potentials (E_p) correspond to the Ru^{3+}/Ru^{2+} redox couple.

[b] $E_{1/2} = (E_{p,ox} + E_{p,red})/2$.

Part 6 – Catalytic tests

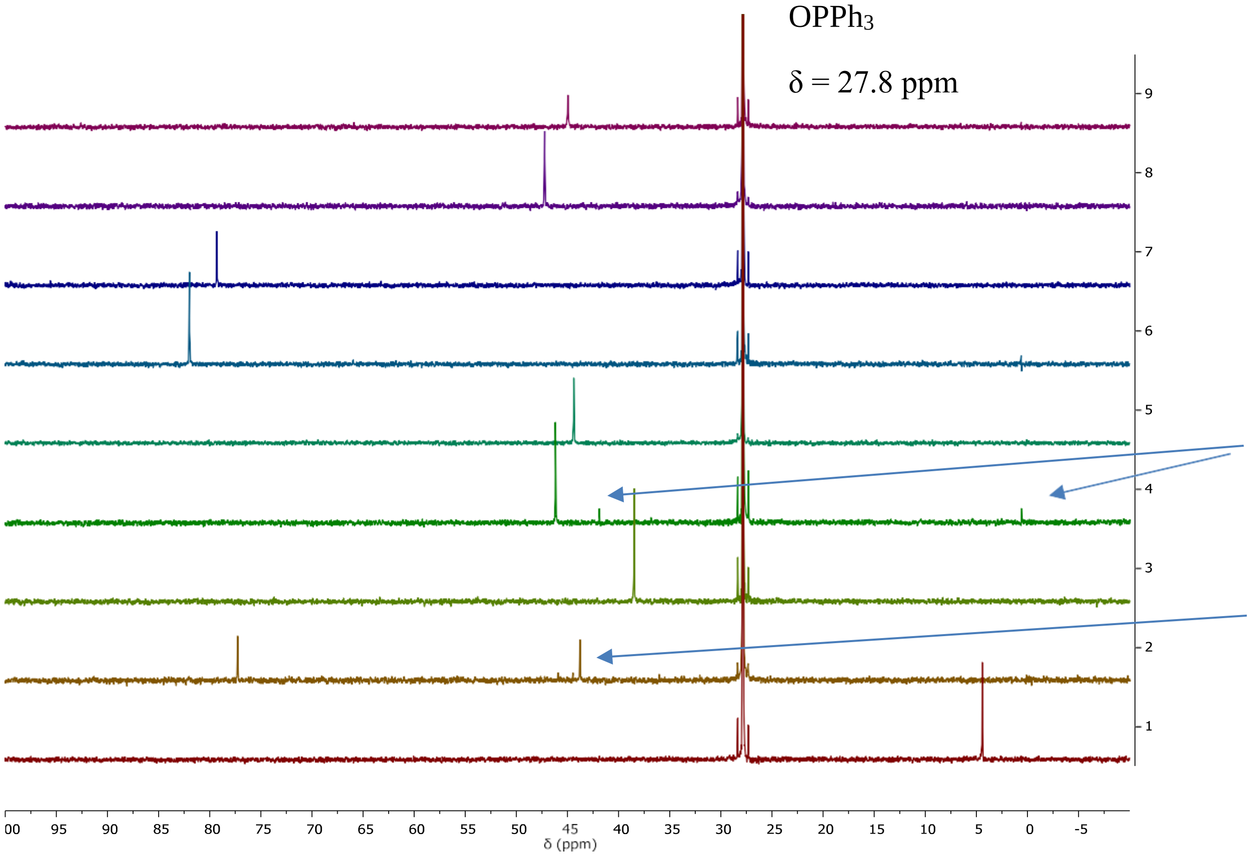

Fig. S70. ^{31}P NMR spectra of the reaction mixtures obtained after heating benzoic acid and 1-hexyne in toluene at 160 °C for 30 min in the presence of $[Ru(S_2COEt)_2(diphos)]$ complexes **1**–**9** (a sealed capillary tube containing Ph_3PO in CD_2Cl_2 was used as an external reference)

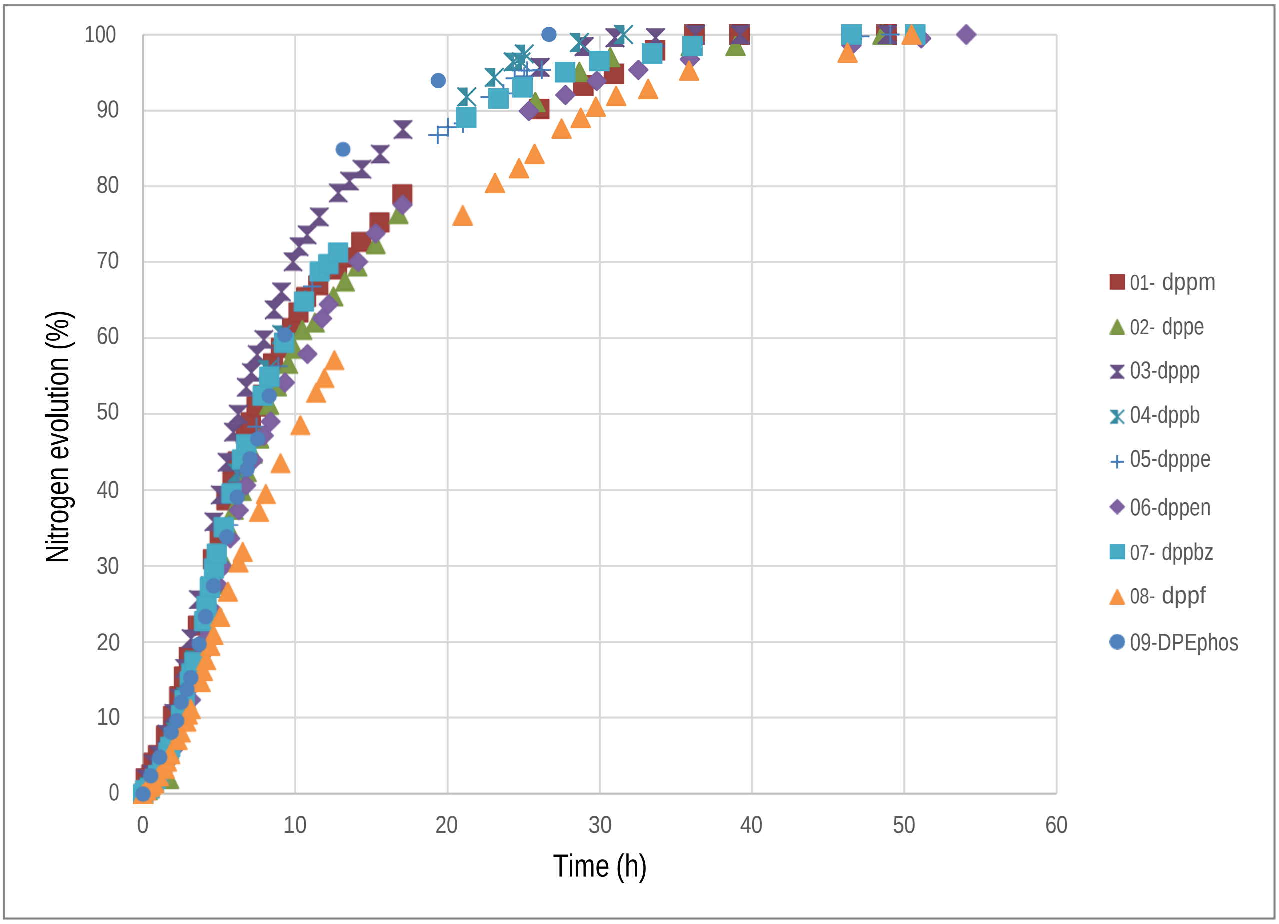

Fig. S71. Rate of nitrogen evolution monitored with a gas burette during the cyclopropanation of styrene catalyzed by $[Ru(S_2COEt)_2(diphos)]$ complexes **1**–**9** at 60 °C

Table S3. Ruthenium-catalyzed ATRA of CCl_4 to MMA at various temperatures[a]

Temperature (°C)	100	110	115	120	125	130	140	150	155	160
Catalyst	Yield (%)[b]									
[Ru(S_2COEt)$_2$(dppm)] (**1**)		0	43	62	78	90	98	100	100	100
[Ru(S_2COEt)$_2$(dppe)] (**2**)				7	12	18	54	81	94	96
[Ru(S_2COEt)$_2$(dppp)] (**3**)				0	2	5	10	51	68	83
[Ru(S_2COEt)$_2$(dppb)] (**4**)				0	0	2	3	21	45	77
[Ru(S_2COEt)$_2$(dpppe)] (**5**)	5	20	38	50	62	72	81	84	84	83
[Ru(S_2COEt)$_2$(dppen)] (**6**)				0	3	7	18	34	95	100
[Ru(S_2COEt)$_2$(dppbz)] (**7**)						3	4	28	42	60
[Ru(S_2COEt)$_2$(dppf)] (**8**)							2	35	39	50
[Ru(S_2COEt)$_2$(DPEphos)] (**9**)				0	0	2	5	14	30	47

[a] All reactions were performed in toluene for 0.5 h with $[Ru^{II}]_0 : [MMA]_0 : [CCl_4]_0 = 1 : 200 : 800$ and $[MMA]_0 = 1$ M. [b] Yields are based on the formation of monoadduct **15** and diadduct **16** and were determined by GC using dodecane as an internal standard (relative errors are ±5%).

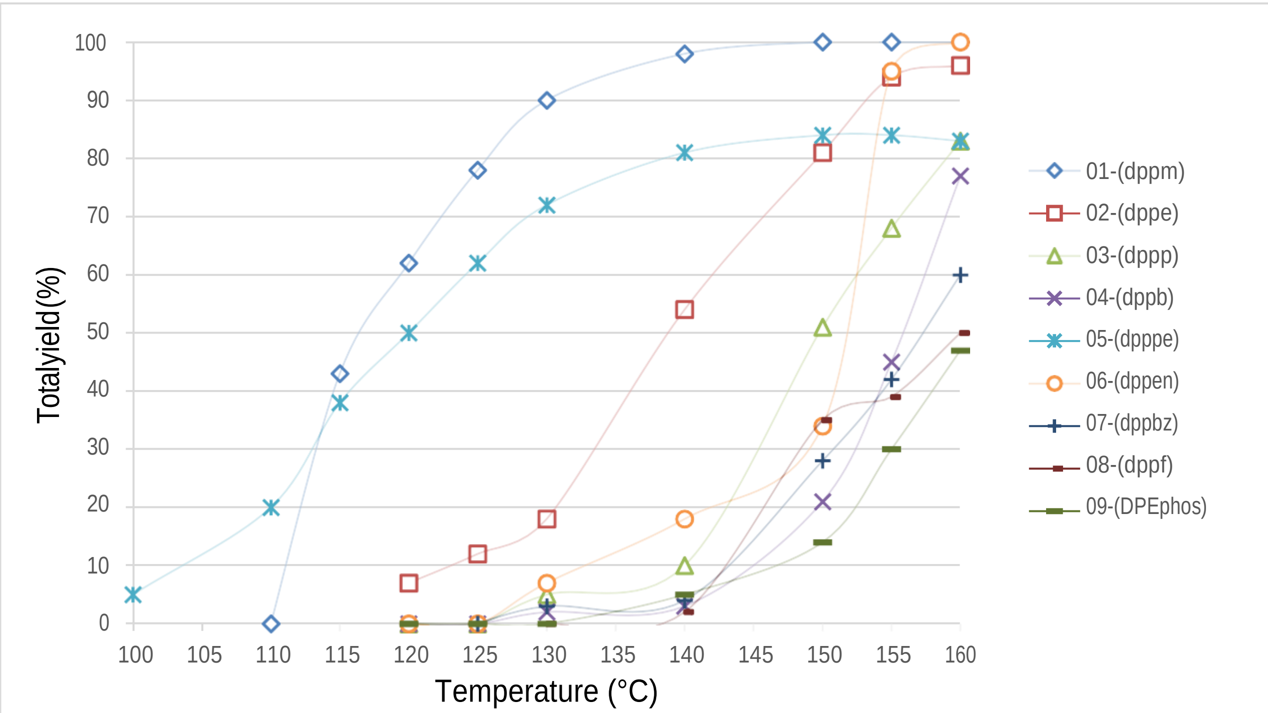

Fig. S72. Plot of the total yields of monoadduct **15** and diadduct **16** for the ATRA of CCl_4 to MMA catalyzed by complexes **1**–**9** at various temperatures (see Table S3 for the experimental conditions).

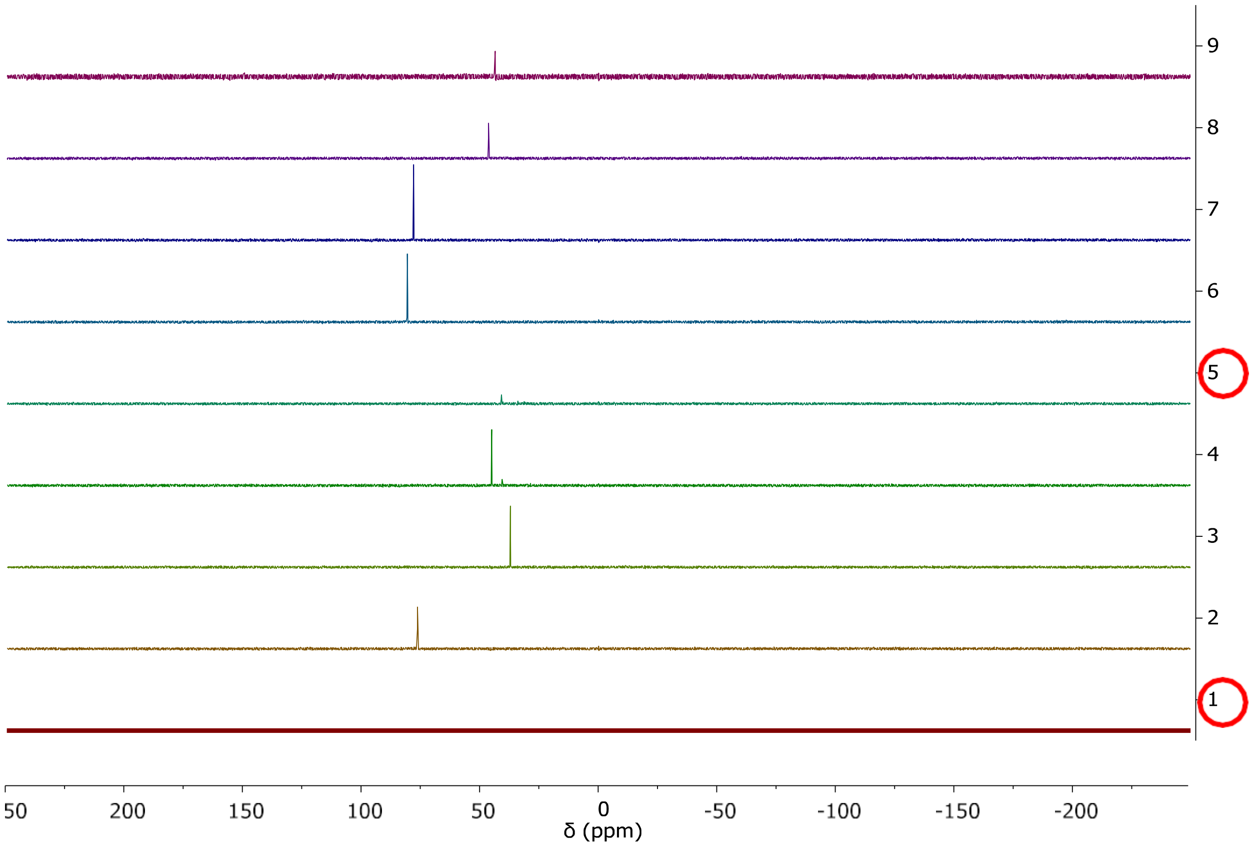

Fig. S73. [31]P NMR spectra of the reaction mixtures obtained after heating carbon tetrachloride and methyl methacrylate in toluene at 140 °C for 30 min in the presence of [Ru(S_2COEt)$_2$(diphos)] complexes **1**–**9** (a sealed capillary tube containing DMSO-d_6 was used for external lock)

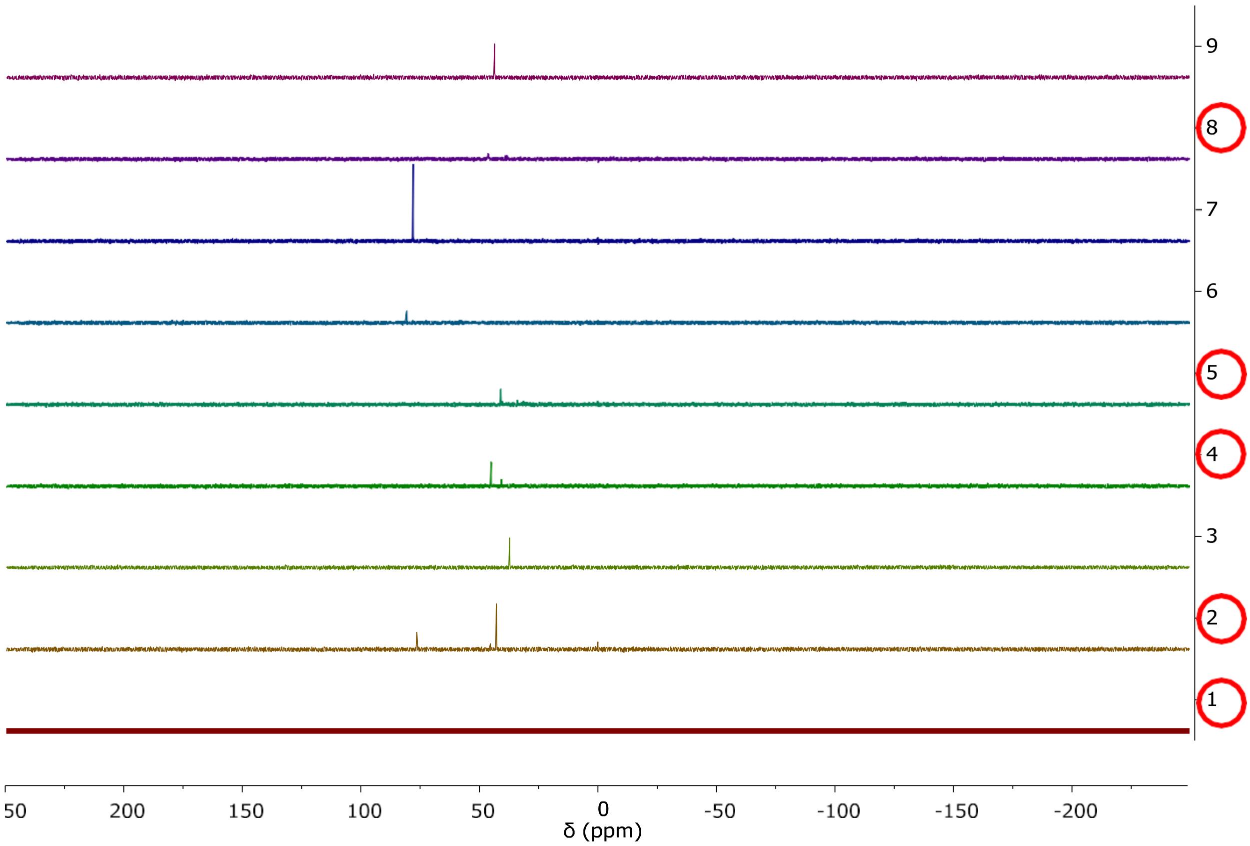

Fig. S74. ^{31}P NMR spectra of the reaction mixtures obtained after heating carbon tetrachloride and methyl methacrylate in toluene at 160 °C for 30 min in the presence of [Ru($S_2COEt)_2$(diphos)] complexes **1**–**9** (a sealed capillary tube containing DMSO-d_6 was used for external lock)